A Bio-Assembly, Mosaic Building, and Informatics System for Cell Biology

by

April Deirdre Blaylock

A thesis
presented to the University of Waterloo
in fulfillment of the
thesis requirement for the degree of
Master of Applied Science
in
Mechanical Engineering

Waterloo, Ontario, Canada, 2007

AUTHOR'S DECLARATION

I hereby declare that I am the sole author of this thesis. This is a true copy of the thesis, including any required final revisions, as accepted by my examiners.

I understand that my thesis may be made electronically available to the public.

Abstract

In the field of regenerative medicine, there is a need to develop technologies that can increase the overall efficiency of imaging and expanding cells in culture and in complex heterogeneous arrangements necessary for tissue construction. Long-term live cell imaging has the potential to significantly enhance our understanding of intercellular signaling pathways and the dependence of phenotype on cell arrangement. A transdisciplinary approach has been taken to bridge the fields of cell biology, robotics, and photonics to create a long-term live cell imaging system capable of single cell handling as well as the acquisition of multiple types of data needed for data mining and a general informatics approach to cell culture. A Bio-Assembly Mosaic Builder and Informatics (BAMBI) system was designed and developed using custom software to control a 3-axis stage manufactured by Galil Inc, and custom 1-axis micromanipulator for robotic operations. The software also employs a Sony charged-coupled device sensor for real-time image feedback and data acquisition. The system is mounted on a Carl Zeiss Axiovert 200 inverted microscope. Custom-built environmental controls are used to maintain the temperature, humidity, and gas conditions for extended live cell work. The software was designed using Visual C++ for the Windows PC platform using an object orientated and modular design methodology to allow the BAMBI software to continue to grow with new tasks and demands as needed. The modular approach keeps functional groups of code within context boundaries allowing for easy removal, addition, or changes of functions without compromising the usability of the whole system. BAMBI has been used to image cells within a novel cell culture chamber that constricts cell growth to a true monolayer for high-resolution imaging. In one specific application, BAMBI was also used to characterize and track the development of individual Colony Forming Units (CFU) over the five-day culture period in 5-day CFU-Hill colony assays. The integrated system successfully enabled the tracking and identification of cell types responsible for the formation of the CFU-Hill colonies (a putative endothelial stem cell). BAMBI has been used to isolate single hematopoietic stem cell (HSC) candidate cells, accumulate long-term live cell images, and then return these cells back to the *in-vivo* environment for further characterization. From these results, further data mining and lineage informatics suggested a novel way to isolate and purify HSCs. Studies such as these are the fundamental next step in developing new therapies for regenerative medicine in the future.

Acknowledgements

Most of all, I would like to thank my co-supervisor Eric Jervis for taking me under his tutelage, sponsoring my graduate studies, and being available whenever I needed his input. He has inspired me to go beyond the limits of my education, to learn and work in the field of stem cell research and tissue engineering. Without his support and guiding influence this work would not have been possible. I would also like to thank my co-supervisor Jan Huissoon for his support in my graduate studies as well as his advice freely offered whenever needed. I would also like to acknowledge and thank my “supervisor” (in spirit), John Medley. Although he was not officially one of my supervisors, he has helped me on a number of occasions (both undergraduate and graduate) and served as an overall force for good during my time at the University of Waterloo. Finally, I would like to acknowledge John Ramunas, who has proof read and provided input on many of the pages in this document. This thesis is only part of the greater work of several students and is truly the result of "standing on the shoulders of giants".

Dedication

I wish to dedicate this thesis to my mother, Sandra Johnman, and my stepfather, the late William Johnman. Both of who have supported my decision to return to graduate school as well as flying me home anytime I needed to be close to my family.

Table of Contents

List of Figures

List of Tables

Chapter 1
Introduction

Cell biology, bioengineering, and microelectronics are fast growing fields wherein advances are being made that can help millions of people who would benefit from their application in regenerative medicine. In cell biology, scientists are working towards an understanding of the fundamental nature of cells to give medicine new ways to treat patients. Bioengineering is a relatively new field so that, when applied to cell biology, is more directed at unraveling the reasons of how and why cells behave the way they do, so that models and technologies can be developed to take advantage of advances in cell and molecular biology. Significantly, the microelectronics industry has revolutionized the methods and the pace with which scientists can perform experiments and analyze results. For example, the advances in computational power using new sequence analysis techniques led to reduction on the expected time it took to map the human genome (Casey, 1999). Inkjet technology has enabled tissue engineers to effectively print "skin" (Boland *et al*., 2003). Laser scanning confocal microscopy has allowed scientists to generate clear three-dimensional views of cells (Pawley, 1995). Each of these successes is due to the fact that a multidisciplinary approach was taken to unite the best of all three fields.

In the field of regenerative medicine, there is a need to develop technologies that can increase the overall efficiency of expanding cells in culture and in complex heterogeneous arrangements necessary for tissue formation. Inter-cell signaling from a three-dimensional arrangement and proper placement of key cell types and support matrix is necessary to create a viable coherent structure that can mimic the tissue type it is designed to replace (Liu *et al*., 2002). Understanding what cell types to use, which configurations work, and what signaling has to take place requires researchers to perform many experiments and develop novel methods to recreate *ex-vivo* conditions, gather data, and finally disseminate that data in a meaningful way. Working on the cellular level is problematic for the research scientist since cells are on the order of 10 micrometers. Robotics assisted cell manipulation can solve the challenge of manipulating single cells, but is still in its early stages of development. The technologies for long-term live cell imaging have, until recently been tedious and user intensive for experimenters to setup and run. Only in the past year have commercial solutions been available that provide high throughput high content live cell screening as opposed to fixed-cell assays. Currently, these products offer mostly “canned” (packaged) algorithms or conventional cell assays that may be good for commercial operations but not as useful for research scientists and engineers who are trying to develop new

experiments and techniques. The present thesis investigates a middle ground approach where technologies from the fields of automated microscopy, robotics, and computer imaging can all be used to enable high throughput long-term live cell experiments at the research level.

The objectives of this thesis was to design and develop an imaging system to provide automated microscopy and live cell robotic micromanipulation to enable researchers to gather large-field long-term live cell data. This system should provide a fully integrated graphical software suite from which to define and conduct automatic time courses, perform robotic pick-and-place operations, and ultimately to view and export data for further processing as needed. Furthermore it should be equipped to gather image mosaics at one or more regions of interest, each mosaic consisting of one or multiple images in three-dimensional space with up to six possible illumination modes through time.

A modular approach was taken to ensure that as each feature was added it could easily be removed or upgraded without compromising the rest of the design. The stability of the system in terms of hardware and software was deemed to be of paramount importance. Therefore, while the imaging system was still in development, it was decided to use it on many of the live cell experiments that were being conducted in the Jervis laboratory. The impact of the system on these experiments and *vise-versa* helped shape its final outcome and application in the field of cell biology.

In this work, a brief introduction to light microscopy is presented. Then, a full literature review is presented on the state of the art in automated microcopy for long-term live cell imaging as well as recent advancements in photonics and robotics for this application. After this, the problem statement is defined and the name “Bio-Assembly Mosaic Builder and Informatics system” (BAMBI) is introduced to describe the system to be designed and developed. The BAMBI design is then described first in terms of hardware and then software. BAMBI has been used in several studies in cell biology and these applications are presented and the results are discussed. Finally, the merits of BAMBI are discussed along with conclusions and recommendations for the future.

Chapter 2
Background

2.1 Light Microscopy

The light microscope has been one of the single most important tools for making scientific discoveries since its invention around the late 16th and early 17th century. Since that time, scientists have developed different microscope configurations and new ways to contrast light through specimens. Many tools have been built to complement the microscope such as automatic shutter control, charge-coupled device (CCD) image capture, and focus control. The compound microscope, the most common in use today, uses several lenses to achieve the magnification. A further revision, the inverted compound microscope, places the objective lens below the specimen rather than above as in traditional systems. This is the preferred method for long-term live cell imaging as it allows the specimen to be placed on the far side of the glass slide instead of between the objective and the slide. This configuration allows much more room for the cell culture environment and additional instruments. For an excellent review of light microscopy see *Fundamentals of Light Microscopy and Electronic Imaging* (Murphy, 2001).

2.1.1 Fundamental Definitions

A brief review of imaging fundamentals is presented to enhance the appreciation for the constraints imposed on system automation.

2.1.1.1 Numerical Aperture

The numerical aperture (NA) of an objective lens is defined by the angle of the light cone accepted by the objective lens and thus it is directly proportional to the ability of the lens to gather light into a resolvable image. It is dependant on the curvature of the lens closest to the glass slide and the index of refraction of the lens material. Generally, higher NAs are desired since they can achieve the better resolution. The greater the incident angle of light on the focus plane the greater the numerical aperture and the better the resolution. A drawback to having high NA is that it requires greater optical correction to account for spherical aberration and chromatic diffraction. High NA lenses also have limited depth of focus and thus place more stringent requirements on the precision of focus.

2.1.1.2 Working Distance

The working distance is defined as the maximum distance allowed an objective between the outermost lens surface and the surface of the specimen slide or coverslip while maintaining a sharp focus (Figure 1). In the inverted microscope position the working distance is shortened by the thickness of the specimen slide. Generally, working distance is inversely proportional to the NA of the objective lens.

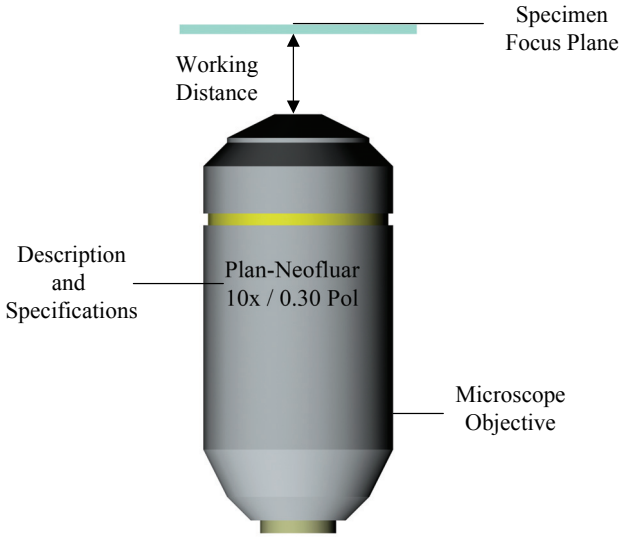

Figure 1: Working Distance for an Inverted Objective

A 10x inverted objective is shown below a specimen slide to illustrate working distance.

2.1.1.3 Depth of Field

The depth of field is defined as the longitudinal resolving power of the objective. It can also be described as the distance from the nearest object plane in focus to that of the farthest object plane simultaneously in focus. Depth of field is only determined by NA where the greater the NA value the narrower the depth of field. The range of values for the depth of field is on the order of micrometers and can also be thought of as the minimum thickness of optical sections that can be attained.

2.1.1.4 Field of View

The field-of-view for an objective is the diameter of the resolvable image, field number, in millimeters as seen at the intermediate image plane. (i.e. it is the maximum diameter of the field-of-view that can be seen at the rated power). If further optics are employed between the objective and the observer the field-of-view can be further diminished. Modern lenses can usually attain a field number around 25 mm.

Field of view can be defined by the following expression:

$$FOV = \frac{N}{M_{Objective} \cdot M_{Eyepiece}} \qquad 2.1$$

Here, FOV is the field of view, N is the field number, and the two terms in the denominator represent the magnification power of the objective and the eyepiece.

2.1.2 Wide Field vs. Confocal Imaging

Wide field microscopy is generally any method of light microscopy that illuminates the entire field-of-view of the sample at a time to generate the image. Confocal microscopy operates by illuminating the sample at a single spot at a time and raster scanning (point-by-point sweep) the entire field-of-view. There are advantages and drawbacks to this method. In confocal microscopy the emitted light is passed from the objective through a small pinhole usually placed in front of a PMT detector. Because the pinhole aperture rejects most of the excited fluorescent signal arising from above and below the focal plane, a laser is typically used for illumination. This actually reduces the point-spread function of the objective lens and can increase the practical resolution by a factor of about 1.4 (White *et al*., 1987). The light beam is usually directed onto the back aperture of the objective lens by a small mirror that can oscillate back and forth to rapidly scan the field of view. This takes more time, up to several seconds, to generate one field-of-view since it involves electromechanical motions to gather the image. One of the most important advantages of confocal microscopy is in the three-dimensional image acquisition. Three-dimensional confocal images are significantly less defocused by the images in the optical layers above and below and can be used to create 3-D representations of the sample. Despite the benefits of confocal imaging, its usage is still limited in research due to the prohibitive cost and

increased acquisition time for experiments. For a complete review of confocal imaging see *Handbook of Biological Confocal Microscopy* (Pawley, 1995).

2.1.3 Differential Interference Contrasting

Differential interference contrasting (DIC) is a form of "optical staining" used to add more contrast to otherwise hard to view transparent specimens when seen in bright field microscopy. This optical staining is achieved by first polarizing then splitting the light path from the lamp, allowing the beams to pass through the specimen, and finally polarizing and recombining the light to form an interference image. The light is first polarized to only allow light vibrating at single angle through to a special prism. The prism splits the light paths into two beams slightly separated where one beam is polarized 90º perpendicular to the other. As the light beams pass through the condenser they are both redirected in parallel but slightly apart toward the specimen. Since each one travels a slightly different path due to varying specimen thickness, slopes and refractive index they will have slightly different path lengths. However, the beams cannot interfere because they are vibrating in perpendicular to each other. After light is collected by the objective it enters another prism where the path difference and the shear are removed. Finally traveling through an analyzer depolarizes the beam and the optical paths are allowed to interfere with one another on the way to the observer. This results in images that have varying shades of contrast creating a pseudo three-dimensional relief of the specimen. For a complete review of DIC imaging, see *Optical Imaging Techniques in Cell Biology* (Cox, 2006).

DIC images tend to be sharper and have excellent resolution. The optical image sections seen through DIC are also somewhat less affected by the planes above and below the focal plane. Additionally, DIC cuts down on the amount of light passed through the specimen relative to the bright field approach thus reducing phototoxicity and maintaining cell viability during long-term live cell imaging.

2.1.4 Fluorescence Imaging

Fluorophores can absorb specific wavelengths of light and re-emit that energy as light at a slightly longer wavelength in all directions. Fluorescence imaging in microscopy takes advantage of the fluorescent properties of some inorganic and organic molecules that act as fluorophores to image specific targets or binding sites in a specimen. Used as a tool in biomedical sciences, fluorophores can be attached to specific antibodies or other ligands that in turn attach to specific

binding sites within the specimen. A similar approach can also be applied genetically when the gene for a fluorescent protein such as green fluorescent protein (GFP) is inserted into a cell (Chalfie *et al*., 1994). By introducing several different colored fluorophores multi-fluorescent images can be taken to image different targets simultaneously. The most common method to image fluorescent molecules in microscopy is by epi-fluorescent illumination (Figure 2).

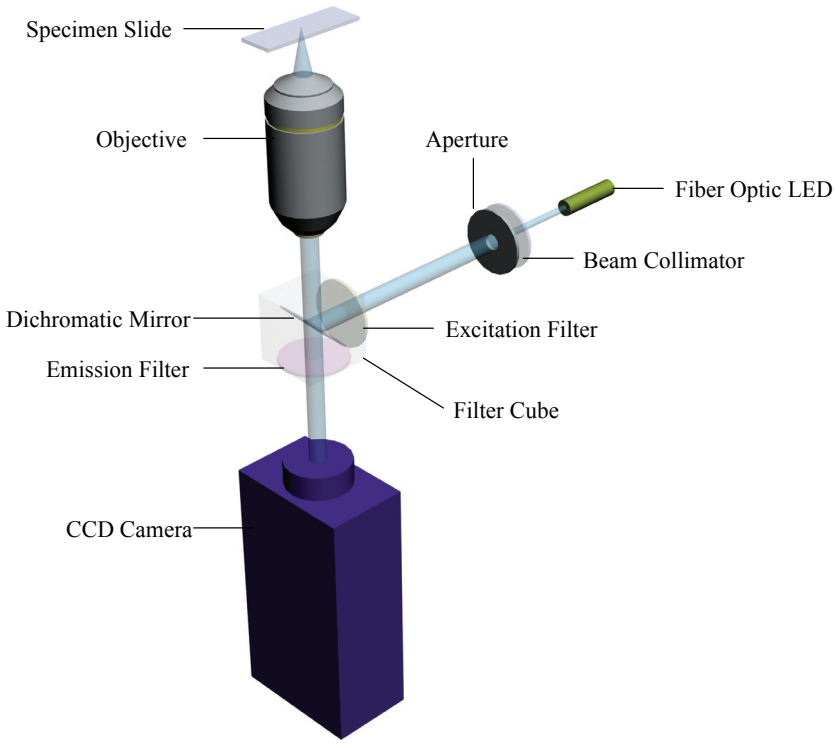

Figure 2: Epi-Fluorescent Illumination

The light path for epi-fluorescent illumination using an inverted microscope and LED source is shown. The light is collimated and passed through a diameter-controlling aperture. The excitation filter blocks all light except the required wavelength. The light that has the excitation wavelength is reflected 90º through the objective and onto the specimen. The light emitted by the specimen travels back through the optical pathway. The emitted light is transparent to the dichromatic mirror and passes through to the emission filter where any stray wavelengths are rejected. The CCD camera collects the final emitted light.

Here the illuminating light source is generated from a light emitting diode (LED) and is carried by fiber optics to the back of the microscope. The light beam is aligned center on the input condenser and passes through a series of filters and then finally through a diameter-controlling aperture. The light beam then enters the filter cube wherein a dichromatic mirror reflects the light upward through the objective where it is focused on the specimen. The fluorophores in the specimen absorb and re-emit the light in all directions. Some of the emitted light travels back

down the beam path of the objective and re-enters the filter cube where it is transmitted through the dichromatic mirror onto the CCD detectors. The dichromatic mirror is manufactured so that it reflects light at a specific wavelength, the excitation wavelength, and transmits light at a slightly longer wavelength, the emission wavelength. This helps to separate the excitation light from the emission light so that emitted fluorescence will be imaged. The excitation and emission filters are optional components designed to further filter the specified wavelengths from entering or exiting the filter cube and serve to reduce background signal from the excitation source.

2.2 Digital Imaging for Light Microscopy

A key requirement for digital imaging in microscopy is efficient and accurate CCD collection of emitted photons. This means that the camera system must provide effective temporal, spatial, and quantization resolution as well as an aspect ratio best suited to the objective field-of-view. It must be able to sense light in the full visible spectrum including near infrared for conventional light microscopy and sometimes ultraviolet for other experimental studies. The camera must also exhibit fairly low noise levels when sensing light as almost all light microscopy used for live cell imaging requires that the illuminating light energy be as low as possible so as to not damage the cells.

CCD cameras use a charge coupled device array in which each sensor (pixel) captures the value of incident light energy by storing it as energy potential. These values are digitally gated off the CCD array one line at a time to form an array of digital values representing the energy potential at each pixel (Forsyth *et al*., 2003). The process of digitizing the coordinate pixel values is called sampling and the process of digitizing the amplitude values is referred to as quantization (Gonzalez *et al*., 2002). The pixels themselves can be arranged in patterns red-green-blue (RGB) for color sensors or ultraviolet-black/white (UVBW) for extended range sensors or simply as full range monochrome black/white (BW) sensors.

The CCD sampling resolution is related to the size of each sensor. Usually the sensors are square and have the same dimension in x and y. Cameras used in digital microscopy have values that can fall in the range of 4 to 6 µm per sensor or pixel. A 10mm x 10mm CCD array with square sensors measuring 4.65 µm would be able to generate a maximum resolution image of 2150 x 2150 pixels. It is important that a camera be able to image the entire field-of-view as seen by the objective to minimize loss of information. If an objective lens with a 25 mm field-of-view were imaged directly onto a camera CCD with no other intermediate lenses, the CCD array has to be

25 mm x 25 mm to capture the entire field of view. In fact, given a 25 mm field-of-view for most objectives, it is common to introduce a 0.6x adapter lens between the camera and the objective, thus reducing the required size of the CCD array to only 15 mm x 15 mm.

An additional consideration pertaining to light microscopy is the fact that the optical resolution also called spatial resolution is limited by the wavelength of the light itself. For an optical microscope, the minimum resolving distance is shown to be:

$$R = \frac{1.22\lambda}{2NA} \qquad 2.2$$

Here R is resolving power, λ is the wavelength of light used, and NA is the numerical aperture of the objective lens (Inoué, 1986). The smallest resolving distance for normal light microscopy, known as Abbe's Limit, is observed at a wavelength of about 220 nm giving a distance of 0.11 micrometers. Given that one must have two samples for every unit of the smallest observable unit to satisfy Nyquist's Theorem and insure no loss of information. (Forsyth *et al*. 2003) It becomes apparent that it may be possible to over-sample the image providing no additional information. This would unnecessarily introduce more damaging light to the cells and increase the data storage size necessary. For example, if light with a wavelength of 505 nm was used with a 40x objective lens with a NA of 0.75 and no additional optics between the camera and the CCD array, the minimum pixel size should be no less than 8.4 μm. Once again, by inserting a 0.6x camera adapter between the CCD array and the objective, the smallest pixel size needed becomes 5.0 μm and the field-of-view is effectively increased by a factor of four.

The final properties important for digital microscopy are quantization (the value assigned to each level of gray) and binning (the number of neighboring light sensors to sum together to generate one pixel value). In the CCD Camera, the bit depth used for the conversion of the CCD potential to a digital value determines the quantization resolution. The common range is between 8-bit, 256 shades of gray, to 16-bit, 65,536 shades of gray, per pixel. Binning modes are made available by the CCD camera and are usually of the form *n* x *n* with *n* being either 1 or 2.

Binning becomes important for fluorescence microscopy where the emitted light is extremely faint and must compete with the noise level to overcome the sensitivity threshold of the CCD

sensors. The relative sensitivity of the CCD camera is dependant on the wavelength of light used, the total magnification, and the total surface area of the CCD neighborhood used per pixel.

The response curve presented in Figure 3 shows the non-linear response of the BW CCD to light energy ranging from near ultraviolet (400 nm) into the infrared (≥700 nm). The CCD is most sensitive in the blue-green region at 505 nm falling off moderately in either direction. The fact that the response curve is still sensitive at wavelengths greater than 700 nm emphasizes the camera's sensitivity to the additional infrared energy or heat that can add noise to the final image.

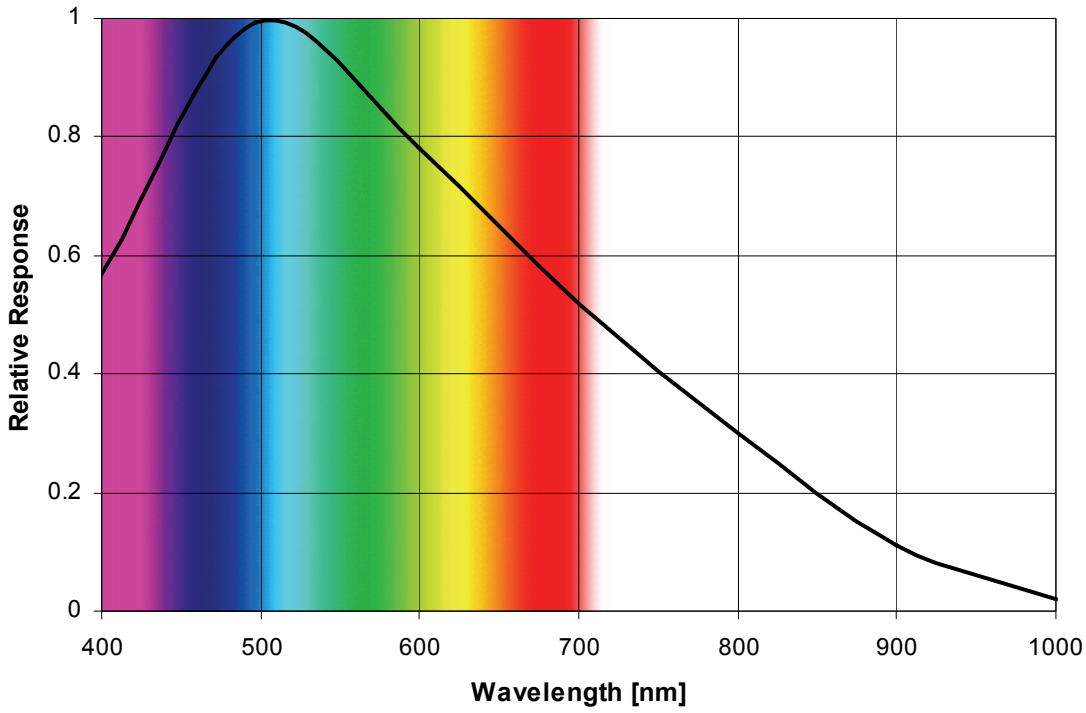

Figure 3: Spectral Sensitivity for Sony XCD-SX910 BW Camera

Shown, is the spectral sensitivity of the Sony XCD-SX910 BW camera for a selected wavelength range. The range of the human visual spectrum (400 to 700 nm respectively) is shown in color. Adapted from the Sony Technical Manual for the XCD-SX910/X710 (2003).

The amount of light incident on a CCD sensor is proportional to its surface area and the binning mode. Increasing the binning mode from 1x1 to 2x2 would increase the sensitivity of light by a factor of four. There would be a trade off between image resolution and sensitivity but the images capture would exhibit a much better signal to noise ratio in the 2x2 binning mode.

The magnification and NA has a significant impact on the amount of light focused onto the CCD array and must also be considered when choosing the binning mode and quantization level. Higher NAs will collect more light than lower numerical apertures thus increasing the quality of the sampled image to the fourth power of the NA. A higher magnification is inversely proportional to the amount of light received to the second power. Generally objectives over 20x used for fluorescent microscopy are of the very high NA variety.

2.3 Automated Microscopy

Automated microscopy is a new tool, fueled by the progression of the microelectronics industry and the need for researchers to push the limits of conventional microscopy. It includes motorized microscope components and accessories to automate the image capture of time-lapse experiments. Z-stacks, a series of optical sections, attained by focusing through a depth range, can be captured automatically with the addition of a focus motor. A z-axis motor with the appropriate software control can allow for correction of microscope focal drift that occurs during time-lapse experiments. A large set of single fields-of-view can be captured and tiled together to form a continuous image or mosaic by the incorporation of an x-y motorized stage. Multi-spectral time courses can be acquired with motorized illumination such as a shutter or filter wheel. All of these features may have an individual software package to control them but the hardest part is building a single software program to make them all seamlessly work together. The nature of long-term live cell imaging requires long run times and the program should be able to operate unattended.

2.3.1 Stage and Focus Automation

The most basic requirement of automated microscopy is the motorized stage and focus control. This will enable the microscope to image areas greater than the field-of-view of the objective by moving from one location to another in the same sample or possibly even across samples from one specimen to another. Many microscopes manufactured for life sciences are designed to support motorized x-y stage control. The microscope manufacturer usually provides this feature as an optional accessory, but it can also be acquired from one of the many after market companies that cater to this need. Almost all stages used in wide field microscopy are designed to move the plate, well, or dish containing the sample while the microscope is held stationary. This allows the sample to be translated through the focal point of the objective as desired. The maximum range of x-y travel will place a limit on the size of plates that can be imaged by the

microscope and can range from 25 mm to 180 mm respectively. Table 1 shows the specifications of several well-known manufactures of motorized stages and z control options.

Table 1: Comparison of different commercially available automated stages and focus controls for microscopy.

Manufacturer	Device Name	Automation	XY Precision*	Z Precision*	Travel Range (mm)
Applied Scientific Instrumentation	MS-2000	Motorized XY Stage	0.8 µm	-	114 x 90
		Z-Focus Knob	-	0.1 µm	-
Ludl	BioPrecision	Motorized XY Stage	3 µm	-	100 x 120
	Piezo Z	Piezo-Z Stage	-	1 nm	0.2
	Z-Control	Z Focus Knob	-	0.15 µm	-
Physik Instrumente (PI)	P-725	Peizo Objective	-	1 nm	0.4
	XYZ M112	Motorized XYZ Stage	0.1 µm	0.1 µm	25 x 25 x 25
Zeiss, Germany	Cell Observer HS	Piezo-Z Stage	-	1.5 nm	100
Applied Precision International	NanoMotion II	Motorized XY Stage	0.1 µm	-	25 x 55
		Motorized Z Stage	-	0.1 µm	1
Prior Scientific	H120	Z Focus Knob	-	0.1 µm	-
	H107	Motorized XY Stage	1um	-	180 x 69

*Precision - The variation of repeated efforts to maintain the same position over a long time, also defined as repeatability.

Most manufacturers, but not all, will incorporate the motorized z-axis as a separate unit from the x-y stage. The most common configuration is to have it attached directly to the microscope fine focus control knob. By rotating the focus knob, usually with a stepper motor, a very accurate relationship between the focal plane and the rotation of the motor can be established. Here the resolution of the focus movement is limited to the fixed value of the stepper's magnetic windings allowing sub micron increments for a known rotation step. Given some backlash in the gear assembly and the setup of the focus control inside the microscope, repeatability remains sub micron. An added benefit of using the focus knob is that the alignment of the z motion relative to the axis of the objective assembly will be as good as the focus alignment of the microscope. If a servo drive is employed instead of a stepper motor, the user can expect to see improvements in the speed of the focus knob as well as less vibration but an auxiliary encoder must be used to accurately determine the position of the z value. In either case, the range of z motion is only

limited to the maximum physical distance between the objective and the sample slide (working distance).

Z-axis automation can also be achieved by having the unit attached as an additional stage insert to the x-y stage or as a telescoping unit placed between the microscope and the objective itself. In either case, the most common method of actuation is via piezoelectric induced motion. Piezoelectric actuators work by passing a voltage through a stack of PZT crystal disks interleaved with thin metal sheets, as each crystal receives the charge it expands up to approximately 1.5% of its original value (Teschler, 2005). This type of actuation is almost instantaneous and can be very accurate. The only drawback is that these systems have limited travel range. Most actuators of this type only offer a range of approximately 100 μm, but some newer versions are now offering ranges up to 400 μm. The increase in travel length is most likely attributed to the addition of an actuation-multiplying device, similar to a lever (Teschler, 2005).

2.3.2 Automated Illumination

The reasons for automating illumination in microscopy are governed by the information requirements of each study. Bright field, DIC, and phase contrast studies generally use a tungsten halogen lamp to provide the source of illumination. In an epi-fluorescent study the source could come from a laser system, a broad-spectrum arc lamp, or a light emitting diode. Confocal applications usually employ a single laser to excite the specimen at any one time, but can include several lasers of different wavelengths. Obviously the confocal application has control built into the system as it is required in order to raster scan the entire field-of-view, but the other systems are usually after-market additions. Halogen lamps such as the tungsten or the broad-spectrum arc lamps are not designed to be turned off and on repeatedly and need a shutter mechanism to block the light when it is not needed. Recently, the need for automated shutters has increased to the point that manufacturers are now including this as a standard feature. An automated shutter is now a standard on the latest version of the Axiovert 100M microscope manufactured by Zeiss, Germany.

Multi-spectral fluorescent experiments that require images to be taken at different wavelengths can use a filter wheel to block out unwanted light only allowing the excitation spectrum through as would be the case when illuminating with a broad spectrum arc lamp. The biggest caveat to using a broad-spectrum light source is handling the deflection of the heat safely. Most broad spectrum light sources, Mercury, Xenon, and Metal Halide, emit infra red light that is absorbed

by the excitation filters causing a great deal of heat to build up. Over time the shutters can breakdown and stick if methods of heat deflection are not employed. A solution to the problem is to use a fiber optic light path that can excite at the desired wavelength without causing heat damage (Carpenter *et al*., 2004).

Light emitting diodes only require a digital logic high or low signal to turn them on or off thus eliminating the need for a shutter. Most LEDs emit light in a specified narrow band wavelength thus reducing the need to implement additional band reject filters. They generate significantly less heat than the traditional broad-spectrum arc lamps and have much longer working lifetimes. Laser light sources are similar to the LED illumination sources in that they emit light in a relatively narrow bandwidth thus reducing the need for additional heat filters. However, lasers can pack a lot more power and must be carefully controlled to avoid effects like cell damage and photo-bleaching from occurring.

2.3.3 Autofocus

In any automated microscopy application, the need to have a robust autofocus system is of great importance especially for any long-term live cell imaging experiments. The need for focal correction arises from unwanted focal drift, a change in the distance between the objective and the desired in-focus plane. The cause of drift can be attributed to temperature gradient, mechanical relaxation, cell movement, or sample settling. Temperature gradients caused by differences in temperature between the stage, microscope, motors and their respective surrounding environments can have a significant effect on the distance between the objective and the desired in-focus plane (Wolf *et al*., 2005). During live cell time course experiments the cell sample and sometimes the microscope itself must be held at a constant temperature, usually 12 - 17º above the ambient room temperature.

Therefore, to overcome these issues, autofocus control must be implemented for automated microscopy systems involving any long-term live cell imaging. Price and Gough breakup autofocus techniques into two major categories (Price *et al*., 1994): positional sensing and image content analysis. Positional sensing could use an interferometric approach such as Molecular Devices Corp.'s ImageXpressMicro™ system that employs a laser to focus light on to a planar surface such as the bottom of a glass slide or cover slip. Another method could also use a digital micrometer between the microscope stage and the objective to report any changes that occur over time (Wolf *et al*., 2005). An image content analysis solution would employ a software algorithm

to generate an optimum focal score for each image sampled in the range of focus. Image content may be analyzed using a closed circuit video feed (Johnson *et al*., 1974) where high energy in the video signal is used as measure of in-focus (Groen *et al*., 1985). Image content can be converted to digital form by means of a frame grabber or directly with a CCD camera and then analyzed for a focal measure as well.

Image content analysis is cost effective and relatively easy method to implement, as it requires no additional hardware other than focus control hardware and a CCD camera for image feedback. Therefore, this section will focus on the various applications of software algorithms used in conjunction with a focus control motor. An image content analysis solution or software solution in general, uses the digital camera to capture images as input to an algorithm that will then generate an in-focus score for each image. By capturing the images through a range of focal values, it can be used to select the best in-focus image and its corresponding Z position. Many different autofocus methods have been employed to varying degrees of success in the literature. (Groen *et al*., 1985; Firestone *et al*., 1991; Geusebroek *et al*., 2000). However, robust autofocus has been shown to be very difficult to achieve in practice.

The problems faced by autofocus algorithms can be summarized by the criteria in which they are evaluated. Groen establishes eight criterions used in the selection and evaluation of focus functions (Groen *et al*., 1985): (1) "Unimodality." There should be no regions of local maxima or minima other than one. Exhibiting multimodality shows that the algorithm is sensitive to other factors that may lead to false maxima. In practice, unimodality cannot be guaranteed (Price *et al*. 1994) but can be reduced by employing less noisy algorithms. (2) "Accuracy." The maxima must be located at the in-focus plane. (3) "Reproducibility." The maxima must be reproducible and sharply peaked. Generally this can be achieved once the results are normalized. (4) "Range." The range focal distances through which the focus function operates should be as large as possible. As the range increases so does the capture time. By incorporating various sampling algorithms, this can be optimized for speed (Geusebroek *et al*., 2000). (5) "General applicability." The function should not be limited to the type of images collected. Significant differences in the performance of algorithms often exist between phase contrast and fluorescent imaging (Price at al., 1994). (6) "Insensitivity to other parameters" such as noise, scratches and changes in lighting conditions. Price has shown that lamp fluctuations can give rise to intensity spikes resulting in false local maxima (Price *et al*., 1994). (7) "Video signal compatibility." This is an issue relating to closed circuit video cameras which can be overcome by using any of the commonly available CCD cameras on the market. (8) "Implementation. The system must be easy to implement."

Here the software autofocus algorithms are generally the easiest to implement due to the digitization of the modern microscope systems.

2.3.4 Environmental Control

Maintaining live cells in culture for automatic microscopy requires that special operating conditions are met while simultaneously allowing optical imaging to take place. This can include conditions such as light transmissibility, temperature, CO_2, pH level, sterility, and osmolarity. Numerous cell culture chambers with widely varying designs have been introduced to meet these needs. They can be boxed compartments that fit over all or only part of the microscope or small chambers designed to fit between the light source and the objective lens.

One of the earliest closed perfusion chambers cited in microscopy literature set the standard for controlled cell incubation chambers for years to come (Dvorak *et al*., 1971). They also introduced eight desirable design characteristics to have for high-resolution light microscopy of cell culture chambers: (1) "Usable with all light microscopy techniques." This requirement meant that the chamber have optically transparent, flat, parallel surfaces with a thickness not exceeding 1.2 mm. This would allow high numerical objectives with short working distances to be used with bright field, phase contrast, and differential interference contrast microscopy. (2) A "closed system." This meant that the culture chamber was safe to handle and immune to pathogens. (3) "Sterilizability." The chamber should be able to be easily sterilized before and after an experiment. (4) "Made from biological inert and non-toxic materials." (5) Designs that allow "rapid cleaning and assembly." (6) Ability to remove the chamber from the microscope and re-locate it with a fixed reference point. (7) Allowed for "long-term maintenance" of the cells. (8) Allow "rapid exchange or replacement of culture media." The problem with characteristic 2, a closed system, is that researches are not able to manipulate the cells once the experiment has begun. This was solved by the introduction of cell culture chamber with a thin gas permeable layer that floated on top of the cell culture medium (Ince *et al*., 1983). Ince's group designed a cell culture chamber that could be used on a microscope that facilitated the automated control of temperature, pH, sterility, and osmolarity of the environment while still allowing free access to the cells. The top lid consisted of a layer of non-toxic mineral oil with heated gas flowing directly over it. The gas flow served a dual purpose allowing it to maintain gas pressure as well as heating the culture to the maintenance temperature. Nowadays, there are many companies that offer long-term live cell imaging chambers for researchers such as Bioptechs Inc. (Butler, PA),

Life Imaging Services (Reinach, Switzerland), Biocrystal Ltd. (Westerville, OH), and Invitrogen Corp. (Burlington, ON).

2.3.5 High Content Screening

High content screening, first introduced commercially by Cellomics Inc. (Pittsburgh, PA) in 1997, has had a major impact in the field of cell biology and lately systems cell biology. The term "high content" refers to the large amount of information that is contained in the images collected by fluorescent microscopy, either confocal or widefield. The term "high content screening" (HCS) refers to the high content microscopy with the addition of the automation and analytical techniques that have traditionally been used for protein analysis, mass spectroscopy, transcription profiling, and DNA microarrays. HCS is generally limited to fluorescence microscopy due to lack of specific markers and algorithms to characterize bright field, phase contrast, or DIC images but some HCS providers do include this option for context reference. The range of applications that can benefit from HCS is growing and improved software, visualization tools, and biological markers are driving this technology into the future. The authors Gough and Johnston provide an excellent review of HCS in "High Content Screening: A Powerful Approach to Systems Cell Biology and Drug Discovery" (Taylor *et al*., 2006). The rest of this section owes much of its merit to their work.

HCS platforms are distinguished by their ability to perform fluorescence based cell analysis in an integrated and automated system that can screen upwards of tens of thousands of samples a day. Gough and Johnston provide a list of five specifications that all HCS systems should have: (1) Sufficient resolution and sensitivity to capture the cellular features of interest. (2) A field-of-view large enough to image multiple cells. (3) Spectral channels to distinguish multiple fluorescent labels. (4) Adequate speed to meet the demands of the screening volume. (5) Flexibility to access a wide range of assay requirements.

At the time of Gough and Johnston's review, 2006, most HCS platforms had only been developed for fixed cell assays or histological assays in that only fixed cell(s) could be assayed. Assays such as these have no temporal connections thereby leaving a lot out of the picture and can even lead to false conclusions (Pepperkok *et al*., 2006). By having HCS platforms that can provide long-term cell maintenance, these problems can be overcome. In the past year companies seem to have caught on to the trend toward high content screening of live-cell cultures and now, more often than not, include long-term live-cell maintenance as a standard feature. (See Table 2.)

All HCS systems are designed to provide fluorescence imaging, whether it be widefield optics with rotating emission bandpass filter wheels or multiple confocal lasers scanning in parallel. In the widefield modality, the system will have a broad range of commonly available filter sets allowing for many different wavelengths. In the laser scanned confocal case the system is limited to the wavelength of the laser installed in the system. However, these systems may provide up to three or four lasers, each with a specific wavelength that can be operated in simultaneous acquisition mode. GE Healthcare incorporates a rotating pinhole disk or Nipkow disk to scan the image confocally while using a broadspectrum lamp with a filterwheel allowing for a greater range of fluorescence than the laser method. Other systems have multiple cameras to acquire images in parallel thus reducing the time required for the single channel variety.

Gough and Johnston make an arbitrary distinction between high-throughput high-content (HT-HCS) and HCS systems by the capacity they have to screen wells. A HT-HCS should be able to image in excess of 50,000 wells a day. There are three such systems, INCA 3000 (G.E. Healthcare), Opera (Evotec), and ImageXpress ULTRA (Molecular Devices) that are HT-HCS systems and are compared in Table 2. They are characterized by having multiple cameras providing three to four channels for simultaneous acquisition. However, careful attention must be made by the experimenter so that there is no crosstalk or spectral overlap between the reporter labels. This is a known problem with near UV excited fluorophores like DAPI and Hoechst DNA labels.

Table 2: Comparison of selected high-throughput and high-content screening systems

System Name	Throughput	Manufacturer	Imaging Modality	Autofocus	Live/Fixed Cell Imaging?
ImageXpress 5000A	HCS	Molecular Devices	Widefield	Software, Laser	Fixed, Both[a]
cellWoRx	HCS	Applied Precision	Widefield	Software	Fixed
KineticScan	HCS	Cellomics	Widefield	Laser	Both
ArrayScan VTI	HCS	Cellomics	Widefield	Software	Both
IN Cell Analyzer 1000	HCS	G.E. Healthcare	Widefield	Laser	Fixed
BD Pathway HT	HCS	B.D. Biosciences	Nipkow Disk	Software	Both
IN Cell Analyzer 3000	HT-HCS	G.E. Healthcare	Confocal	Laser	Both
Opera	HT-HCS	Evotec	Nipkow Disk	Laser	Fixed
ImageXpress ULTRA	HT-HCS	Molecular Devices	Confocal	Laser	Both

[a] Optional Component.

HCS and HT-HCS are still new technologies and rely on strict protocols to be used for their reliable operation. Research is driven by novel configurations and setups that are challenging to automate, thus only a few applications of live cell microscopy can be performed on these systems. Some systems offer an open software architecture allowing the user to create custom modules that can be added at a later time.

2.3.6 Automated Microscopy Software

One of the most important parts in employing automated microscopy is having software that can effectively orchestrate the image/data acquisition, visualization, and analysis (Taylor *et al*., 2007). The design and implementation of such software is a very demanding problem, especially for live cell imaging. A number of recently developed biological assays have lent themselves well to automation and as a result there are many software choices out there to choose from. However, products can range from open source highly unspecific yet customizable to all-in-one commercial software packages that are very specific in application and hard to customize. Researchers must select the software that best matches their requirements, but in the end there is always an inevitable trade off between customizability and functionality.

Automating the process of live cell imaging is an especially demanding task as it must be able to adapt under dynamic conditions. As the science progresses, new and more complex assays are being developed all the time, which require new algorithms and procedures to be implemented. Live cells studies may require the ability to focus on a region of interest (ROI) at one moment and then move to a different ROI at a later time. This is especially important when ROIs are mitotic cell divisions or the assay incorporates live cell tracking. Another confounding factor is that in most high throughput systems it is not possible to make modifications after the experiment has started (Pepperkok *et al*., 2006).

It is important to quantify the features that are required for automatic microscopy software. Automated image analysis should incorporate image segmentation of regions of interest, classification of those regions, and tracking of the regions desired (Pepperkok *et al*., 2006). The analysis software should be intuitive and user friendly, provide a real time display of the analysis results, and provide the tools to visualize, manipulate, and compare the data (Taylor *et al*., 2007). The data and images acquired should be stored and made available in a relational database structure (Andrews *et al*., 2002). Most literature sources stress the importance of image analysis and data mining over the actual acquisition capabilities.

A comparison of software solutions is presented in Table 3. The software programs are rated in five categories for comparison. Throughput - the throughput needed for the application it is intended for. Research applications generally require no more than 50,000 images a day, but they can be installed on a conventional automated microscope. Acquisition - the ability to control the hardware for automatic data/image capture. Analysis - the ability to process the data and images collected. This is the first step in quantifying results. Database - the ability to store the images and data in a relational database. This is important for running queries based on any results from the analyses to provide the researcher with a fast tool for new discoveries. Customization - the degree to which the program functionality can be altered. Some programs are inflexible and are designed for a specific purpose. Add-on software modules may allow for a larger range of applications but do not add to user customization. Macros and batch processing may not add customization to the applications, but will add to the ease of automation. Open source code, specific programming toolboxes, or incorporating programs like MATLAB actually enable the user to add new functionality to the program as needed. However, the more flexible the software programs the more demanding it can be for the programmer to implement it (Lamprecht *et al*., 2007).

Table 3: Comparison of selected automated microscopy software programs

Software Title	Throughput Application	Manufacturer	Acquisition	Analysis	Database	Customization
Cellenger	HCS	Definiens	No	Yes	No	No
BioApplications	HCS	Cellomics	No	Yes	No	No
KineticScan	HCS	Cellomics	Yes	Yes	No	No
CellProfiler	HCS, Research	Open Source	No	Yes	No	MATLAB[a]
BioConductor	HCS, Research	Open Source	No	Yes	No	R[b]
ImagePro Plus	HCS, Research	MediaCybernetics	Yes	Yes	Yes	Macro Language
IN Cell Investigator	HT-HCS	G.E. Healthcare	Yes	Yes	No	Toolbox
MetaXpress	HT-HCS	Molecular Devices	Yes	Yes	Yes	Macro
MetaMorph	HCS, Research	Molecular Devices	Yes	Yes	No	Macro, VB[c]
ImageJ	Research	Open Source[d]	No	Yes	No	Java[e]
AxioVision	Research	Carl Zeiss	Yes	Yes	Yes	Batch, VBA[f]

[a] Requires MATLAB and image processing toolbox. [b] R programming language. [c] Microsoft's Visual Basic programming language. [d] National Institutes of Health. [e] JAVA programming language. [f] Microsoft's Visual Basic for Applications.

2.4 Cell Manipulation

Some long-term live cell imaging experiments require the ability to manipulate cells directly. This may be to establish clonal colonies from a single cell, arrange cells in a specific pattern that mimics the cell structure *in-vivo*, or re-implant cells in a host after live cell imaging. Tissue engineers need to be able to work with small population sizes in order to create a structure that is just as intricate and diverse as the naturally occurring tissue and yet still be able to produce a large enough cell density in the order of one million cells per cubic centimetre to be useable. Automated cell manipulation may solve the challenge of overcoming large population sizes but it still in its early stages of development. There are many different methods of cell manipulation already developed that may or may not be suitable for single cell manipulation. Several technologies that show promises in the field of cell manipulation are cell based printers, optical manipulation, dielectrophoresis, photopatterning, and microfluidics.

2.4.1 Ink-jet Cell Printing

Commercial off-the-shelf ink-jet printers have been successfully modified to print organic materials and cells onto solid supports (Boland *et al*., 2003). This technology enables the patterning of microarrays for uses such as protein, antibody, and DNA combinatorial reaction studies. It can also be used to pattern cell libraries and cell arrangements that may mimic the actual respective organ or tissue to be replicated.

The system employed by Boland and Wilson consisted of a modified Hewitt Packard 500 series ink-jet printer that was broken out of the casing and mounted on a glass sheet that was in turn mounted on a wooden frame (Boland *et al*., 2003). For cell printing, the standard ink cartridges were replaced with a custom built 9-needle (30 gauge) version that was fed from nine separate compartments. This allowed the print head to accommodate up to a maximum of nine possible cell solution/substrate combinations. The print head is mounted onto a bar and is allowed to move width wise across the surface of the glass. A second bar and wheel assembly provides the lengthwise motion of a sample overtop of the glass surface. The sample to be ‘written’ upon is a glass cover slip that is taped to a transparency sheet that is in turn needed to provide the width surface necessary for lengthwise movement by the wheels. A custom built graphical user interface allowed the printer to be easily programmed by providing it with a picture of the array deposition and a color code for the cell compartments to be used.

The ink-jet based cell printer could pattern cells at a minimum of 50 μm between droplets, 1.5 cells per drop, and cover an area of 1 square inch per minute. Using a cell solution of bovine aortal endothelial cells at 1 $x10^5$ cells/ml and printing them on a basement membrane of 3 mg/ml Matrigel™ they achieved an overall 75% cell viability. The results show that this technology has some advantages such as having high throughput, low cost components, and being easily automated.

A challenge for ink-jet cell printing technology is that, although it is automated, it is programmed in a feed-forward technique that does not allow for real-time quality control feedback that would be necessary for repeatability of results on the cellular scale. For example, if a cell array were patterned in one experiment it would be very hard to duplicate the original conditions in subsequent runs even though it had the same program due to variances in the cell deposition (one or two cells per droplet). Another challenge for ink-jet cell printing is that it is limited by its current resolution of 50-μm-deposition pitch. Although on large scales this would not be a problem, when making tissues that depend on cell-cell adhesion, the distance would be far too great to overcome without having the cells migrate themselves, which in turn may distort the desired original construct. More challenges such as needle clogging, cross contamination, and sterility of the print head will have to be addressed before this technology can be fully realized in a commercial sense.

2.4.2 Laser Cell Printing

Laser cell printing (Ringeisen *et al*., 2004; Barron *et al*., 2004) has been used to generate large-scale cell arrays, adjacent arrays of different cell types, and three-dimensional layered cell patterns. In one experiment, a laser printer known as matrix-assisted pulsed laser evaporation direct write (MAPLE DW) was used to pattern pluripotent embryonal carcinoma cells (P19) onto a thin layer of Hydrogel™ (Barron *et al*. 2004). In another experiment an improved printer based on the MAPLE DW known as biological laser printing, BioLP, is used to pattern heterogeneous arrays and 3-D cell layers using human osteosarcoma cells (MG63) and mouse endothelial cells (EOMA GFP) (Ringeisen *et al*., 2004).

In MAPLE DW, the system uses a pulsed laser to focus energy just below a cell to vaporize the substrate causing an explosive gas bubble that in turn ejects the cell forward onto the receiving medium. The P19 cells were placed in a biopolymer medium at a concentration of 1.5 x 10^7 cells/ml and spread out as a thin layer onto a 2.52 cm diameter transparent quartz disk. The laser

was positioned on the other side and normal to the quartz surface so that it could focus on the interface between the quartz and the biopolymer. The laser wavelength used in this study was 193 nm and was chosen so that the water contained in the supportive bio-layer mainly absorbed the laser energy. Using a CCD camera that was pointed confocally with the incident laser light a user could select the portion of the bio-layer and cells that were to be printed. The receiving surface for cell printing was a glass slide with a thin layer biopolymer coat. This coating is necessary to decelerate the transferred biomass, provide support, and a viable growth medium for the P19 cells. A single pulse of laser energy, approximately 400 mJ/cm^2, with a spot size of 100 x 125 mm^2 was enough to insure the transfer of about 10 cells at a time. The results of the experiment showed that the cells were very sensitive to the velocity they were transferred at and the thickness of the receiving medium. The initial ejection velocities of the cells can range from 50 to 1000 m/s that would cause deceleration values to be too great for cell viability. Hydrogel™ coatings of 40 mm were found to be necessary to provide enough deceleration time to maintain a >95% viability.

In BioLP™ the system is based on the MAPLE DW™ printing device but makes a significant change by inserting a barrier between the focal point of the laser and the biomaterial. Other changes include the ability to write different cell types into heterogeneous arrays and form three-dimensional layers. The BioLP set up is as described in the MAPLE DW system above except that the quartz disk is coated with a thin (35 to 85 nm) layer of metal or metal oxide (Au, Ti, or TiO2) between the bio-layer and the quartz surface. The barrier absorbs most of the incident laser energy and in turn transfers energy in the form of heat to the bio-layer containing the cells.

The experiments showed that the BioLP could pattern MG63 cells onto a Matrigel™ substrate ranging from 50 - 200 mm thick. It could perform multiple transfer operations to seed different cell types by changing the quartz cell solution disk with a different one containing different cells and re-registration of the disk to the substrate surface. Using a cell concentration of $3x10^5$ cells/cm2, a laser spot size of 100 mm, and laser fluence energy of 160J/cm2 resulted in 3 - 10 cells placed per 100 mm spot on a 600 mm spaced array. The deposition speed was reported to range from 15 to 100 drops per second dependant on laser pulse frequency. Cell viability was reported as being very close to 100% based on a live/dead cell assay. Another experiment showed that the printer could be used to deposit cells in a multi-layer based pattern by adding more Matrigel™ to the receiving surface and re-printing.

Both techniques of laser printing have the ability to deposit cells at high speed with very good viability and can be automated with a CAD/CAM system. Cell viability concerns seem to have been remedied by the BioLP by the introduction of an energy absorption layer. As well, the problems found in ink-jet printing such as sterility, nozzle clogging, and cross contamination are not applicable to this 'non-contact' method of transferring material.

2.4.3 Acoustic Cell Printing

An acoustic method for printing cells is very similar to the laser printing method in that it uses focused energy to eject a cell from one surface to another. The difference in the acoustic case is that sound vibrations produce the energy necessary for transfer. An acoustic printing device has been developed and used to transfer nanoliter volumes between microplates for possible work on cell-based assays (Ellson *et al*., 2003). Other applications claimed by this technology in the patent literature include ejecting a single cell from a fluid onto a surface for patterning surfaces, creating arrays or simply for sorting cells (Mutz *et al*., 2002).

The acoustic cell transfer system consists of a moveable transducer located below a microplate that contains the solution to be transferred. The transducer can be positioned below a desired microwell on the plate and then a passed radio frequency energy that it in turn can convert to sound waves which can eject the target. Depending on the amount of energy, the frequency used, and the fluid properties of the solvent the system can be made to transfer specific drop volumes in the nanoliter range.

Since there have been no published results for cell viability or fidelity of cell patterning using this technique it is hard to evaluate it's effectiveness. It has the advantage of being automated with the use of CAD/CAM technology like other cell printing technologies. The transducer makes no contact with the transferred medium and therefore poses no contamination or pore-clogging problem as an ink-jet device would. A major challenge this technology faces is that it requires that the transferred media be in a range of specific viscosity and surface tension. Current work (Ellson *et al*., 2003) used DMSO at concentrations in the order of .1% to maintain fluidity for nanoliter droplet formation and ejection. Solvents like DMSO would not be desirable for studying cell-to-cell interactions or creating any kind of tissue construct as it breaks down adhesion and degrades cells. Another challenge for tissue engineering with this technology is that the receiving surface must be inverted above the microplate for biomass transfer. This limits the range of receiving cell array mediums that can be used and tissues deposited.

2.4.4 Rapid Prototype Cell Printing

A close cousin to the ink-jet cell printer, BioAssembly Tool™ (BAT), uses both pneumatic and positive displacement ejection needles to create three-dimensional tissue constructs (Smith *et al*., 2004). The BAT system brings cell printing up from microscopic to the macroscopic by being able to create large tissue constructs on the order of centimeters in length and height with 90 μm resolution. It has successfully been used to extrude human fibroblasts suspended in a polyoxyethylene /polyoxypropylene matrix with 60% cell viability. It has also successfully co-extruded bovine aortic endothelial cells with collagen type I onto a flat sheet with 46% to 86% cell viability depending on the size of needle used.

The BAT system is fully automated. It consists of a motorized x-y stage (5 mm travel) with four syringes, traversable in the z-direction (5 mm travel), made up of one positive displacement and three pneumatically operated. Each nozzle is supplied with a video camera, a fiber-optic light source, and individual electrical temperature controls. The stage itself is fitted with a water jacket for temperature control while the whole assembly is fully enclosed in a working chamber that is both thermostat, and humidity, controlled. The BAT also has the ability to extruded individual cells and has been shown to viably extruded co-cultures of cells and polymer matrix. Finally, since there is more than one syringe it can load multiple cell types to simultaneously create three-dimensional multicultural constructs.

Although BAT has overcome many issues such as the cell matrix getting too dry or too cold by monitoring and controlling temperature and humidity, it still suffers from many of the same issues as ink-jet cell printing. This includes nozzle clogging, possible cross contamination, and sterilization issues. The minimum internal diameter used for syringes was 90 μm which is about 2 - 10 cell widths wide in most applications. This means that cell-to-cell communication and adhesion is not repeatable and therefore limits the ability to create a structure *in vitro* that truly represents a structure *in-vivo*.

2.4.5 Optical Trapping

Optical trapping employs a laser to provide the pushing force necessary to trap and manipulate cells for many different applications. This technology relies on the difference of refractive properties between the cells and the surrounding medium that in turn allows the light to form a vector of force as it is absorbed, refracted, and transmitted through the cell material. Various techniques have evolved over the years but each one still relies on the same basic principals

mentioned above (Uchida *et al*., 1995). Optical trapping can be simply used to push cells in one direction called optical transport where the laser force only supplies a pushing force in the beam propagation direction. A single laser focused through a high numerical aperture lens can focus the beam at very high angles of incidence directed toward the center of the beam that can be used to grip the cell as an optical tweezer enabling selective movement in any direction transverse to the average beam path. Combination of the two above techniques results in a levitation trapping scheme where one laser is used to position the cell transversely, an optical tweezer, and a second beam to move the cell up and down, optical transport. More recent technologies such as holographic beam splitting and beam sharing can form a plurality of beamlets that can be patterned into many types of caging shapes to manipulate cells (Gruber *et al*., 2004).

The first biological application of optical trapping used a single laser as an 'optical tweezer' to hold and manipulate living viruses and bacteria (Ashkin *et al*., 1987). Focusing Gaussian laser light through a high NA objective lens of a microscope creates a gradient that points to the center of the beam thus creating a single beam trap. This experiment was able to trap and move a motile bacterium, 0.5 to 1.5 μm in length, with an argon (green) 514.5 nm laser at powers as low as 3 to 6 mW. It was found that the bacteria were optically damaged at powers in the range 10-20 mW within a half-minute. Obviously the laser is a two edged sword in that the larger the trapping power the greater the risk of harming the cell. The laser light used in this experiment was in the green spectrum, which is easily absorbed by the cell, and it would be better to use a wavelength with less absorptivity such as the near infrared.

Another experiment employing optical trapping used computer-generated holograms to move colloidal silica microspheres in an array of 400 independently controlled optical traps (Curtis *et al*., 2002). Holographic Optical Tweezers (HOT), as it is called, can employ a diffractive optical element or a real-time configurable special light modulator to break up the laser beam into many individually controlled traps that can be used to move particles in 3-D space. A benefit of using a HOT to move biological cells is that since there are many beams available to move a cell, their respective power can be much lower thus eliminating the hot spot problem caused by using a single high power beam (Gruber *et al*., 2004).

Many biological applications for optical trapping exist such as cell sorting, measuring mechanical properties of cells, cell purification, studying cell-cell interactions, cell arraying, and creating three-dimensional structures. A method for high-resolution sorting of sperm cells has been proposed using holographic optical traps to 'funnel' cells that are appropriately identified by a

fluorescence threshold (Gruber *et al*., 2004). The adhesion strength between cells has been studied using optical levitation and optical tweezers. In this experiment the cells were brought into contact by stabilizing one in the end of a micropipette while a second cell was attached to it using levitation and optical tweezing. They were allowed to bond for 30 seconds and then the cell held by the optical trap was 'pulled' away. The trapped cell eventually broke from the forces involved that were estimated to be as large as 30 pN (Uchida *et al*., 1995). Three-dimensional structures or layered patterns of cells are usually embedded in a medium such as Hydrogel™ or collagen to immobilize the cells, provide structure, possible chemical signals, and promote cell growth. By using a holograph optical trapping scheme it is proposed that gel based cell sorting can take place even after the gel structure is finalized (Gruber *et al*., 2004). Since HOT can move cells in three dimensions it is possible to extract cells that are in-gelled by melting of the gel by the optical traps that can expose exit pathways. Alternatively, the whole gel can be melted and the cells rearranged, held in place by optical traps and re-solidified.

BioRyx 200™, a commercial embodiment of the holographic optical trapping technology described above, has been developed and available for purchase by Arryx Inc. since 2002. It can create up to 200 simultaneous optical traps that are powerful enough to control up to 30 μm sized objects and can be independently maneuvered in all three dimensions. It employs a 2 Watt 532 nm diode-pumped solid-state laser.

One of the most recently published methods for maneuvering cells using optical trapping uses a diode laser bar to control a larger trapping zone (Applegate *et al*., 2004). The laser diode bar is unique in that it does not form a trap at a point or plurality of points, rather it can create a continuous line of action between 1 and 100 mm in length. It uses a laser diode bar at 980 nm in wavelength that is capable of producing 3 Watts of average power. The laser is directed through a low NA objective lens, then through an optional mask, reflected by a mirror and refocused through another low power objective before being focused at the target. The mask used in the experiment consisted of two razor blades that only allowed a sliver of the laser bar through to the focus, but could be translated back and forth as desired. This allowed for translation of a single trapped cell. The laser diode bar was able to trap a line of bovine red blood cells in a PDMS microfluidic channel with an unspecified flow gradient. This technology could be used to perform cell sorting in microfluidic chambers with a fraction of the energy required by other optical trapping methods. It also has the advantage of being relatively simple when compared to the computationally intensive holographic optical trapping technology.

Laser cell manipulation is fast becoming a viable method for maneuvering cells for many different biological applications. However, there are some challenges yet to be over come.

Most of the lasers used a wavelength in the range of 530 nm. The problem with this wavelength is that although it can place more force on biological cells it is also absorbed very well by them. Larger wavelengths, such as the laser diode bar at 980 nm, would not be as readily absorbed by cells which would improve cell viability after trapping. Another challenge facing laser-trapping technology is that it can only be employed on surfaces that are optically transparent and only within the small range of focal depth offered by the optical aperture. This limits the range of cell deposition possible for creating multidimensional structures. Most of the laser-trapping experiments have been conducted in a highly aqueous medium due to the large forces that would be needed to overcome the viscous friction to move a cell though a thicker medium.

2.4.6 Dielectrophoresis

Dielectrophoresis works on the fact that electric fields exist between a single charged electrode and its surroundings. A microelectrode tip can be made to repel or attract a biological cell by applying a charge with a specific frequency (Schnelle *et al*., 1999). This experiment used square wave signals in the range of 100 kHz to 40 MHz and 5 to 28 volts peak-to-peak to power a microelectrode just under 5 μm in diameter. By switching between the frequencies a single yeast cell was selectively captured and released by the attractive and repulsive potentials thus induced. The attractive field strength was shown to drop off rapidly as distance between the cells and the microelectrode was increased. This is beneficial in that it allows for single cell manipulation in larger cell population solutions.

Single electrode dielectrophoresis can cause damage to the biological cells membrane if too much voltage is applied. The long-term effects on cell viability with dielectrophoretic manipulation need to be studied. Experiments must be made to characterize the amount of voltage needed to move a particle through a thicker medium or a medium with a velocity gradient.

2.4.7 Photopatterning

A method for creating Hydrogel™ microstructures with living cells using photopatterning has been demonstrated (Liu *et al*., 2002). This tissue engineering technology can be used to form complex three-dimensional tissues structures with one or more different cell types.

Photopatterning uses a polyethylene glycol (PEG) based Hydrogel™ to encapsulate the biological cells into a scaffold that is in turn crosslinked using UV light. A pre-treated glass slide, to allow bonding at the surface, was flattened against a Teflon™ base and sealed. A pre-polymer solution containing PEG diacrylate, HEPES buffer solution, and a photoinitiator was combined with human hepatoma HepG2 cells and injected through channels in the Teflon to fill up the free space between the glass and the base. A photo mask was printed using a high-resolution line printer and placed upon the glass surface. A 10 mW/cm^2 UV light at a wavelength of 365 nm was used to initiate cross-linking in the pre-polymer solution. After solidification the glass slide was removed from the Teflon mould and washed with HEPES buffered saline solution that removed the uncross-linked pre-polymer leaving behind the cell biopolymer pattern. This process was repeated to create intricate three-dimensional structures such as fibrous micro weaves.

The impact of photopatterning on cell viability was reported as not significant. UV light has the potential to cause cell damage by introducing free radicals, however it was reported that the biopolymer acted as a free radical sink. The results of the photopatterning showed that there is a lower limit to how small the features created could be. It was shown that features sizes less than 200 μm resulted in larger features, up to 200% at 50 μm, than the intended size.

2.4.8 Microfluidic Cell Patterning

Microfluidic cell patterning is the novel combination of fluid dynamics in microchannels and cell patterning by deposition of biopolymers and cells. A microfluidic chamber or stamp, as it is called, is a three level structure composed of two layers of transparent elastomer, polydimethylsiloxane (PDMS), sandwiched together. The top layer contains the channels that are needed to cross over the structure, the bottom layer contains the channels need to cross under the structure, and the union of the two PDMS layers provides the upper and lower halves of the complete structure. A method for the fabrication of microfluidic stamps that contain three-dimensional channels has been described in literature (Anderson *et al*., 2000). The biological applications for microfluidic cell patterning can include creating cell and protein arrays for biosensors and drug screening or for creating tissue constructs (Chiu *et al*., 2000). This requires that cells in a biopolymer matrix must be deposited into structured arrays via the microchannels by fluid gradients imposed at the entrance and exit channels. The deposition of cells using three-dimensional microfluidics was successfully demonstrated using bovine capillary endothelial (BCE) and human bladder cancer (ECV) cells (Chui *et al*., 2002). Two cell structures were

created: a series of concentric squares and a checkerboard pattern with tiny capillaries linking them together. This provided a proof of concept that more complex structures could be created using these techniques.

In another study, three types of cells were successfully layered into a heterogeneous tissue using a three-dimensional microfluidic system (Tan *et al*., 2004). Layering cells one after another is possible in microfluidic stamps because of contraction of the biopolymer matrix caused by cells themselves. The process of contraction is controlled by three factors: cell type, cell concentration, and time. In this case, the goal was to create a three layer arterial type tissue composed of human lung fibroblasts, umbilical vein smooth muscle, and umbilical vein endothelial cells. The final 3-D structure produced by the experiment was characterized as being well organized. Although it maintained the distinct layer pattern, there was still significant cell migration between the layers that must be overcome if this type of tissue is to make it into clinical trial.

The microfluidics approach to cell patterning, although very good at actually patterning tissue structures, will have to overcome challenges to be a commercially viable tissue-engineering tool. Using fluid gradients or capillary action to transfer cells will not guarantee repeatability of results. The flow of cells cannot be easily controlled on a cell-by-cell basis but rather are seeded *en masse* with a probability that one will attach to the surface at a given site. This will limit the efficiency of single cell work such as the study of single stems cell fates in microwells where many wells were constructed and only a fraction of them were populated, by chance, with a single cell (Chin *et al*., 2004).

Chapter 3
Problem Statement and Objectives

3.1 Problem Statement

In regenerative medicine it has become of great importance to understand the underlying mechanisms of behavior and function of cells within the human body. There is a need to relate the physiological characteristics of cells with time and function through visual reporters such as fluorescent markers. To do this, cells must be isolated and observed in culture while responding to different conditions in order for us to understand how cells change with respect to their environment. Previous studies have been limited by the lack of automated tools to culture and observe these live cell interactions over long time periods until recently. With the great advance in computer data storage capacity and digital camera technology in the past few years' researchers are now able to take the next step forward in long-term live cell research. In this study, a fully automated microscopy system has been developed for the PC to facilitate long-term live cell imaging.

The system, entitled the Bio-Assembly, Mosaic Builder, and Informatics system (BAMBI), will combine the process of laying down cell types in media, capturing the events taking place, image content visualization, and data export for the purpose of data mining and informatics. Throughout its development BAMBI will continually be used by researchers for different applications within regenerative medicine. These applications will provide the crucial inputs and feedback on the BAMBI design allowing it to grow and respond to specific needs. BAMBI can be thought of as a true work-in-progress that will continue to evolve beyond the specifications presented in this thesis.

3.2 Objectives

The design criteria for BAMBI has been divided into two sections: Primary and secondary objectives. The primary objectives are considered to be hard goals that must be met by the system. Some of these goals were present at the beginning of this work, and some were additional requirements that were added during development to support the various experiments in the lab. The secondary objectives are meant to serve as guiding principles for the overall system design.

3.2.1 Primary Objectives

3.2.1.1 Automated capture of multiple fields-of-view through time

Previous work (Ramunas *et al*., 2007) has outlined the need for more than one field-of-view to be taken during a single time course experiment. Being able to observe a low probability event requires that one have many events to observe. The benefit of capturing a very large array of fields is that one can go back to the beginning of the time course, zoom-in, and play these events forward again while observing them in greater detail. The increase in the amount of data captured allows more statistically rigorous observations with a higher probability of capturing the events of interest.

3.2.1.2 Capture of three-dimensional fields-of-view through time

The capture of a three-dimensional image can be achieved by taking images of multiple optical sections through the z-axis of the specimen. In previous work (Moogk *et al*., 2007), it was shown that a 3-D time course was necessary to identify the key cell dynamics within a human islet of Langerhans. A 3-D time-course can provide a wealth of information about cell-cell interactions in three-dimensional cell aggregates.

3.2.1.3 Automated capture using multiple fluorescent light sources

With the introduction of fluorescent labeling techniques in the past decade it has become necessary to provide an imaging system that can operate in the fluorescent domain. Allowing for multiple fluorescent channels enables different markers to be excited and recorded during the same live cell experiment.

3.2.1.4 Robotic handling of cells for pick-and-place operation

The ability to capture and release individual cells allows research to be conducted on a single cell level. Previous work (Ramunas *et al*., 2007) used BAMBI to recover individual cells subsequent re-implantation in live mice to ascertain the pluripotency or "stem cell like" qualities of the cell. As much of the operation of pick-and-place operations should be performed by the robotic interface so that it might be automated in the future.

3.2.1.5 Automated robotic micromachining of multi-well arrays

The ability to manufacture microwell arrays enables many simultaneous experiments to be conducted at the same time under the same conditions. The automation of the machining process alleviates the user from the tedious repetition of hundreds of commands.

3.2.1.6 System is robust against failures

The software should be implemented such that failures or system crashes are handled gracefully. There should be precautions in the software or hardware to avoid potentially damaging or creating hazardous conditions. When in automatic mode, the user may not be aware a crash has occurred. Therefore, in the event of a failure, care must be taken to insure motors should not be left in a runaway state or other devices like lights are left "on". Consideration will be given to BAMBI as it is intended to be run on Microsoft's Windows XP™. Windows XP is not a true real-time operating system and therefore there is no way to absolutely guarantee that the software can always react to failures when they occur. The way around this is to provide an additional layer of hardware support for failure conditions. An example would be the addition of a failsafe timer on the heater or light circuits that would deactivate the device if left "on" too long.

3.2.2 Secondary Objectives

3.2.2.1 Software is easy to navigate and use

The software should retain a standard Microsoft Windows XP application look-and-feel. This would include maintaining a similar menu layout to well known programs such as Adobe Photoshop™ and Microsoft Word™. The software should include a help menu to assist the novice user in any part of the application.

3.2.2.2 Software allows modifications to be made during a live experiment

The ability to react to changing conditions or make adjustments to the way in which data is being collected after the experiment has already been started is a key feature of BAMBI. Almost all of the high content screening systems available commercially lack this seemingly simple yet very important functionality. Having lost potential data due the inability to alter an experiment mid-run can be expensive ethically, in the case of sacrificial donor cells, and financially due to time lost and reagents used.

3.2.2.3 Software stores all data in a format easily exchanged with other programs

Given that BAMBI serves as the front end for a wide range of data mining applications, any output data should be in a format that can be easily opened by the receiving application. Any relevant textual data should be stored in a well-known or accepted format that could be opened directly by any spreadsheet program such as Microsoft Excel™, IBM Lotus 1-2-3™, and Borland Quattro Pro™.

3.2.2.4 Software is easy to upgrade and modify

The field of cell biology is a dynamic environment where new markers and techniques are continuously being developed and tested. The researcher should be able to add new routines and capabilities to BAMBI with as little effort as possible. This should include the use of good coding methods such as object-orientated programming and modular or encapsulated design. The final code submitted should be fully documented and, ideally, available in html document format.

3.2.2.5 Software will provide the user with a real-time display during all operations

During data capture, robotic micro machining, or pick-and-place operation BAMBI should provide the user with "real-time" feedback. This could include helpful diagrams, heads up display of the current motor status, and display of the currently captured image. If an experimental run is active, it should provide information about where the system is in relation to the experiment as a whole, how long it has been running, and a forecast of the time left. User interface elements should be responsive to the user, even under heavy computational stress conditions. This could include the use of multiple threads, efficient message handling, and multiple interrupts.

3.3 Architecture of BAMBI

BAMBI can be represented as many functions, each one devoted to a specific task, and all of them linked together in a mutual communication network. Figure 4 provides an overview of these functions and how they relay information to each other.

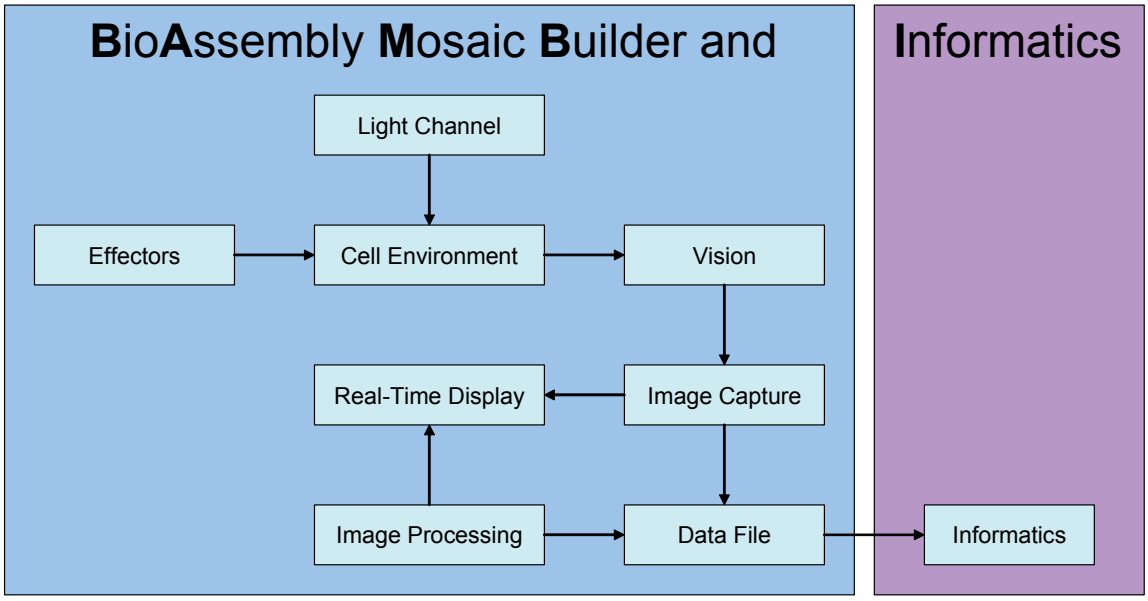

Figure 4: BAMBI Overview

This figure shows the breakdown of the BAMBI acronym and its main functions. *BAMB* represents the functions that are required for "real–time" data collection and *I* represents the functions that can be performed post-collection.

Here BAMBI is divided into two parts: The *Bio-Assembly Mosaic Builder* as one and *Informatics* the other. The first part encapsulates all the "on-line" functions that must take place during an actual experiment run. Where as the second part, informatics, is traditionally an "off-line" function that can be done anytime after the experiment has taken place. The first section forms the scope of this thesis work while the Informatics section has been left to others to develop in parallel. However, rather than break BAMBI up into *BAMB* and *I*, all references made to BAMBI from this point forward will refer to work done for this thesis unless otherwise noted.

The figure shows the many functions BAMBI must provide to facilitate long-term live cell imaging. The cell environment box represents the state of all the dependant conditions that are needed to support the cell(s) including the dish, reaction chamber, or slide containing the sample. This includes the cell(s) media, temperature, CO_2 concentration, and humidity. The effectors box represents all the ways we can control the variables in the cell environment. This includes any robotic end effecter or manipulator used for cell pick-and-place operations, CO_2 levels, and humidity and temperature regulation. The light channel box represents any type of light source that can be used to image and contrast or excite fluorescence in cells. This would include the control of the shutter as well as light box. This is really a subset of the effector box, but is shown

separately for clarity of purpose. The vision box represents the process of imaging the field-of-view by the CCD camera. The image capture box shows that there must be a way to control the digital camera and grab the frames acquired for further display or processing. The image-processing box represents the tasks that can be performed on the captured data. This could include feature tracking, autofocus, and image contrast and enhancement for live viewing. The real-time display box represents the graphical user interface for the program. It provides a heads up display of the current image data gathered from the image capture process during a live experiment. Ultimately the final result, a data set and associated image set must be stored in a format that can later be retrieved. This is the job of the data file box. It provides all the functions necessary to collect this data and make it available to the image processing box as well as any other program that may be required.

The large bounding box encompassing all the functions in *BAMB* from Figure 4 represents the overall software package. Each piece of hardware usually has its own set of drivers and software required to control it. The purpose of this software is to make the individual pieces work in harmony and communicate effectively with each other. Each function in *BAMB* shown in Figure 4 is further broken down and described in complete detail in the subsequent chapters: Chapter 4, *Hardware Design and Implementation*, and Chapter 5, *Software Design and Implementation.*

Chapter 4
Hardware Evolution and Implementation

4.1 Hardware Components

The BAMBI hardware components can be divided into seven general categories as shown in Figure 5 below.

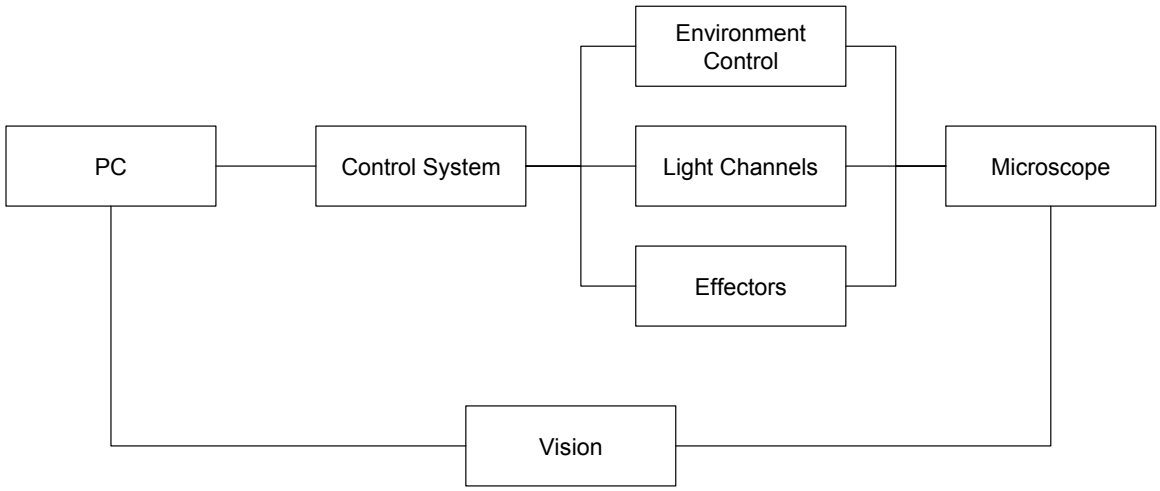

Figure 5: BAMBI Hardware Control Pathway

This figure illustrates the control pathway for the hardware components used in the BAMBI system. The personal computer (PC) runs the software for the control system and is used to communicate with all the devices as well as the vision system.

The personal computer (PC) houses the servo controller cards and feedback devices as well as running the software that orchestrates the communication between all components. The software program is represented by the control system and is responsible for control of the environmental settings, microscope illumination, end effectors, and the vision system. The environment control box represents the temperature, CO_2, and humidity regulation. The light channel represents the electromechanical shutter for the broad-spectrum lamp and the electronic operation of the array of fluorescent light channels. The microscope and vision boxes represent the inverted microscope on which all experiments are performed and the CCD camera attached to it.

4.2 Microscopes

Three microscopes have been modified to work with the various configurations of BAMBI. Each is an Axiovert 200 inverted microscope manufactured by Carl Zeiss, Germany. All microscopes have the same features and specifications respectively and are herein referred to as M1, M2, and M3. Most of the BAMBI 4-axis prototype work was conducted on M3, with the final 8-axis design implemented on M1 and M2. Each microscope was fitted with a 5x, 10x, 20x, and 40x objective. The optical specifications, including working distance and NA of the objectives are summarized in Table 4.

Table 4: BAMBI Microscope Objectives – Specifications

Magnification	Numerical Aperture	Working Distance	Field of View	Correction	Contrast Method
5x	0.12	9.9mm	23mm	A-Plan	Phase 0
10x	0.30	5.5mm	25mm	Plan-neofluar	Phase 1
20x	0.50	2.0mm	25mm	Plan-neofluar	DIC
40x	0.75	0.5mm	25mm	Plan-neofluar	DIC

4.2.1 Optimizing CCD Sensitivity

A big concern for long-term live cell imaging is avoiding cell damage from illumination sources. As light can cause genetic mutations, cell death, and other unwanted reactions, it is always best to limit light exposure to minimum amount necessary to achieve the goals of the experiment. In the case for fluorescence studies, overexposure of the exciting wavelength can cause bleaching of the fluorophores that can invalidate the consistency of the results for long term comparative studies. The amount of energy needed by each of the CCD elements to register a non-zero value sets the bar for the minimum amount of light needed to capture an image. A balance must be made between the amount of light needed by the CCD camera to generate an acceptable image and the health of the cells. Given that overall magnification, NA of the lens, and camera binning effect the amount of light that reaches the CCD elements, there are choices that can be made to make such experiments feasible (see Table 5).

Table 5: CCD Relative Light Sensitivity Chart

Rank	Objective	NA	Camera Adapter	Camera Binning	Relative Sensitivity
1	40	0.75	0.5	2x2	1.00
2	20	0.5	0.5	2x2	0.79
3	10	0.3	0.5	2x2	0.41
4	40	0.75	0.5	1x1	0.25
5	40	0.75	1	2x2	0.25
6	20	0.5	0.5	1x1	0.20
7	20	0.5	1	2x2	0.20
8	10	0.3	0.5	1x1	0.10
9	10	0.3	1	2x2	0.10
10	40	0.75	1	1x1	0.06
11	20	0.5	1	1x1	0.05
12	5	0.12	0.5	2x2	0.04
13	10	0.3	1	1x1	0.03
14	5	0.12	0.5	1x1	0.01
15	5	0.12	1	2x2	0.01
16	5	0.12	1	1x1	0.00

Table 5 ranks the relative sensitivity of various combinations of optical elements and camera binning modes. The camera binning mode is a hardware controlled feature supported by most microscope rated CCD cameras that allows the energy received by a group of pixels to be summed to a single value. By increasing camera binning from 1x1 to 2x2, the CCD sensitivity is increased by a factor of 4, and noise is reduced. The downside is that the resolution of the image is reduced by the same amount. The numerical aperture (NA) of the objective lens plays the most important role in increasing sensitivity as the intensity is proportional to $(NA)^4$. The combined magnification of the objective and the camera adapter affect both the size of the field-of-view and the light intensity. Here, the light intensity is proportional to the overall $(magnification)^2$. The end result becomes a choice between the size of the field-of-view, the camera resolution, background noise, and exposure levels tolerated by the cells.

4.3 Environmental Control

Each microscope was provided with an environmental control system to enable long-term live cell imaging. The environmental control system regulates temperature, CO_2, and humidity. To accomplish this, a large insulated box with various panels for experimenter access was constructed and placed around the microscope. A gas line, attached to a 3000 psi CO_2 tank with

a regulator, is fed into the box. Temperature is maintained with a conventional hand-held hair dryer with feedback control provided by a digital temperature gage. The hair dryer is mounted inside the box and the temperature gage is mounted to the microscope stage. M3 was fitted in one environment box, while M1 and M2 shared a larger environment box. The M1and M2 setup allows for a control setup to be conducted in parallel under the same conditions on each microscope. M3 is also fitted with a laminar HEPA filter flow hood inside the environment box to maintain a sterile environment for open culture experiments on the microscope stage. This system maintains horizontal laminar flow of filtered air through the entire work area of the enclosure thus maintaining sterility. This allows M3 to be used for cell pick-and-place operations without contamination of the cell culture. M1 and M2 can only be used in a "closed" chamber configuration.

4.3.1 Environment Box

The environment box is crafted from panels of 1 inch thick aluminum foil faced foam sheathing. The sheathing has a thermal resistance R-value rating of 6.5 that is common for most home sealing applications. The sheathing is cut into square panels and fastened together into a box with aluminum angle brackets for support. All the connections and exposed edges are sealed with aluminum foil tape.

4.3.2 Temperature Regulation

A simple hair dryer and temperature sensor are used to control the temperature inside the environment box. The resulting inside temperature can be maintained between 36 and 37º as is needed for live cell experiments. The heat is supplied by a commercially available 1600 Watt hair dryer manufactured by Revlon Corporation operating from a standard 125V 60Hz power supply. Heater control is managed with solid-state relay connected to a standard wall outlet for power, and a PC computer for the control signal. The heater is controlled "shot gun" style, either "on" or "off", depending on the logic state of the 5-volt control signal with "on" corresponding to 5 volts and "off" corresponding to 0 volts. A USB analog and digital input/output device by Labjack ™ Corporation (CO, USA) installed in the host PC sends the signals directly to the relay via software command. The heat sensor is an EI1022 temperature probe from Electronic Innovations Corp. (CO, USA). The analog output from heat sensor is connected to the analog to digital converter on the Labjack device. This signal is then used as feedback by the software program to regulate the temperature. Once the heat sensor is calibrated by comparing it's readout

with an actual calibrated thermometer that is placed beside it inside the environment box it can be used to maintain a temperature within +/-1º from target.

4.3.3 Cell Culture Environment Chamber

The cell culture environment chamber design allows for CO_2 and humidification controls for long-term live cell imaging. Temperature is maintained by the microscope environment box as described previously. A three-dimensional cutaway of the complete chamber resting on the BAMBI end effector is shown in Figure 6.

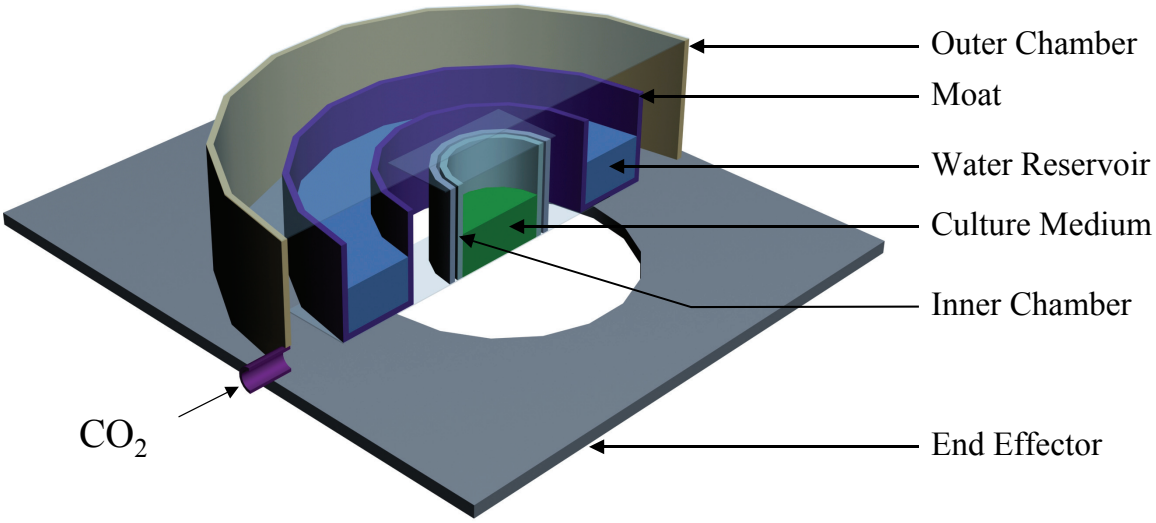

Figure 6: Cell Culture Environment Chamber

Three-dimensional cutaway of the cell culture environment chamber, as it would appear when laying on top the BAMBI 3-axis end effector.

The cell culture environment chamber features a low profile and three mutually parallel thin glass sections for optimal DIC imaging. The glass slides are micro cover slips with a thickness range between 0.14 and 0.17 micrometers. All slides are kept in parallel configuration to avoid light aberrations. The total height of the environment chamber is 20 mm - 25 mm depending on the application. For DIC experiments, the height of the chamber is a critical factor, and must be no more than 25 mm to allow room for the condenser to focus through specimens attached to the bottom of the inner chamber.

The line out from the CO_2 flask is fed directly into the outer chamber inlet as shown in the bottom left of Figure 8. The flow of the CO_2 is deflected by the wall of the moat upon entry to

chamber that prevents concentrated flow into the inner chamber. Humidity is provided by natural evaporation of the nano-pure water contained in the moat that encompasses the inner chamber. The outer chamber may be lifted off at anytime to provide access to the inner cell culture chamber or to refill the moat. Sterility is maintained by the coverlid of the inner chamber. Gas exchange with the culture medium occurs through passive diffusion between the contact of the inner lid and the inner cell culture chamber.

4.3.4 CO_2 Regulation

The CO_2 gas is provided from a 4500 psi rated steel tank with a two-stage regulator. The first stage regulates the gas pressure between 0 to 4000 psi and the second stage regulates the pressure between 0 and 30 psi. A final pressure of approximately 1 psi is used for CO_2 perfusion during live cell time courses. A 5 mm diameter hose is connected to the secondary stage and stepped down to 2 mm before connection to a 0.2 μm filter. The purpose of the filter is to remove any possible bio-active contaminants. A second 2 mm diameter hose is run from the filter to a sealed flask half filled with nano-pure water. The outlet of the hose inside the flask is such that it lies at the bottom of the flask and is completely submerged by the water. The CO_2 gas is then allowed to bubble up through the water. This effectively humidifies the normally dry CO_2 gas before entry into the cell culture environment chamber. A 2 mm diameter outlet hose channels the humidified CO_2 from the flask to the environment chamber. All hose lines including the flask are sterilized (autoclaved) before they can be used for a live cell experiments. In the case of M1 and M2 they share the same CO_2 line and therefore a splitter is attached to the outlet hose on the flask. Each subsequent line to the M1 and M2 cell culture environment chambers has a rotameter to ensure that each chamber gets the same CO_2 flow rate.

4.4 BAMBI End Effectors

The end effectors used in BAMBI are a 3-axis stage and a single axis micropipette. The 3-axis stage provides the motion for all three directions in space (x, y, z) and the micropipette is allowed to translate up or down for an "injection" like motion. Together these two end effectors allow for automated panning of the cell culture, focus control, and pick-and-place operations.

4.4.1 Three Axis Stage

A 3-axis Cartesian robotic stage is used to mount and move a sample through the microscope's focal point. A drawing of the complete three axis robotic stage is shown in Figure 7. The stage is made up of three linear actuators that are mated to each others moving surface to form the x, y, and z perpendicular motions of a traditional Cartesian robot. The y-axis is attached directly to the moving part of x-axis and the z-axis is attached to the moving part of y-axis with a 90-degree mounting bracket. A custom designed cell culture mounting plate is attached to the z-axis linear actuator to hold the live sample. Full drawings of the cell culture plate are provided in Appendix A. 4-5.

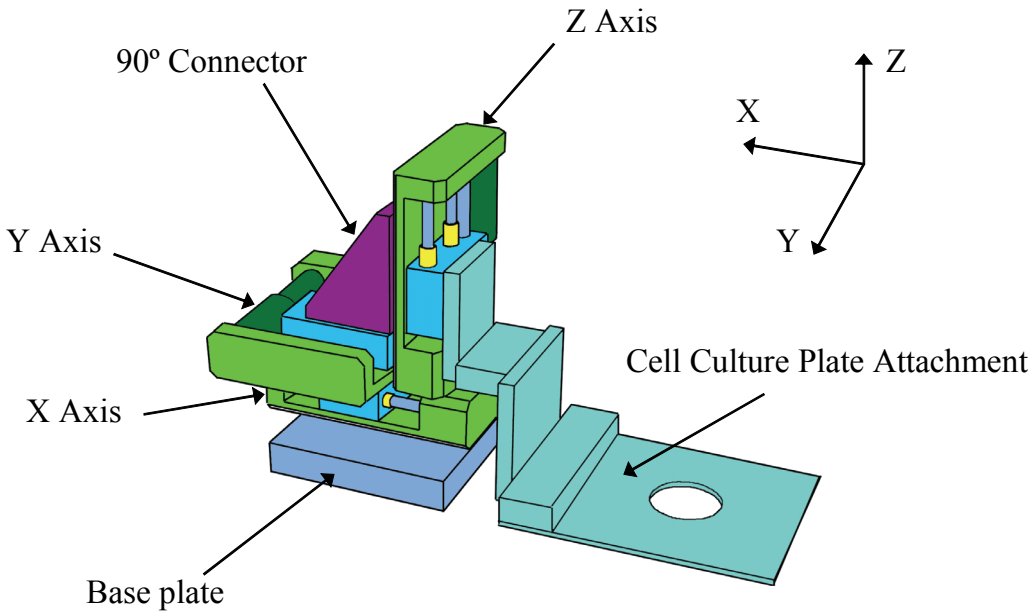

Figure 7: BAMBI Three Axis Stage

A drawing of the three axis stage with an attached cell culture holder. The coordinate axes in the top right indicate the directions of positive motion for the linear actuators. All three actuators are mutually attached. Y is attached to X and Z is attached to Y via a 90-degree connector. X is directly attached to the base plate that is in turn attached directly to the microscope platform.

The three actuators are Ultra-High-Resolution Micro-Translation Stages manufactured by Physik Instrumente (PI), Germany. The actuator's encoders have a design resolution of 0.007 µm and a 25 mm travel range giving a total working space of 25 cm^3. They can achieve a minimal incremental motion of 50 nm and move at speeds up to 1.5 mm/sec. A small DC motor with a Backlash compensated leadscrew powers each actuator. The unidirectional backlash is limited to 2 µm for each axis. However, there is some interplay between all three axes that is evident when

any one axis is changing directions. Additional side lash also occurs due to the free play and frictional effects of the two bearing rods, shown in yellow in Figure 7, within a single actuator. The mounting plate for the cell culture is attached to the z actuator stage and is made out of aluminum for reduced weight. The coordinate origin used for the robot is arbitrarily located but could be located anywhere since movement is assumed to be completely translational.

4.4.2 The Single Axis Micropipette

A micropipette is used to perform single cell pick-and-place operations for live cell experiments. A long glass needle with a very small diameter called a micropipette is attached to the moving surface of a linear actuator. The linear actuator is mounted to the microscope stage via a modified manual controlled x-y stage panner. The linear actuator can be positioned at any angle between 0 and 90º relative to the microscope stage. The long axis of the micropipette is in parallel with the direction of translation to create an injection type motion.

The linear actuator has the same design and manufacture as the aforementioned Ultra-High-Resolution Micro-Translation Stages by Physik Instrumente. The micropipette is made from a thin tube of glass with one end drawn out to tiny tapered opening and a plastic tube attached to the other. The micropipette tip is only about 3-5 micrometers in inner diameter when used to grip cells in culture and 15-30 μm when used to draw cells inside. The tube is filled with media and is attached to a manually controlled syringe that can move very small to large volumes via a fine and course adjustment thumbscrew. The actual pressure inside the tube is sensed with a digital pressure transducer to give the operator feedback on the amount of force necessary to keep the cell attached or inside the micropipette. As it is difficult to tell from direct viewing which direction the current pressure gradient is, the digital display is very helpful in this regard.

4.5 Light Channels

An electromechanical shutter and a LED illumination panel control the illumination for long-term live cell experiments. For broad spectrum "white" illumination a shutter is used to swing in and out of the light path as necessary. For fluorescent illumination an array of LED's are selectively turned on and channeled into the back port of the microscope.

4.5.1 Light Shutter

The light shutter is an electromechanical shutter used to block light from the tungsten-halogen lamp (HAL) on the Axiovert 200 microscope. This is illustrated in Figure 8 where the shutter is shown between the light source and the condenser of the microscope. The light facing side of the shutter is coated with a thin layer of aluminum to effectively block both the heat and light from the source. The arm is swung into or out of the light path via a voice coil actuator held in opposition with a spring. The spring is used to return the swing arm back to position once the voice coil's signal is disabled. The system is controlled by a simple 5-volt on/off signal provided by a computer. . The shutter is actuated by a voice coil and spring.

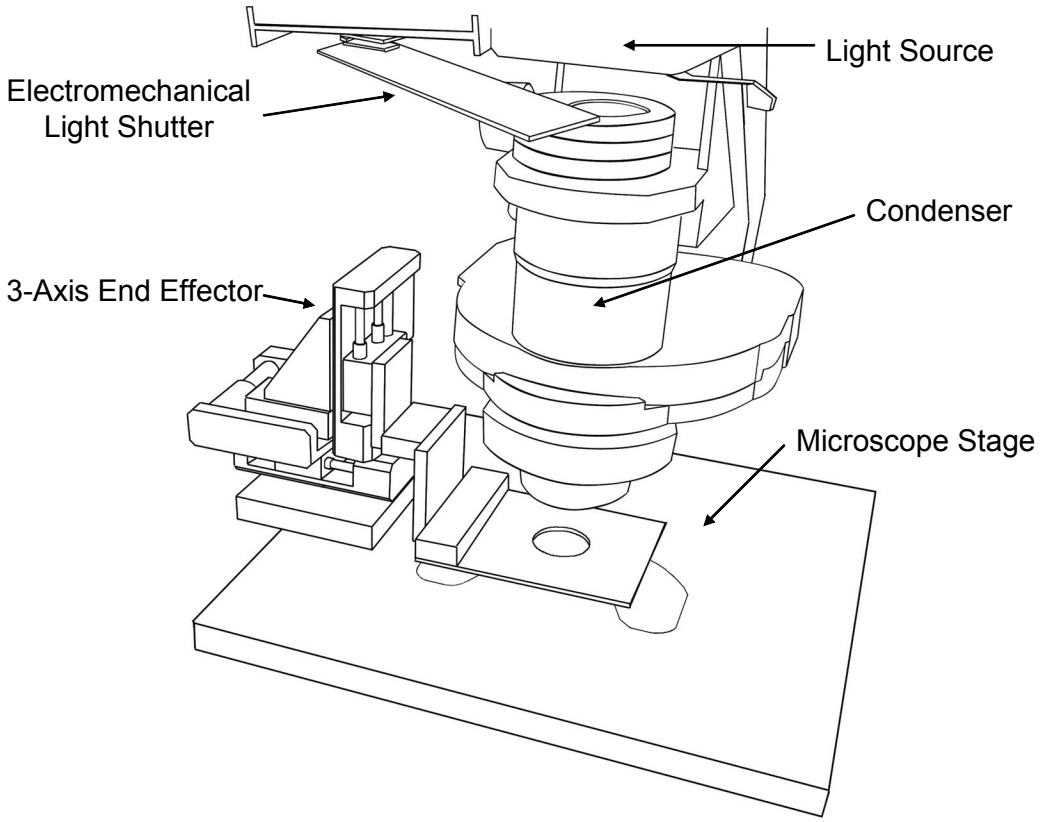

Figure 8: Electromechanical Light Shutter

The broad spectrum light shutter is shown between the light source and condenser of the Zeiss Axiovert 200 microscope. The shutter is shown in the open position, allowing light to pass through the condenser and into the sample.

4.5.2 The LED Array

The LED Array is a computer controlled light panel that can deliver amplified light at a specific peak wavelength to the microscope for use in fluorescent imaging. The LED Array system is essentially a box with five fiber optic exit ports, each with its own filter holder and LED light source. Each light can be turned on or off by software control. A 15-pin ribbon (only 5 plus 1 ground are used) connects the BAMBI 8-axis Control Module to control the LED channels. A special fiber optic five-to-one adapter conjoins the five ports into a single fiber. The resulting fiber optic line is routed to the back of the Axiovert 200 microscope. The complete connection diagram is shown in Figure 9.

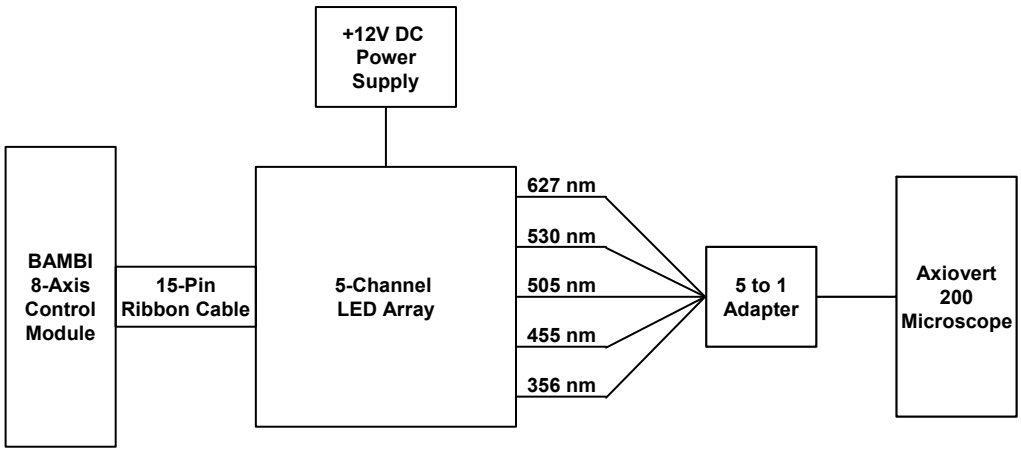

Figure 9: 5-Channel LED Array Connection Diagram

This is the connection diagram for the 5-channel LED light array. Power is supplied to the box via a single 12v DC power supply to drive the five LEDs. Each LED output is routed via 100-micron diameter fiber optic cable to a custom built 5 to 1 adapter. The resulting 100-micron diameter fiber optic cable is then attached to the back port of the Zeiss Axiovert 200 microscope.

One problem with using a fiber-optic light source arises when more than one LED is spliced into the fiber. For example, a tri-color fiber optic channel would require that only 1/3 of the light energy from each source be allowed to enter the channel. 1/3 of the maximum illumination potential may result in low excitation levels and thus low emission levels. Thus camera sensitivity becomes a critical factor as the signal to noise ratio will drop by 2/3 per channel.

4.6 Control System

The control system for BAMBI has gone through several major revisions and many incremental improvements as the experimental studies progressed. The original BAMBI consisted of a 3-axis stage and 4-axis ISA legacy controller card manufactured by Physik Instrumente, Germany. Problems with migration from Windows 95 to Windows NT led to the purchase and implementation of a completely new system. The new system consisted of a 4-axis PCI controller card supplied by Galil, USA and a new 3-axis modular stage from Physik Instrumente, Germany. This is the current system on M3. The need for dual microscope control for M1 and M2 led to the development of an 8-axis system. This consisted of a single 8-axis PCI controller card connected to two 3-axis stages, one for each microscope. Each of the new controller configurations, 4 and 8-axis, in addition to the legacy 4-axis system will be discussed in the following sections.

4.6.1 4-Axis Legacy Control

The original BAMBI setup consisted of a C-812 4-axis ISA controller that communicated with the PC via the IBM ISA bus. Four transistors provided the current for each DC motor in an H-bridge arrangement from the controller card itself. Communication with the card was possible by using a handshaking protocol that included writing to two different addresses and reading from one. This card was designed and built in 1991 to run under Microsoft DOS and Windows 3.1. Additionally, it could also operate under Windows 95, 98, and 2000 as they allowed full access to these access read/write memory locations. However, it could not operate under the more recent Microsoft operating systems such as Windows NT and Windows XP since they blocked access to these memory locations for security reasons. At the time BAMBI was in development, the University of Waterloo Chemical Engineering Computer Services had banned the use of all Microsoft operating systems released before Windows NT or XP from the Campus Network due to inherent security risks in the older software. The manufacturer considered the controller card a "dead product" (Legacy) and therefore there was no driver available for Windows NT or XP. This required that a new driver be written to access the protected memory on the C-812 for use in Windows NT and XP.

This driver was completed during my undergrad co-op term in 2003 at the University of Waterloo. The resulting driver is distributed under GNU public license and is made available in the accompany software CD for this thesis. The performance of the driver, however, was

hindered by the fact that there was a faulty read address on the controller card. The effect this might have on the movement commands for the axes either reduced or increased the target value by one digit or in other words an order of magnitude. Although it happened rarely, its effects would be devastating for the running experiment. As a result, this system was scrapped and completely replaced with a fully supported and modern 4-axis controller system.

4.6.2 4-Axis Control

A 4-axis control system employing a 4-axis controller card and custom 4-axis driver was implemented on M3 to drive the 3-axis stage and 1-axis micromanipulator described above. A diagram showing the overall servo loop is presented in Figure 10.

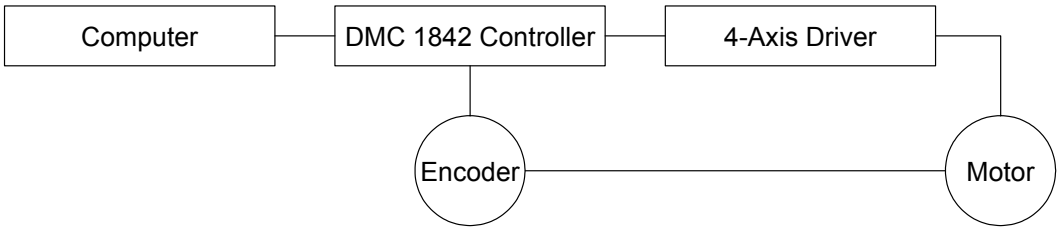

Figure 10: 4-Axis DC Servo Loop

This diagram shows the servo loop for the 4-axis DMC 1842 controller showing the basic elements including the computer, controller, amplifier or driver, motor and feedback encoder.

A PCI "Econo" series 4-axis controller card manufactured by Galil Motion Control, Inc. (CO, USA) is used to control the 4 axes. The "Econo" series controller does not supply power directly to the DC motors as the C-182 does and therefore required additional hardware (4-Axis Driver) to drive the motors. The controller can supply either a pulse width modulated (PWM) or a +/- 10-volt analog (16 bit DAC) command signal for normal DC motor operation. The card features 8 uncommitted digital outputs and 8 uncommitted TTL (0-5 volt) inputs. The bi-directional FIFO (first in first out) buffer on the controller card provides communication on the PCI bus. A Galil ICM-2900 Interconnect Module is used to breakout the analog and digital signals to and from the card. A more complete picture is presented in Figure 11 showing the wire connections for the complete control system for one axis.

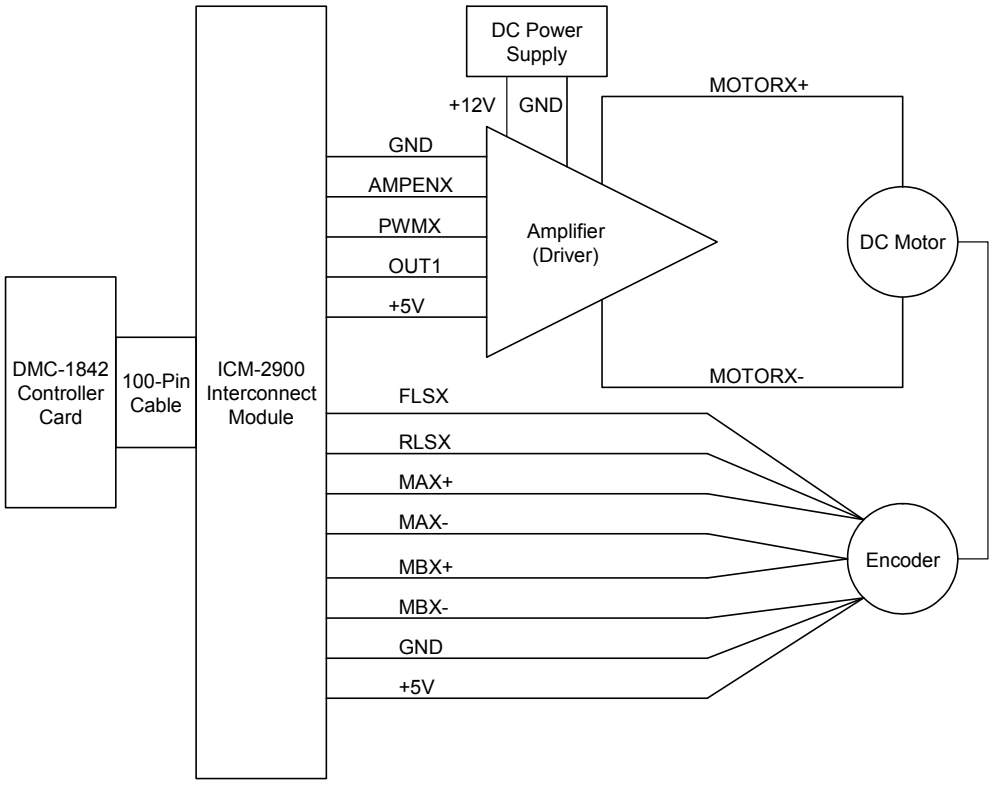

Figure 11: 4-Axis Interconnect Diagram

The complete wire connection pathway for the x-axis servomotor is shown in this diagram. The remaining 3 axes are connected in exactly the same manner. The link between the DC motor and the encoder represents the physical connection within a single encased assembly. FLS: Forward limit switch. RLS: Reverse limit switch. MA: Motor A channel quadrature. MB: Motor B channel quadrature. OUT: Digital output. GND: Ground or reference voltage. PWM: Pulse width modulation. AMPEN: Amplifier enable signal.

4.6.3 4-Axis Driver Module

A custom built 4-axis driver was designed and implemented to supply the power, drive the motors, and manage the wire hookups between the 100-pin cable and the motors. This includes the ICM-2900 interconnect module, amplifier (Driver) and DC Power supply shown in Figure 11. The driver utilizes the PWM signal provided by the controller card to create the DC voltage for the motors. The PWM signal is a steady stream of pulses at a constant period with varying pulse width or duty cycle. Figure 12 shows the effect of various pulse widths on the DC motor. If the duty cycle of the PWM is 50% the effective voltage being passed through the motor is zero and the motor speed is also zero. If the duty cycle is 0% the motor experiences the negative full

source voltage and the motor will drive at full reverse velocity. If the duty cycle is 100% the motor experiences the positive full source voltage and the motor drives at full forward velocity.

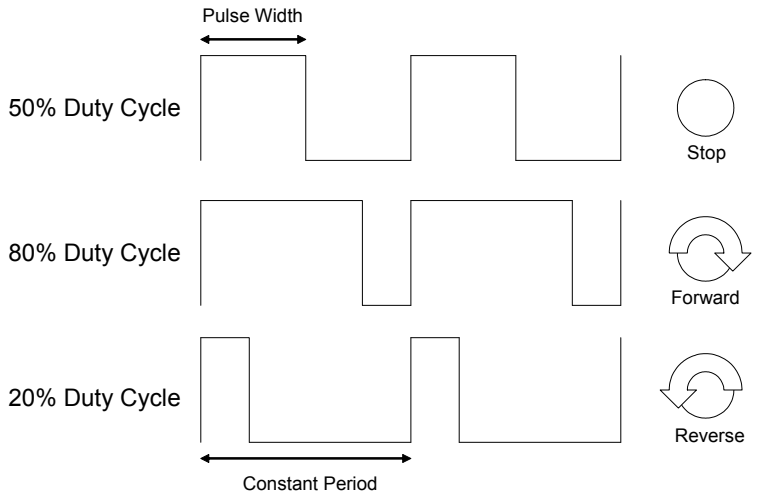

Figure 12: Pulse Width Modulation for DC Motor Control

Pulse Width Modulation (PWM) is shown with varying pulse durations and their effect on the direction of the servomotor motion. The 50% duty cycle results in a stop condition. The 80 % duty cycle results in a forward rotation. The 20% duty cycle results in a reverse rotation. The frequency of the pulse is always the same.

Internally the driver makes use of a full H-bridge to power the motor. The PWM signal is used in a locked anti-phase configuration. Splitting the PWM signal into two and inverting one of the signals creates the locked anti-phase condition. The resulting two signals are then used to drive each side of the H-bridge. The circuit diagram in Figure 13 illustrates this.

This circuit requires the amplifier enable (AMPEN) signal to be high in order for power to be supplied to the motors. This preserves a safety feature that is used by the Galil controller card to cut power to the motors in the case of an unexpected timeout or fault condition. The driver also requires that a logic low signal be provided on one of the digital out lines (ENABLE) to enable the corresponding motor. This was a design feature to allow the controller to effectively switch between two motors per output channel. Thus, the controller capacity can be doubled from 4 to 8 axes respectively. To date, this feature has not been fully implemented. Managing two motors from one channel requires duplicate driver hardware and custom software to save motor states between the two drives.

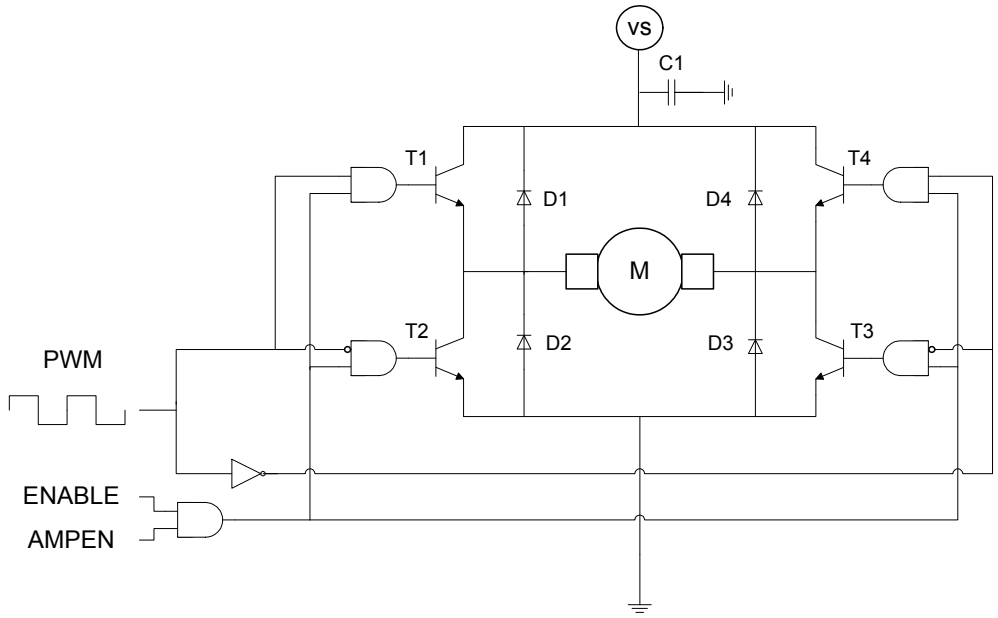

Figure 13: Full H-Bridge Driver

This diagram shows the full H-bridge driver in locked anti-phase configuration that is used to drive a single DC motor. The 'H' refers to the pathway the voltage is allowed to flow through the motor between the four NPN power transistors. The 4-axis controller provides PWM (pulse width modulation), ENABLE (auxiliary enable), and AMPEN (amplifier enable) signals. The DC voltage source, VS, (+12V, 1A) is used to power the motor. The PWM signal is split and one signal inverted (locked anti-phase) to provide the two input signals to left and right sides of the H-bridge.

The operation of the motor is governed by the state of the four transistors T1 through T4 that form the four corners of the "H" and the motor forming the "bridge". If the upper left and lower right transistors are 'open' and the rest closed then current is allowed to flow from the source, across T1, through the motor, across T3, and out to ground. Conversely, if the lower left and upper right transistors are 'open' and the rest closed then current is allowed to flow from the source, across T4, through the motor, across T2, and out to ground. The external bridge of diodes (D1-D4) is made by four fast recovery elements (recovery time < 200 ns) to prevent voltage from flowing backward in the circuit and possibly damaging the motor. A truth table showing the results of the various combinations of the three control signals and their effect on the motor are given in Table 6.

Table 6: 4-Axis DC Motor Truth Table

Inputs			Motor
ENABLE	AMPEN	PWM	
H	H	H	Forward
H	H	L	Reverse
L	X	X	Free Running
X	L	X	Free Running

H=High, L=Low, X=Don't Care

It is important to note that if either ENABLE or AMPEN go low the motor enters a free running stop condition and not a breaking condition. This allows the motor to be moved manually by hand without resistance if needed. Ideally, the voltage source is equivalent to the maximum positive working voltage of the motor. In this case the motors are rated at +/- 15 volts but the power supply is only 12 Volts. The maximum velocity the motors can safely travel is 200,000 counts per seconds that corresponds to a DC power supply slightly under than 12 volts with no load. Since the loads will be very small, the amount of over-voltage necessary would be minimal, and the less expensive 12V power supply becomes a better choice. A complete circuit diagram and parts list for the 4-Axis driver module can be found in Appendix B.2.

4.6.4 8-Axis Control

An 8-axis controller design was implemented to simultaneously control a 3-axis stage and 1-axis micromanipulator on both M1 and M2. This design employed an 8-axis PCI "Accelera" series controller made by Galil Motion Control. The controller card features 24 uncommitted, isolated inputs and 16 outputs as well as 8 uncommitted analog inputs. The controller provides an analog signal between –10 and +10 volts with 16-bit DAC resolution for DC motor control but does not supply an alternative PWM control signal like the 4-axis "Econo" model. However, it does provide a similar amplifier enable signal for each axis to power down the motor in case of a hardware fault or timeout. The card communicates via the PCI bus using a FIFO and dual Port RAM buffer for fast reading and writing. The minimum update rate for the 8-axis configuration is 125 μs respectively.

4.6.5 8-Axis Driver Module

Like the 4-axis control system, an additional driver module was designed and built to transform the control signals provided by the controller card into the required voltages for the motors.

However, since the 8-axis "Accelera" controller card does not provide PWM, a different circuit was required to translate the analog command signal. Additionally, the new design allowed for improvements to be made over the original 4-axis driver. This included breakout screw terminals for all inputs and outputs offered on the Galil 8-axis card, auxiliary –12, +12, and +5 volt power connectors, LED readouts for all digital activity including motor error, limit switch contact, home position, and motor movement.

The 8-axis driver hardware is housed in a 400 mm x 260 mm x 150 mm EM-06 chassis by Circuit Specialists Inc. (AZ, USA). The chassis features two internal mounting rails and 1.5 mm thick aluminum front and back plates. The front and back plates were customized for the driver hardware and two internal shelf units were constructed to fit the internal mounting rails and to provide support for the internal components. The complete mechanical assembly for the 8-axis driver module can be found in Appendix A.2.

The 8-axis driver uses the "Accelera" -10 to +10 volt analog command signal to drive the dc servo motors. The driver employs a differential amplifier driver circuit to translate the analog command signal into the current necessary to power each of the motors (see Figure 14). The input signals to the circuit are the amplifier enable (AMPEN), enable (ENABLE), and the analog command signal (CMD). The AMPEN and ENABLE signals must both be logic high for power to reach the motor. Like the 4-axis circuit, the AMPEN signal preserves a safety feature of the Galil controller to turn off the motor during fault or timeout situations. It is also used by software to turn on or off a motor. A switch on the front panel of the 8-axis driver module provides the second ENABLE signal. Each axis has a physical toggle switch that is used to select between servo or stepper motor operation. This allows either a stepper motor or servomotor to be used with the Galil “Accelera” controller. However, the stepper circuit driver hardware was not essential to the BAMBI project and will be completed in future work. In any case, the actual switch must be switched to the servo side for normal servomotor operation. The final input to the driver circuit is the CMD signal that is supplied by the Galil “Accelera” to control the motors. The circuit is designed to amplify the CMD signal 1:1.2. That is, given a 10-volt command signal, 12 volt will be applied across the contacts of the servomotor. The complete electrical schematics and parts lists for the 8-axis driver module can be found in Appendix B.3.

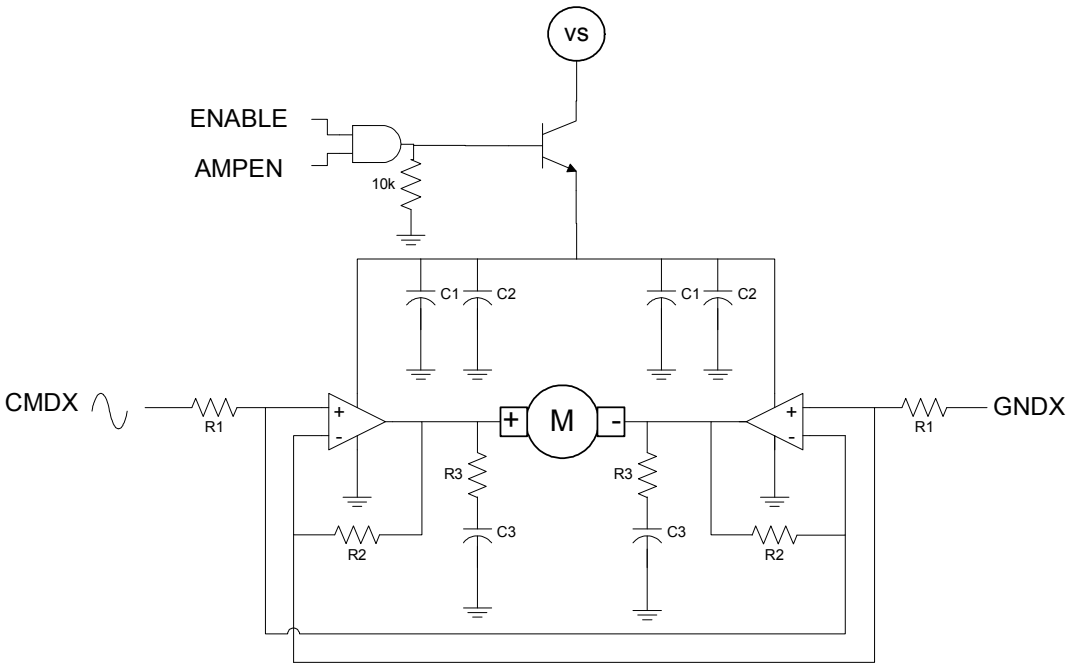

Figure 14: Differential Amplifier Driver

This diagram shows the differential amplifier driver circuit for the x-axis. The remaining seven axes use the same circuit design. This circuit accepts six input signals: Power supply ground, CMDX (+/- 10 volt analog command signal provided by the Galil controller), GNDX (reference ground for the CMDX signal), AMPEN (TTL amplifier enable signal provided by the Galil controller), and ENABLE (the additional TTL enable signal provided by a manual switch on the front panel). Each amplifier supplies current to the motor from the power source (VS).

Chapter 5
Software Development and Implementation

5.1 The Dynamic System

It is important to define the dynamic relationships between the various components of the BAMBI system. In Figure 15, a simplified picture is shown of a sample plate positioned between the objective lens and the light source of an inverted microscope. This diagram shows the individual coordinate spaces attached to the 3-axis plate, camera, and sample. When working with three coordinate systems it becomes important to define the relationships between each of them and how they relate to the image space used by the computer and seen by the user on the computer screen.

The dynamic model for robot space is derived from the positive directions of motion for the linear actuator for each axis. The robotic slide or end effector can move in any of the x, y, and z directions which can best be described as a right-handed Cartesian system where all three axes of motion are mutually perpendicular and linear. Each axis of motion has an independently controlled corresponding DC motor. The positive direction of the axes indicates the incremental motion of the DC motor. An assumption is made at this point that there are no cross correlation terms between any of the axes and that they travel in perfectly linear paths. Obviously there is some interplay between the axes due to friction and small deviations in straightness of travel and will have to be accounted for by software.

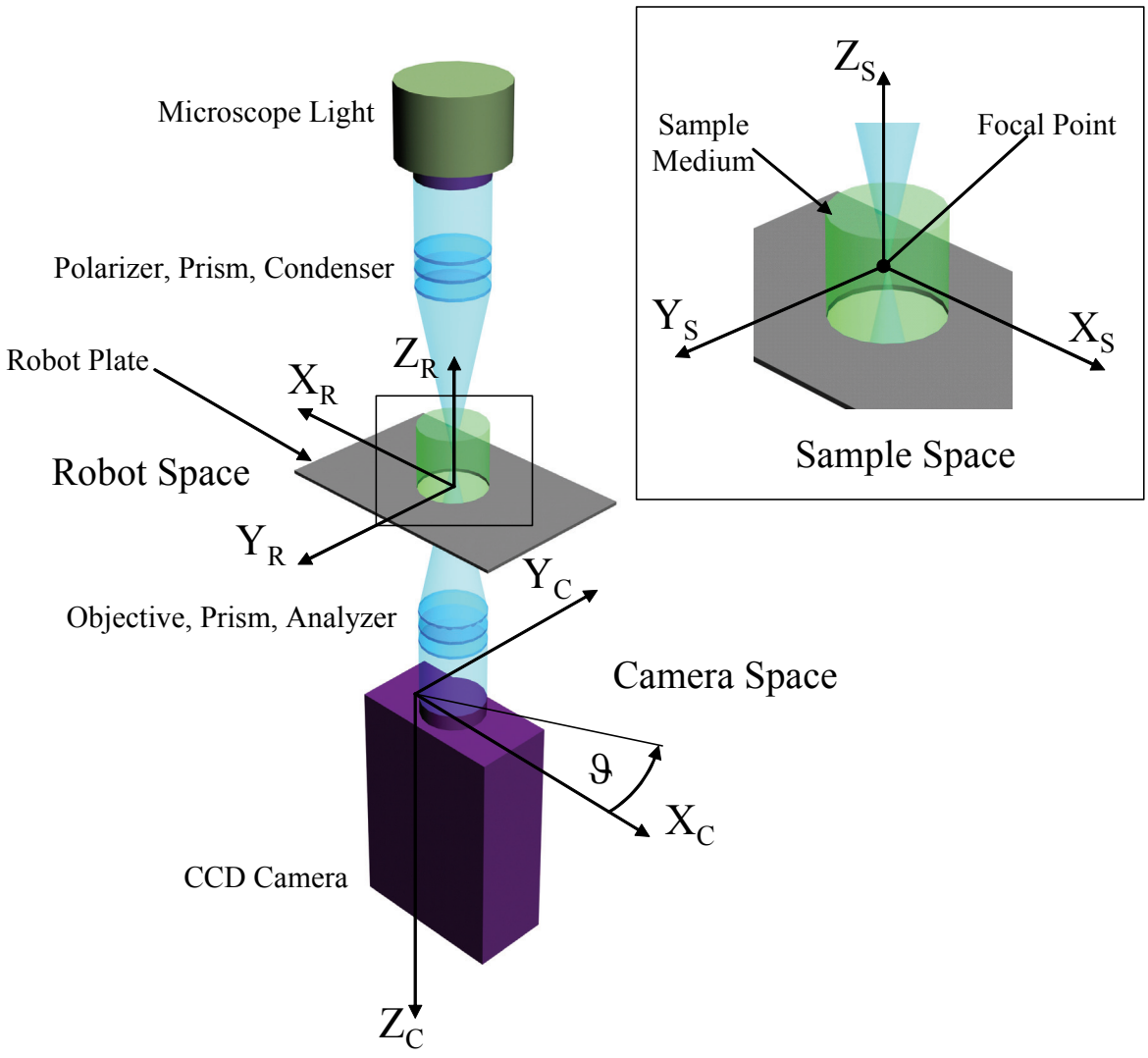

Figure 15: Robot, Sample, and Camera Coordinate Space

A simplified diagram of the light path for in an inverted microscope and the Cartesian coordinate systems attached to the robotic plate, specimen sample, and camera. Robot space represents the coordinate system relative to the robot manipulator. Sample space (inset) represents the coordinate system attached to the chamber, slide, or dish containing the sample. Camera space represents the coordinate system attached to the camera itself.

The dynamic model for the robot is shown below as a state vector p_R, which represents the position of the robot given the state of its motors (x_R, y_R, z_R).

$$p_R = \begin{bmatrix} x_R \\ y_R \\ z_R \end{bmatrix} \tag{5.1}$$

The dynamic model of the focal point within the sample is also defined in a left-handled coordinate system. The origin of the coordinate system is completely arbitrary but it is shown to be at the center of the current focal point within the sample in Figure 15 (inset). Like in robot space, the dynamic model for the sample is shown below as state vector p_S, which represents the position of the focal point within the sample.

$$p_S = \begin{bmatrix} x_S \\ y_S \\ z_S \end{bmatrix} \tag{5.2}$$

Camera space is shown at the bottom of Figure 15 and represents the image the observer would see. However, only one degree of freedom is offered by the fact that the camera can be rotated within its attachment to the microscope about the axis normal to the x-y plane. The dynamic model for the camera is shown below as a state vector p_C, which represents the position of the camera at any given rotation, θ_C, in the direction shown in Figure 15.

$$p_C = \begin{bmatrix} \vartheta_C \end{bmatrix} \tag{5.3}$$

Image space is illustrated in Figure 16 and defines the coordinate system attached to the image the observer would see when looking directly at the computer screen. The origin in the upper left hand corner coincides with the origin of the axis in camera space and represents the first pixel in the upper left corner of the CCD array. This is identical to the camera space. The left hand coordinate system was chosen to match the coordinate system used by the Microsoft Graphical

Device Interface (GDI) architecture and to provide an intuitive top down view when looking at the screen.

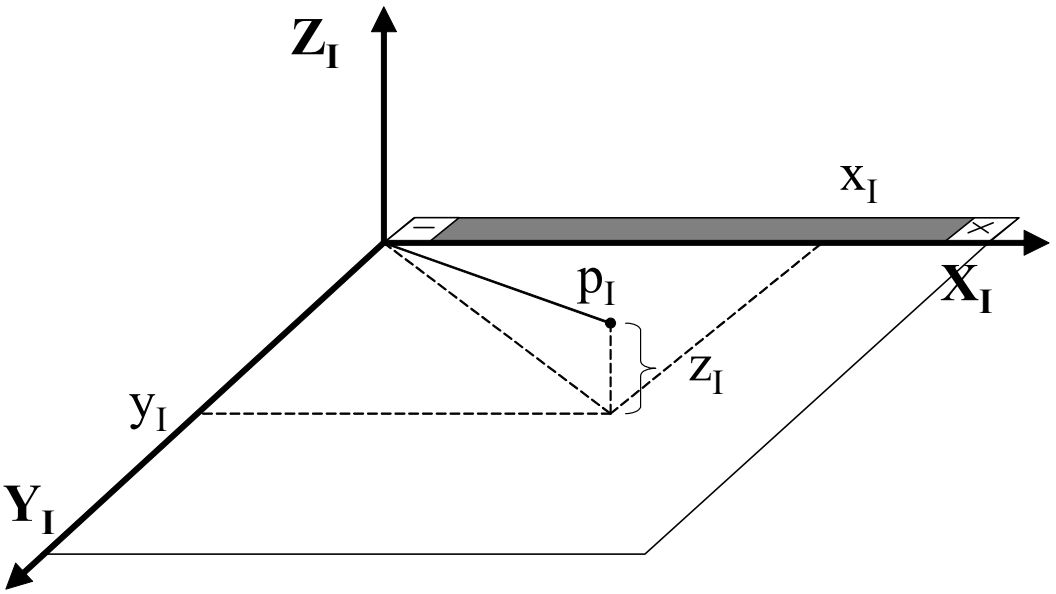

Figure 16: Image Space

A representation of the coordinate system attached to the image space when observing the capture image on the computer screen. This is a left-handed coordinate system wherein the z-axis comes out of the screen toward the observer. The image origin coincides with the position of the focal point in sample space and the first pixel of the CCD camera array.

The dynamic model for any position in image space is shown below as a state vector p_I, which represents the position the focal point within the sample.

$$p_I = \begin{bmatrix} x_I \\ y_I \\ z_I \end{bmatrix} \qquad 5.4$$

Given that image space and sample space are flipped 180º along the x-axis to each other, this is again flipped 180º along the x-axis by the optics of the system. Therefore, holding the camera

angle at zero, image space and sample space are related by Equation 5.5 where A is the scaling vector accounting for the power of the optics.

$$p_I = A \cdot p_S \tag{5.5}$$

The scaling vector is shown in 5.6, where α is the multiplied magnification factors of the microscope objective and camera adapter lenses. The magnification for is the same in both x and y directions but is unity in z.

$$A = \begin{bmatrix} \alpha & 0 & 0 \\ 0 & \alpha & 0 \\ 0 & 0 & 1 \end{bmatrix} \tag{5.6}$$

The relationship between image space and the position of focal point within the sample space given the angle of rotation of the camera, ϑ_C, and the x, y, and z positions of the robot is solved in the solution below.

Given T is the translational matrix from robot to image space we get:

$$T = \begin{bmatrix} 1 & 0 & 0 \\ 0 & -1 & 0 \\ 0 & 0 & -1 \end{bmatrix} \tag{5.7}$$

Given $R(\vartheta)$ is the rotational matrix from robot to image space provided the angle, ϑ, of the camera as shown in Figure 15 we get:

$$R(\vartheta) = \begin{bmatrix} \cos(\vartheta) & \sin(\vartheta) & 0 \\ -\sin(\vartheta) & \cos(\vartheta) & 0 \\ 0 & 0 & 1 \end{bmatrix} \tag{5.8}$$

The combined transformation is the product of the two transforms in Equations 5.7 and 5.8:

$$R(\vartheta)\cdot T=\begin{bmatrix}\cos(\vartheta) & \sin(\vartheta) & 0\\ \sin(\vartheta) & -\cos(\vartheta) & 0\\ 0 & 0 & -1\end{bmatrix} \tag{5.9}$$

The equation to map coordinates from image space to robot space now defined as the product of Equations 5.9 and 5.4 and the inverse of the magnification vector A is shown in Equation 5.10.

$$p_R = A^{-1}\cdot R(\vartheta)\cdot T\cdot p_I \tag{5.10}$$

To map robot space to image space, both sides of Equation 5.10 must be multiplied by the combined inverse transform to yield the final result in Equation 5.11.

$$p_I = A\cdot\left[R(\vartheta)\cdot T\right]^{-1}\cdot p_R \tag{5.11}$$

The fully solved form of the Equation is shown as Equation 5.12.

$$p_I = A\cdot\begin{bmatrix}\dfrac{x_R\cdot\cos(\vartheta)}{\cos(\vartheta)^2+\sin(\vartheta)^2}+\dfrac{y_R\cdot\sin(\vartheta)}{\cos(\vartheta)^2+\sin(\vartheta)^2}\\ \dfrac{x_R\cdot\sin(\vartheta)}{\cos(\vartheta)^2+\sin(\vartheta)^2}-\dfrac{y_R\cdot\cos(\vartheta)}{\cos(\vartheta)^2+\sin(\vartheta)^2}\\ -z_R\end{bmatrix} \tag{5.12}$$

Ideally the camera angle could be held constant at 0º which would significantly simplify the mathematics as shown in the following:

$$p_I = A \cdot \begin{bmatrix} x_R \\ -y_R \\ -z_R \end{bmatrix} \quad 5.13$$

5.2 Software Implementation

5.2.1 Autofocus

Having reliable autofocus for long-term live cell experiments is critical to the success of the study when left in unattended operation. Without autofocus the experimenter must make these unavoidable adjustments by hand often and throughout the entire course of the study. In long-term live cell imaging studies, the time needed between focal corrections may range from every five minutes to every hour depending on the conditions. The reasons for focus control are many: temperature drift, mechanical settling, cell movement, and servomotor drift. Not only are the drift effects significant, they can be long lasting as well.

During the initial heat-up phase the focus will drift significantly, but will eventually reach a kind of equilibrium after one or two hours. However, since the temperature controller will introduce a small cyclic variance due to the cycling of power to the heater, this will be seen as a small oscillation in the focal plane. The mechanical settling of the microscope focus mechanism is usually problematic at the beginning of a time course and tapers off over time but never stops changing. A big problem is the servo motors themselves as they will generate heat while in operation and can impart significant changes to the focal plane. Since motors are not always in constant use, i.e. waiting for the time to elapse for the next acquisition cycle, they will also impart an oscillation effect on the focal plane.

BAMBI has implemented several autofocus algorithms over its lifetime and each one has proven to be unreliable for long-term live cell imaging so far. Some of the problems encountered with autofocus are having multiple focus curves, vibration, background noise, varying experimental conditions, and the limited time required for focus. Multiple focus curves are generated when there are several objects at different depths within the focal range that are *in-focus*. Vibration can hamper any work on a microscope as it causes significant blurring of the images. Generally, vibration is dampened out as much as possible before starting a run; however a single vibration event during an autofocus correction procedure could have unpredictable results. Once focus is

lost, it is usually hard to get back programmatically. Background noise can confuse some algorithms that define good focus as the amount of information contained by an image such as a derivative or entropy approach. Performance of an autofocus algorithm can be very dependant on the type of Illumination used (Sun *et al*., 2004). Various cell cultures and media conditions can also play a role in how well the focus function performs.

The focus function chosen for BAMBI performs well over a wide range of conditions including Bright Field, DIC, and fluorescence illuminations (see Equation 5.14). Normalized variance is a statistical measure of focus that weighs the deviation of intensity from the background with a power function.

$$F_{normalized\_variance} = \frac{1}{H \cdot W \cdot \mu} \sum_{x=0}^{Height} \sum_{y=0}^{Width} \left(i(x,y) - \mu\right)^2 \qquad 5.14$$

The benefit of using this method is that is not as sensitive to noise compared with the gradient or derivative methods. However, the problem of having multiple in focus objects causes a great deal of confusion. This can be caused by having cells imaged in a microwell, where the well walls themselves exhibit *in-focus* features. Other environment factors like the surface of the glass slide or gap chamber can also cause confusion.

The next step in developing this algorithm further is to have BAMBI only allow the focus function to be calculated inside small window selected from within a field-of-view. This way only the object of interest inside the window will be optimized for focus. Other techniques could be tested, such as implementing a fuzzy approach to make the best guess as to which focal maxima to select or combining several autofocus functions and taking a weighted average.

5.2.2 Automatic Image Stitching

BAMBI implements the automatic tiling or stitching of images in a very straightforward manner. Because the accuracy of the servomotors are well within a micron when backlash is corrected for the images can simply be tiled according to the value of the servo motor coordinates for each image. Applying Equation 5.13 to convert from motor units to pixel locations is all that is required provided the rotation of the camera is precisely 0º. As well, BAMBI does not have to account for lens aberration since the objectives used are highly corrected and introduce very little optical error to the images themselves.

5.2.3 Backlash Compensation

Backlash exists in practically every mechanical system that involves friction, gears or drives. It can occur whenever a mechanism changes its direction or rate of travel. Its cause is well known and is usually designed out of the system as much as possible before it is manufactured. An example of a backlash characteristic is shown in Figure 17.

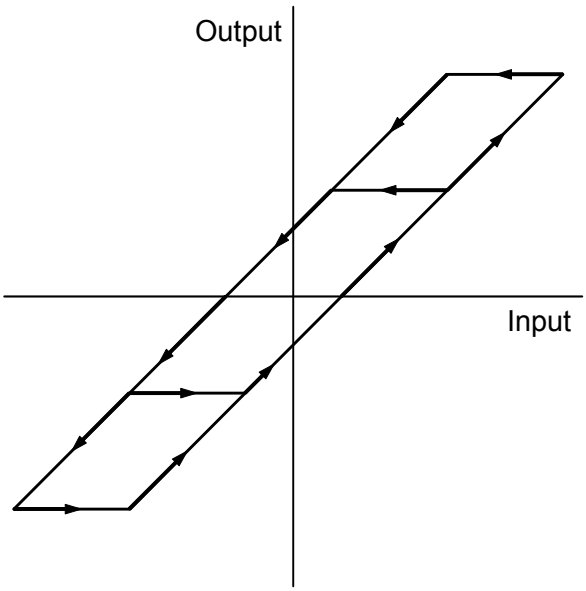

Figure 17: Static Backlash Characteristic

Each time the direction of movement changes sign there is a loss of contact in the gears between the load and the motion. This figure is adapted from (Lewis *et al*., 1997).

Each of the Galil M-112 micro-translation servos is backlash compensated to less than 2 μm by the use of precision lead screws and gear head. Linear guides with precision ball bearings insure that the straightness of travel deviates no more than 0.5 μm. These linear guides are manufactured with very tight tolerances to reduce backlash and maintain low friction. However, in actual operation when the servo changes direction there is a small amount of sidelash that occurs. Sidelash is a term for the complementary backlash experienced by the orthogonal direction of motion. That is, if the x-axis direction of travel was stopped and reversed, there would be a small change in the y-axis position. This is due to the small amount of free play between the linear guides and the moment of inertia generated by the offset location of the servo lead screw.

When BAMBI is working at high magnifications a backlash of 2 μm can be quite significant and must be compensated for by other means. Backlash correction can be achieved by the introduction of a position sensor on the load (end-effector) with feedback to the control algorithm. This is called Dual-Loop-Feedback-Control. Because the micro-translation stages are complete solutions with shrouded compact components it would be too costly and bulky to add more hardware to implement. In light of this difficulty, two software approaches to correct for backlash have been investigated and implemented in the BAMBI software.

The first method shown in Figure 8 works on the principle that the once backlash is measured for each servo's direction of travel it does not change with time. The correction is performed each time the direction motion changes sign. This method also requires a homing movement to be performed prior to use to ensure the servomotor is not currently dwelling in the backlash non-contact region when the first movement is made. This was implemented by having the servos all move in the negative direction, well beyond the backlash value and then forward again the same distance. This ensured that the servos had no free play between the load and the motion in the forward direction. Figure 18 shows how the algorithm would work for a single axis.

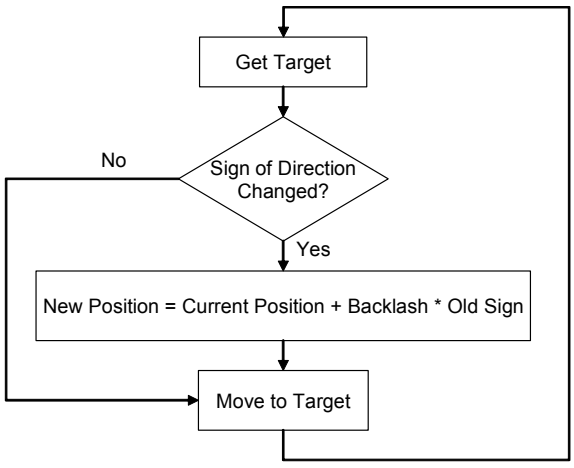

Figure 18: Backlash Correction Method 1

This figure shows the logic for negating backlash when the backlash value has been measured for a servo. When the sign of the motion command changes the current position is overwritten with the new corrected position value before the movement command is allowed to continue.

The drawback to this method of correction is that the position values of the servos are rewritten each time the servo changes direction; therefore, a small amount of round off error will be introduced to the system each time the direction changes. When this algorithm was implemented on BAMBI it was shown to drift over time due to this effect. A possible solution to the problem would be to avoid overwriting the position value and use an offset variable whenever reporting positions back to the program. That way there would be no loss of information due to round off, because the offset is only applied whenever the position is reported. Another confounding problem with this method was only observed during live cell imaging when the temperature effects became an issue. Live cell imaging requires the environment chamber to be heated to 37º Celsius. Additionally, the trajectory of the robot is composed of one hundred waypoints or more, which will heat the motors up to 53º Celsius depending on the speed and torque settings. The temperature has a huge effect on the value of the backlash, possibly due to the high gear ratio. The effects on the backlash are of a cyclic nature due to the capture cycle of the arrays. The motors heat up during a capture cycle and cool back down while waiting for the next cycle to begin.

The second method of backlash correction is a more straightforward approach. That is, each point in a trajectory or path is always approached from the same direction for each servo (see Figure 19).

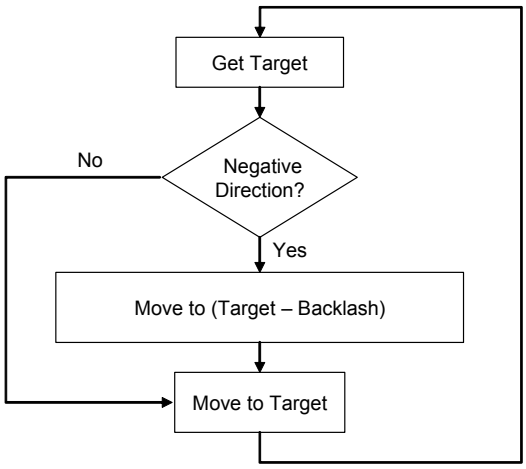

Figure 19: Backlash Correction Method 2

This figure shows the logic for negating backlash by approaching the target from the same direction each time. The value of the backlash correction is slightly greater than the actual measured backlash to avoid temperature and torque effects.

Like in the previous method, this technique still requires a homing maneuver to take place before the first movement is made to ensure that the servo does not start in a non-contact region. It is not subject to the round off errors in the first method and would always work provided the backlash correction was greater than the actual backlash to account for temperature and torque effects. The implementation of this algorithm on BAMBI proved to be successful. There was still drift in the position of the servo due to the cyclic heating of the motors during operation, but it was minimized compared to first method. The drift in position due to temperature effects could not be avoided and tended to oscillate less and less as the experiment continued.

One drawback to this method is that it requires a more complicated the trajectory path to ensure each waypoint is approached from the same direction. It significantly increased the number movements needed. It also requires more communication and coordinated timing between the Galil controller card and the BAMBI application. Some application threads had to wait on the backlash maneuver to complete before completing their function. This required additional process threads to be created and inter thread communication to be implemented to coordinate their actions.

Ultimately, the second method ensured there was no free play between the motor and the load regardless of the temperature when approaching from the same direction. The distance required to correct for backlash was approximately three times the measured backlash to ensure that the distance corrected for would not be susceptible to heat or torque effects. If a backlash correction was needed it was found that it was better to perform a backlash correction maneuver for all three axes to minimize the co-variance or sidelash effects between the adjoined axes mentioned earlier. For these reasons, the second method of backlash correction was chosen to be used in the final BAMBI design.

5.2.4 BAMBI Image Space

BAMBI software uses the left-handed coordinate system described in Figure 16 to draw the images on the screen. That is, the camera image is displayed in this format with the horizontal direction corresponding to x and the vertical direction corresponding to y. Elevation, z, is positive in the direction coming out of the x-y plane, the computer screen, towards the observer. Angles are measured about the z-axis starting at the x-axis and increase in positive value in the clockwise, x to y, rotation. Since the image is in units of pixels there must be a mapping between pixels and actual motor units given the magnification of the camera and the objective lens. If we

assume the camera to be orientated such that its x and y axes are exactly parallel to the x and y axes of the image space then we can eliminate the rotational term in Equation 5.10 to get the position of the robot in motor units as a function of image position:

$$p_R = A^{-1} \cdot \begin{bmatrix} x_I \\ -y_I \\ -z_I \end{bmatrix} \tag{5.15}$$

Here, A is the magnification vector of the objective and camera adapter lenses or the scaling values between the camera and image space. Displaying an image on a computer screen requires that the units are in terms of pixels. Therefore, an additional step must be taken to relate the screen pixels with motor units. The final equation relating the position of the robot to image space given magnification, pixel size, and motor unit size is:

$$p_R = A^{-1} \cdot C \cdot M \cdot \begin{bmatrix} x_I \\ -y_I \\ -z_I \end{bmatrix} \tag{5.16}$$

The two additional constants are C, the size in millimeters of one element on the CCD array, and M, the number of motor units per millimeter. This equation assumes that C and M are the same for both x and y directions. If this is not the case, then C or M could be replaced with a vector of constants instead. The z term in such a vector would be arbitrarily chosen to match one of the x or y directions resulting in a volumetric representation of pixel size called a voxel. Both of these constants can be found in the specifications of the servo/encoder and digital camera used. In the case for BAMBI, the Galil M-112.1DS motors have a count of 145636 motor units per millimeter, and the Sony XCD-SX910/710 cameras have a square pixel size of 0.00465 millimeters per pixel.

5.2.5 Mosaic Capture and Trajectory Generation

The process of capturing images for a long-term live cell imaging can be very different from one experiment to the next. It depends strongly on the type of information needed and the constraints/conditions imposed by the cells themselves. Experiments can range from a single field-of-view captured through time using only DIC illumination to many fields-of-view

spanning x, y, and z captured through time at different intervals for both DIC and fluorescent illumination. The hardiness of the cell types will determine the exposure time or how often they can be illuminated before damage starts to occur. If the goal of the experiment is to find a low frequency event then many fields-of-view will need to be imaged with enough optical resolution to answer the questions the experiment is designed to solve. As resolution goes up, the number of fields-of-view needed will also go up. A balance must be made between the resolutions required, the size of the image field and the exposure cycle time allowed by the cells and the physical limits of the robot itself.

BAMBI divides possible experiments into three categories: 2-D time courses, 3-D time courses or hypercubes, and multi-channel fluorescence. These three categories can be used alone or in combination to generate a complete live cell imaging time course.

5.2.5.1 2-D Time Course

The 2-D time course is a monolayer consisting of one or more fields-of-view located anywhere in a defined 2-D plane (See Figure 20). This will generate a 2-D image mosaic through time easily viewable on a 2-D workspace. The plane that the images or waypoints will be generated on can be created by several methods. The user can define a starting position in (x, y, z), a row and column grid spacing, and the number of waypoints in the x and y direction. This holds the z-axis constant and automatically generates the waypoints to fill in the space defined.

Alternatively, the user can define a three points on the bounding area of a rectangular 3-D plane. That is, the plane is defined by the (x, y, z) positions for the upper left, upper right, and lower right corners. Given the row and column grid spacing the program will fill the plane with as many waypoints that can fit in the bounded region. The program will generate the z component of any waypoint given its row and column (*m, n*), the step sizes Δx and Δy, and the gradient components $\frac{\partial z}{\partial x}$ and $\frac{\partial z}{\partial y}$ (See Equation 5.17).

$$Z_{(m,n)} = Z_{(0,0)} + n \cdot \frac{\partial z}{\partial x} \cdot \Delta x + m \cdot \frac{\partial z}{\partial y} \cdot \Delta y \qquad 5.17$$

This approach enables straightforward 2-D image mosaic construction when the ROI in the specimen is not strictly parallel to the microscope's axis.

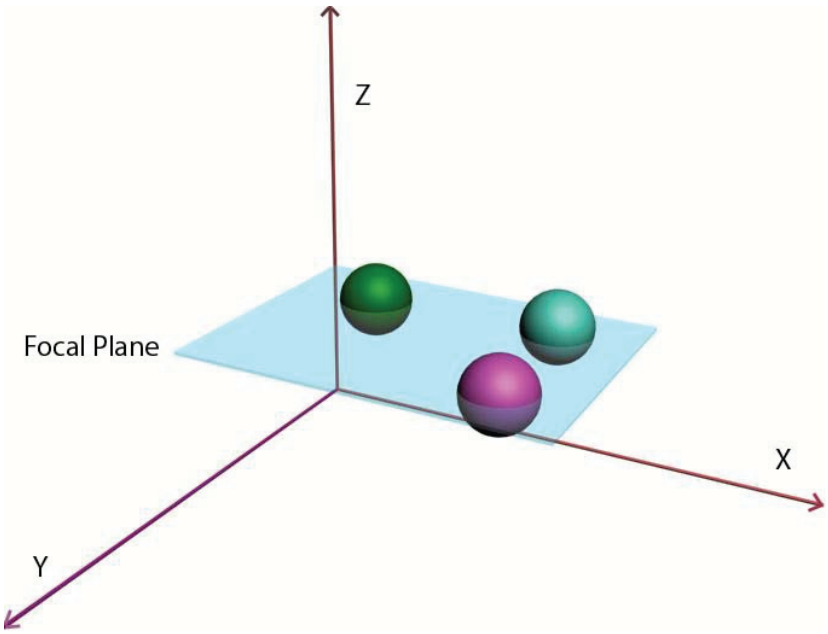

Figure 20: 2-D Time Course

A 2-D time course is shown as a single plane of focus through the objects of interest. The plane represents the region in XYZ space wherein image locations are to be placed. The three balls represent spherical cells that are in the region of interest (ROI) of the cell culture.

The trajectory or path generation is simply a matter of generating the waypoints in the correct order for image capture. The BAMBI software makes a distinction between two image capture paths for a 2-D Time course: the top down *S-curve* or the top down left to right *Zigzag* trajectories (see Figure 21).

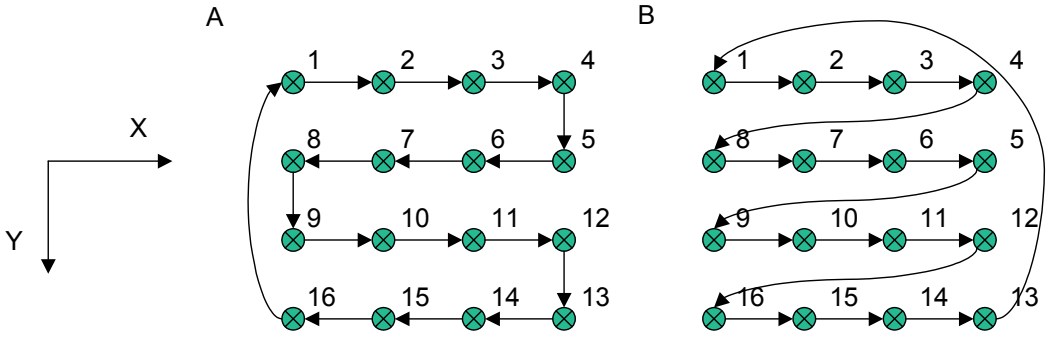

Figure 21: 2-D Time Course Paths

Two robotic stage path patterns for collecting a 2-D set of images. A. S-Curve pattern. B. Zigzag pattern. The stage takes less time to complete the S-curve pattern than the Zigzag, but is less amenable for real time visualization.

The S-curve method provides a does not have to return to the far left column after it captures each row, therefore it has a shorter path to follow resulting in faster cycle times. This is especially important when there are many fields-of-view to acquire with short cycle times. Another benefit is that when the images are later stitched together to form a mosaic, the shorter paths translate to shorter time intervals between fields-of-view directly above or below one another. That is, the smaller time interval between images in the row above or below minimizes live cell movement between the frames. A drawback to this method is that it requires additional processing and attention to the way in which the image data is opened in other editor programs. It breaks the continuity of batch processing algorithms that rely on monotonically increasing file offsets to access data in the file structure. (i.e. if the mosaic is to be inversed or flipped and the final row contains less than the full amount of columns, they must be zero padded with blank data before flipping). However, this problem can be overcome by using the actual logged coordinates of each image to load the raw image files rather than a predefined path.

5.2.5.2 Hypercubes

An extension to the 2-D time course is a 3-D time course called a hypercube (see Figure 22). The added dimension is in the z direction thus creating a volume of waypoints in the space (x, y, z). Others have referred to this as 4-D image acquisition with the extra fourth dimension defined as time, indicating that it is in fact a 3-D time course (Burglin, 2000). Similar to the 2-D time course, the hypercube can be defined by a point (x, y, z) in 3-D space with defined rows and columns an additional grid spacing, Δz, called a slice.

As before, the user can define a hypercube by selecting 3 points on the boundary of a plane in 3-D space and specifying the row, column, and slice step size. The gradient method is used to calculate the first surface (top plane) and the z-slices are just offsets from this plane. To calculate the z positions, x and y are held constant and an offset is applied to the z value for each waypoint below it. Therefore, in a strict sense, the hypercube may not be exactly orthogonal. However, these effects are small and can be ignored with no impact to the results of the study.

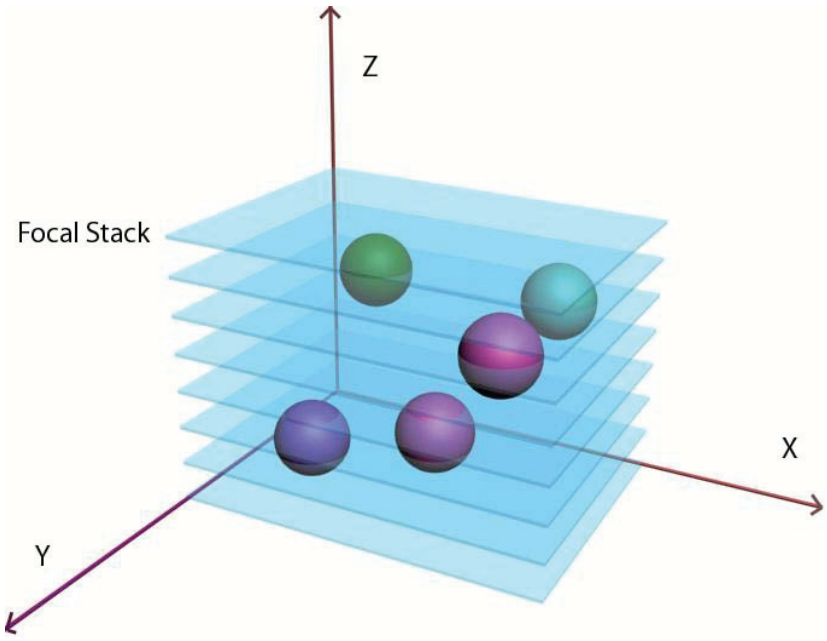

Figure 22: Hypercube

A 3-D time course is shown as a stack of eight focal planes in 3-D sample space. The spheres represent cells or cell aggregates that are in the culture medium.

The transparency of the cells, the media, the contrasting method, and the numerical aperture of the object lens determine how far the waypoints can effectively span in the z direction. Almost all hypercubes must be imaged with DIC or a very high NA lens to help remove the unwanted light from above and below the image plane. Under these conditions is possible to provide a confocal-like result with depths as great as 25 um.

The path generation is identical to the 2-D time course except for each waypoint in the first surface (top plane) there are an additional set of waypoints created incrementally in the negative z direction. The negative z direction corresponds to an upward motion of the stage. The upward motion of the stage helps to reduce focal drift resulting from gravitational settling in the mechanical system. Figure 23 shows how the path would be generated for the first row of either of the 2-D time courses presented in Figure 21. The same procedure is applied for any subsequent rows.

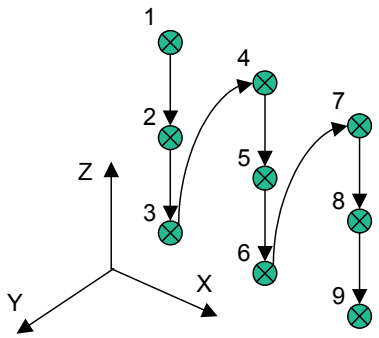

Figure 23: 3-D Path Generation

This figure illustrates the robotic stage trajectory pattern for the first row of a 3-D set of images. The waypoints 1, 4, and 7 lay on the top surface of the 2-D plane and are generated according to the *S-curve* or *Zigzag* pattern specified. The next waypoint in the trajectory, 10 will be located on the top surface, below 7 if the *S-curve* pattern is chosen and below 1 if the *Zigzag* pattern is chosen.

5.2.5.3 Multi-channel Fluorescence

Multi-channel fluorescence imaging is an extension to the concept of the hypercube in that it adds an additional dimension to the time course. The hypercube now becomes a vector **H**, composed of the three spatial dimensions (x, y, z), time t, and illumination ρ (see Equation 5.18).

$$\mathbf{H} = \langle x \quad y \quad z \quad t \quad \rho \rangle \tag{5.18}$$

BAMBI is equipped with a LED array that can be used to illuminate the cells with up to five different excitation wavelengths. Multi-channel fluorescence significantly increases the amount of information that can be gathered from a long-term live cell study. BAMBI can take advantage of the fluorescent properties of some inorganic and organic molecules that act as fluorophores to image specific targets or binding sites in a specimen. By introducing several different colored fluorophores multi-fluorescent images can be taken to image different targets at the same time point, respectively.

5.2.6 Mosaic Blocks

The amount of information that can be contained in a single square centimeter of a specimen slide is extremely large. Of course, this depends on what features the experiment is looking and this in turn will determine the magnification, illumination, and cycle times. This forms the upper limit to the amount of space that can possibly be imaged for a given study. Sometimes the features of interest or ROI are sparsely located throughout a large area and other times they are close together in a few small groups or aggregates. In either case, there are regions of the space that contain no valuable information and regions that do; therefore it makes sense to only image the ones that do. BAMBI solves this by introducing dynamic mosaic blocks.

Mosaic blocks are a set of waypoints that have been defined in 2-D or as a hypercube for a specific ROI. An experiment can have more than one mosaic block. Each block embodies a complete long-term live cell imaging study unto them selves. They contain all the information necessary to navigate to the points, capture the images, store the data, and report back to the main program. They can be dynamically created and destroyed at any point in the experiment, allowing the user to capture a newly found feature of interest or stop imaging an area that cells have died or is no longer of value. Another special feature of mosaic blocks is that they can grow in size, shrink, and even move within the space as needed.

5.2.7 Mosaic Block File Structures

BAMBI stores the setup information for all mosaic blocks in a single file with the filename extension “bam”. The BAMBI "bam" file format is fully described in Appendix C.1. Each mosaic block has its own set of files for actual data storage. The data storage files come in pairs for each illumination source used by the block. The actual image data is stored in a raw “flat file” format composed of consecutive 8-bit pixel values with the extension “raw”. The actual position the robot, timestamp, and identification information is stored in a corresponding comma-separated file with the extension “csv”. If the illumination source is fluorescent then the image files are further separated into two raw formats, one for fluorescent and the other for DIC illumination. (See Figure 24.)

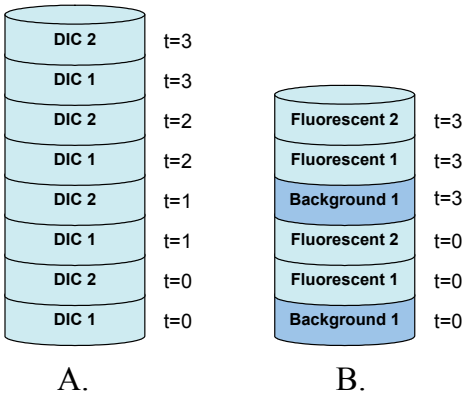

Figure 24: Mosaic Block Raw File Structures

This figure shows the files structure for a single mosaic block composed of only 2 fields of view (1 and 2) captured in both DIC and fluorescent illumination. The sample period shown for DIC and Fluorescence is t=1 and t=3. A. The file storage pattern for DIC (could also be phase contrast or bright field) illuminated images. B. The file storage pattern for the fluorescent illuminated images.

Because fluorescence illumination is not as bright as DIC, several images are taken and summed to create a single viable image. When this is done, the background noise present in the images is amplified. To remove this effect, a set of background images is taken without any illumination and is subtracted from the summed fluorescence image. The same number of background images are taken as the fluorescence set. They are only taken once at the beginning of each fluorescence cycle at the first waypoint. The background noise is not dependant on location as much as it is on the camera properties like dead pixels and small differences in the CCD element sensitivities.

5.2.8 Mosaic Capture Algorithm

At the heart of BAMBI's mosaic capture operation is a set of logic trees that allow the individual mosaic blocks to be captured completely independent of each other, but share the resources in a concurrent fashion. It is important that the resources which are in different process threads such as the camera, shutter, illumination, and robot are only manipulated by one mosaic block at a time. This is accomplished by the use of a single outer control loop that is closed by an *OnTimer* event handler. (See Figure 25.)

The *OnTimer* logic algorithm is shown as an outer control loop that allows entry into three possible logic blocks: *OnTimerFunction*, *LEDLogic*, and *DICLogic*.

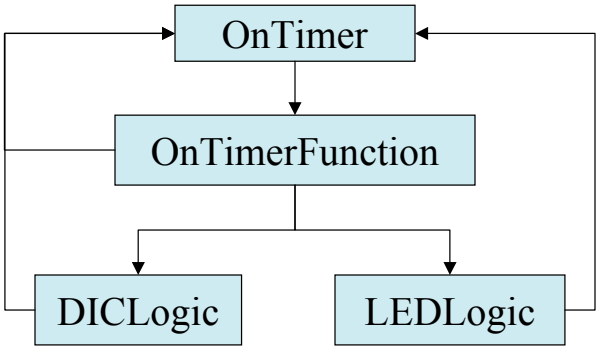

Figure 25: Outer Control Loop

The mosaic capture algorithm's outermost control loop is governed by a Windows event timer that is captured by the *OnTimer* message handler. If the appropriate timeout is received the *OnTimer* handler calls the *OnTimerFunction* function which can in turn call the DIC and LED logic algorithms.

The first block is the *OnTimer* function is a message handler that intercepts the windows timeout message. If the appropriate timeout is received it calls the *OnTimerFunction*, otherwise it releases the timeout message and waits for the next one.

5.2.8.1 OnTimerFunction

The *OnTimerFunction* purpose is to determine if the user has chosen to stop the data capture process, and if not, passes the control on to the appropriate logic block (see Figure 26). It checks to make sure the user has not *stopped* or *paused* the mosaic builder, if so it resets the timer and exits. If the mosaic builder has not been stopped or it checks to see if a mosaic block is in active capture mode, if so it will check the *iChannel* variable to see if it needs to be sent for LED or DIC processing. If not, it will activate the block and check to see if there are any LED Blocks present. If there are no LED blocks it passed control to the *DICLogic* function, otherwise it passes control to the *LEDLogic* function.

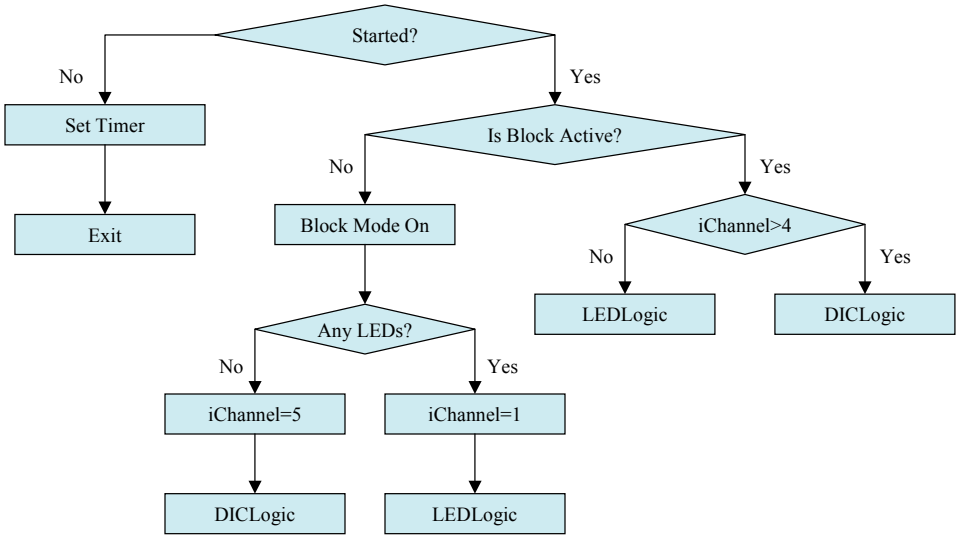

Figure 26: OnTimerFunction Logic Tree

The mosaic capture algorithm's *OnTimerFunction* checks the status of the program to ensure that the user has not paused or stopped the mosaic builder. If it is in the *started* state its job is to determine if a block is in active capture mode, if not it will turn it on. Its job is to pass control to the correct illumination block for further processing.

5.2.8.2 LED Logic Tree

The function of the LED logic tree is to capture the LED, background, and corresponding DIC images. The algorithm (See Figure 27) first checks to see if it is in LED mode. That is, has it already started processing the mosaic block? If not, it checks to see if any of the LED captures are ready to be taken. Most LED capture times span a cycle of 2 hours or more and so more often than not, the module will usually set *iChannel* to 5 and reset the timer. This action will cause the *OnTimerFunction* function from above to redirect the block to *DICLogic* for processing instead. Only if there are LEDs ready to be captured, does it activate the LED mode and move the robot to the first waypoint in the mosaic and reset the timer. The robot takes time to get to the first location, so rather than wait for it to get there, resetting the timer will pass control back to the program until the robot is ready. If LED mode is activated, it checks to see if the robot has reached the waypoint and has stopped moving, a state known as *on target*. If the robot stage is not *on targe*t the routine simply resets the timer and passes control back to the program. If the robot stage is *on target*, the routine checks to see if a background image has been taken at this waypoint. If not, it takes the appropriate number of background images for each LED channel

that is ready, resets the timer, and exits. Background images are taken with the camera shutter speed and gain settings for the respective LED image to be taken, but with the LED light off. If the background image has been taken, it checks to see if the LEDs are finished. If not, it will capture all the LEDs that are ready to be taken for this waypoint with the appropriate camera shutter speed, gain, and LED light enabled. During an image capture event such as LED accumulates, control is not released back to the graphical user interface (GUI) until the image capture finishes. The timing of the LED was found to be such a critical part of data collection that it was allowed to have full access to the executing thread. Future editions can evaluate this feature in more detail, perhaps allowing the GUI to operate inside an additional thread. In either case, the control of the thread during image capture will not be given up until the images are acquired for the waypoint. The extra GUI thread would only allow the user to click on buttons that would have no actual effect until the images were captured. Once the images are collected, it enables the DIC illumination, sets the timer, and passes control back to the program.

Once all the LEDs are finished, it checks to see if the DIC images have been taken. If not, it checks once more to see if the DIC Illumination is enabled. Because the user actually sets the preload for the spring-loaded electromechanical switch, it can open and close at different rates from one experiment to another. This code will allow for an additional check on an addition feedback device such as a limit switch or light sensor to indicate that the shutter has indeed opened. If the light is not yet enabled, it resends the command to open and resets the timer. If the light is enabled for DIC Illumination it sets the camera shutter and gain for DIC and captures the image, closes the shutter and immediately checks to see if there is another waypoint in this mosaic block to move to.

If the DIC images have all been taken for a given time point the routine checks to see if this waypoint was the last one in the mosaic block. If it isn't, it moves the stage to the next waypoint, resets the timer and exits. If this is the last waypoint it turns off all the active modes, resets the timer and passes control back to the program. This restarts the process so that the next mosaic block that is ready can be processed.

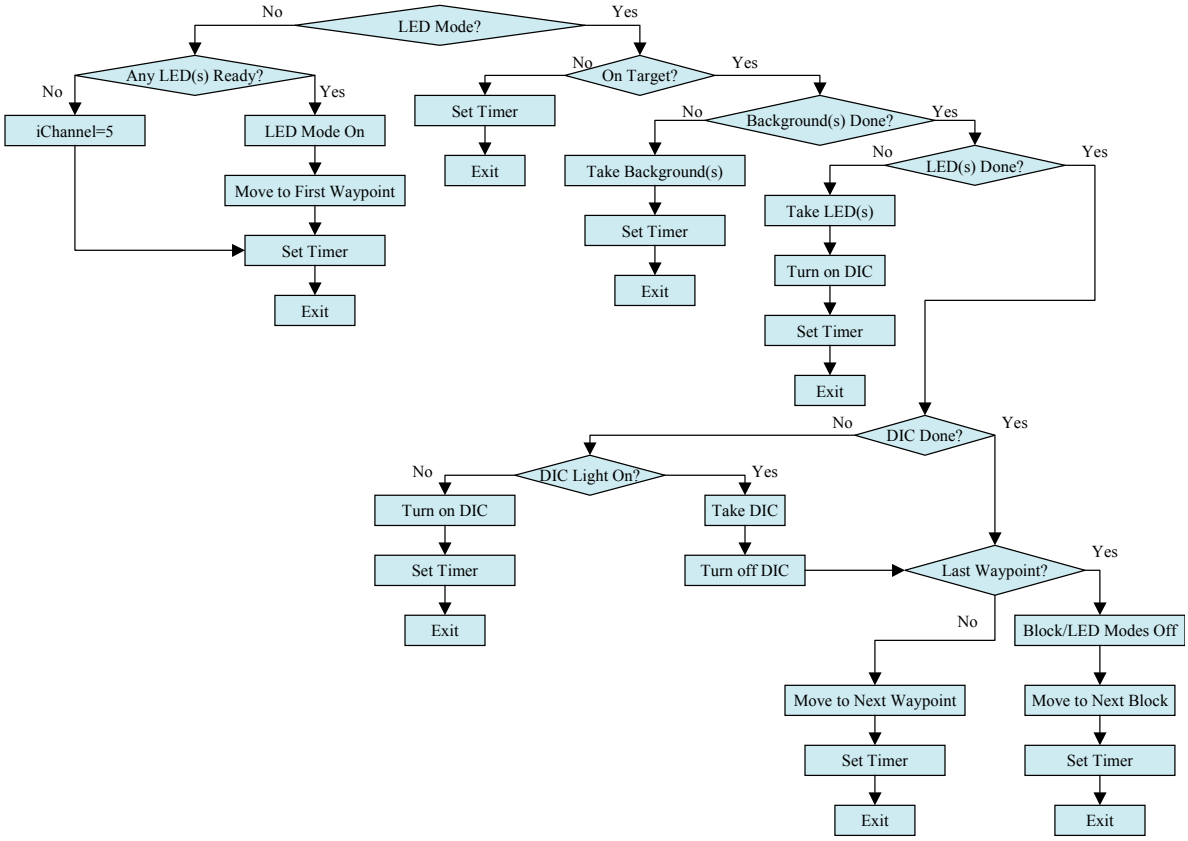

Figure 27: LED Logic Tree

The mosaic capture algorithm's LED logic tree is responsible for the capture of all the LED illumination images and their corresponding backgrounds. It also takes all the DIC images for that time point to keep the context between DIC illumination and the fluorophores.

5.2.8.3 DIC Logic Tree

The DIC Logic tree is responsible for the capture of DIC illumination blocks that do not require fluorescence for the time point (see Figure 28). The function checks to see if it is in DIC mode. That is, has it started the DIC image capture process? If not, it checks to see if it is time to take a DIC image for this block. If not, the algorithm turns block active mode *off*, moves the internal pointer to the next mosaic block, resets the timer, and exits the function. If it is time to take the DIC images, the routine turns on the DIC capture mode, moves the robot to the first waypoint in the mosaic block, turns the DIC light *on*, resets the timer, and passes control back to the program.

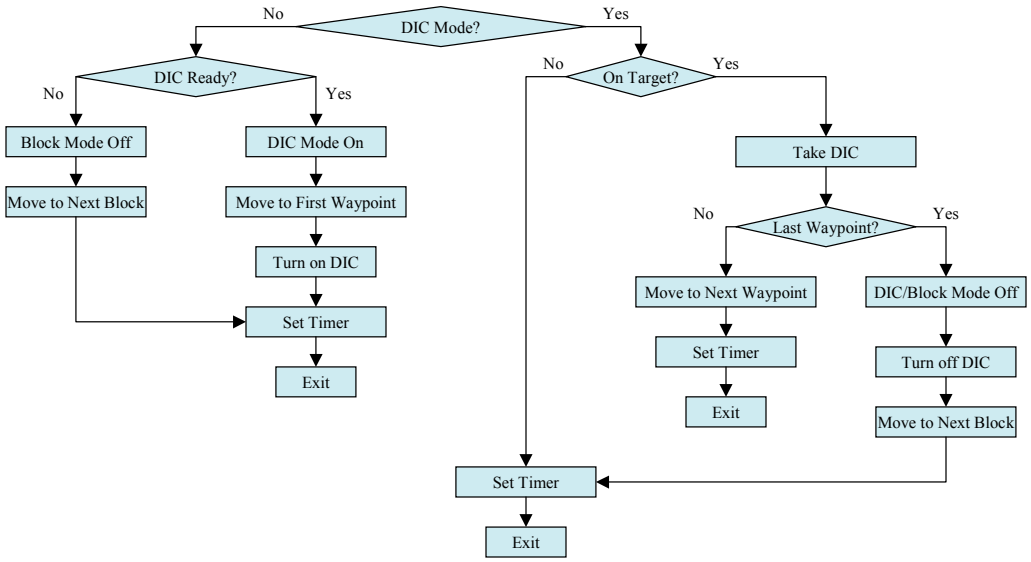

Figure 28: DIC Logic Tree

The mosaic capture algorithm's DIC logic tree is responsible for the capture of all the DIC illuminated images that do not need fluorescence at that time point.

If the DIC mode is active when the program enters the DIC logic tree, it checks to see if it is *on target*. If not, the robot is still in motion and the routine resets the timer and exits. If the stage is *on target*, a DIC illuminated image is collected and the algorithm checks to see if this was the last waypoint. If so, it will turn the block mode off, close the DIC shutter, move the internal pointer to the next mosaic block, reset the timer, and exit the function. Otherwise, the routine moves the robot to the next waypoint without closing the DIC shutter, resets the timer, and exits.

5.3 Graphical User Interface

From the user perspective the software program is divided into four distinct groups that are tethered by a single dialog interface (see Figure 29). The Mosaic Editor group provides a GUI to load raw image files, display them in various ways, and allow editing of images and time courses. The Robot Control group provides a Navigation Panel through which the user can directly interact with the robot, view robot properties, and change its settings. The Camera Window group provides the real time display of the images currently being captured via the Sony camera and can save these images as snapshots or movies. The final group, Mosaic Builder provides the user with all the tools and controls needed to set up automatic long-term live cell capture of

mosaic blocks. This includes setting up the trajectory paths, illumination conditions, and managing them.

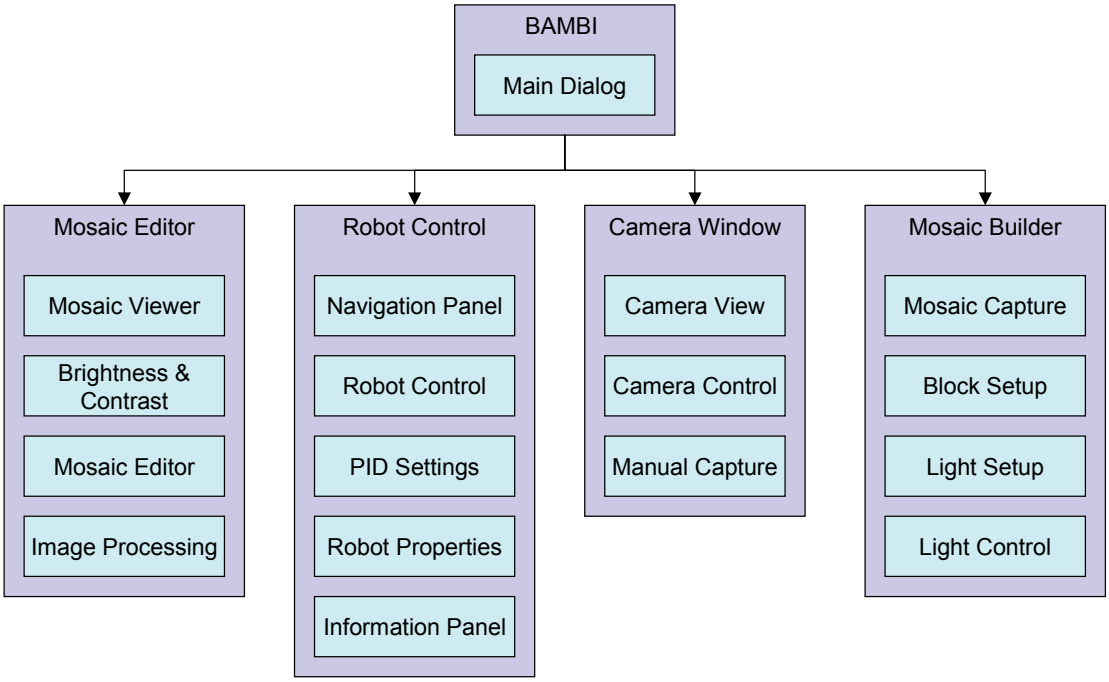

Figure 29: BAMBI Software User Interface

The BAMBI software is divided into four functional groups that are all accessed via a single dialog interface. The Mosaic Editor provides the GUI for mosaic display and editing. Robot Control exposes all the functions necessary to interact with the robot. Camera Window provides a GUI for the real-time display of the camera. Mosaic Builder provides GUIs to set up, control, and save data from long-term live cell imaging experiments

5.3.1 Mosaic Editor

The Mosaic Editor group provides a set of tools that allow the user to load, edit, view, and export captured time course files. The first task of the Mosaic Editor is to display the Mosaic Editor Window GUI (see Figure 30). This widow provides a menu the user can interact with. The first menu choice "Edit" allows the user to open any raw mosaic block file for display. This can even include a time course that is currently being captured on BAMBI. File integrity is maintained by accessing the data in *read only* mode. Once a time course is opened only one field of view is displayed on the screen at one time. The Mosaic Editor Window places four slider bars at the edge of the display to allow the user to navigate the mosaic block by row, column, slice, and time point.

The "Select" menu allows the user to select regions of interest in the form of a bounding rectangle. The user can export the selection as an image or movie if given a range of time points. The editor can save images and image sequences in several formats: raw, avi, jpg, and tiff.

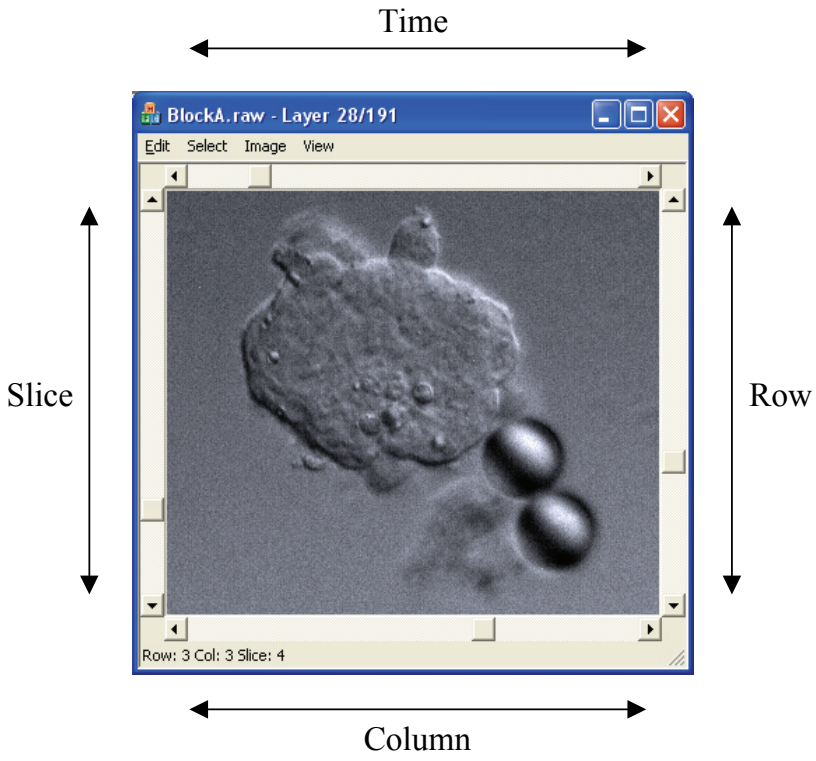

Figure 30: Mosaic Editor Window

The Mosaic Editor Window provides all the functions to load, view, edit and save BAMBI mosaic blocks. It can display the images as single frames or in a tiled mosaic view. Selected ROI from the time courses can be saved in image or movie format.

The "Image" menu allows the data to be displayed in different ways. The actual data set can be reordered to suit different capture patterns and images can be flipped or inversed.

When navigating 2-D or 3-D multi-frame mosaics, the "View" menu allows for 3 modes to view images on screen: One-up, Four-up, and All up. One-up will display a single field-of-view in 3-D space given the row, column, slice, and time point as determined by the position of the four slider bars. Four-up mode increases the display to include exactly four adjacent imaged at a time for a given time frame and region in space. Four-up mode effectively decreases magnification by a factor 2 but still maintains the base resolution for display. The All-up mode as the name suggests displays the entire tiled mosaic at the same base resolution for a specified time point and depth

(in the case for a hypercube or 3-D time course). The user can play the movie forward or backward through time, zoom in or out, and adjust the brightness and contrast settings. The brightness and contrast settings are very important controls to identify features in fluorescent data sets, as the dynamic range of the pixel intensities can be very small.

The Mosaic Editor is able to accommodate very large raw files, often 300 Gigabytes or more, with millisecond load times while navigating the image set. This is possible because the editor only loads into memory the current images that are displayed. This removes the limit imposed on most image editors that must load the complete file into memory before viewing.

5.3.2 Robot Control

The Robot Control group encapsulates all the functions required to view, edit and manipulate the devices attached through the Galil controller card. This currently includes the 3-axis stage and single axis micromanipulator, electromechanical shutter, and LED array panel. Various dialogs or panels can be accessed to control each of these processes. When the Robot Control group is activated for a given microscope, it creates a GUI dialog called The Navigation Panel (see Figure 31).

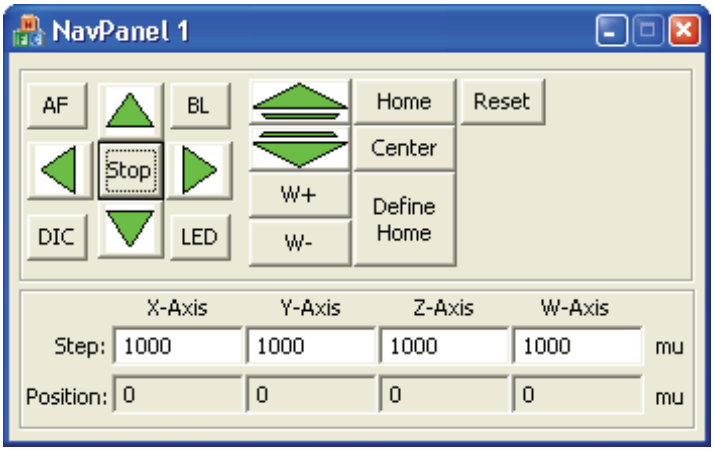

Figure 31: Navigation panel

The navigation panel is a pushbutton interface for manual control of the robot (3-axis stage and 1-axis micromanipulator). The colors of the direction arrows indicate the state of the motors. Green: motors are on. Yellow: motors have tripped a limit switch. Red: motor is off.

The function of the Navigation Panel is to provide the user with a pushbutton interface to control the robot. Direction arrow keys are provided to move all four motors by manual user mouse click command. The directional arrow keys are color coded to help identify the state of the motor

without adding too much clutter to the screen. Green indicates that the motor is turned on and is able to move in the direction indicated by the arrow. Yellow indicates that that the motor has encountered a limit switch in the direction indicated and will not travel in that direction any further. Red indicates that the motor is off and both directions of travel are not possible until it is turned on. An emergency stop button is provided to halt motor movement in all directions if needed. The user can also define a home position, home, and center on home as needed. The reset button is provided to reset the motors if an error during manual operation is encountered. This cycles the motor control *off* then *on*. The BL button is used to turn the backlash correction *on* or *off* for manual motor operation. When using the Navigation Panel in conjunction with a time course, the backlash correction should be enabled to keep the current position inline with the waypoint positions. If the user is not navigating for a time course, backlash correction can be turned off to increase the speed of the robot. The step sizes for manual control are user configurable and are shown in motor units only. The actual robot position is also displayed in motor units for each axis. If more motor detail is required an additional dialog called the Information Panel can be opened from the Main Dialog window.

The Information Panel displays the current state and configuration settings for each motor. This includes the dynamic information: torque, velocity, and static information: reference position, actual position, position error, stop code, and step size. Apart from step size, additional motor settings like torque, velocity, and acceleration can be configured from within the Motor Settings dialog.

BAMBI makes use of a proportional, plus integral, plus derivative (PID) controller to manage motor motion. This feature is provided by the Galil card itself, but the PID parameters must be provided for and tuned by the user via the Systems Properties Dialog. This dialog provides the user with a GUI to set and tune the PID setting for each motor as necessary (see Figure 32). This dialog was designed to allow the user to quickly change settings and immediately observe the results of those changes by having BAMBI automatically generate the step response. The step response for any given set of PID values can be displayed by pressing the *Get Step Response* button.

Generally, once the parameters are set for a motor they do not need to be changed unless the motor is replaced. However, due to varying operating conditions, such as heat and varying mass of the loads, it may become necessary to tune the parameters. If this must be done during a live cell imaging experiment, the time to tune the motors must be as short as possible. The automatic

step response feedback can significantly speed up tuning the system if the user is knowledgeable in reading a step response graph.

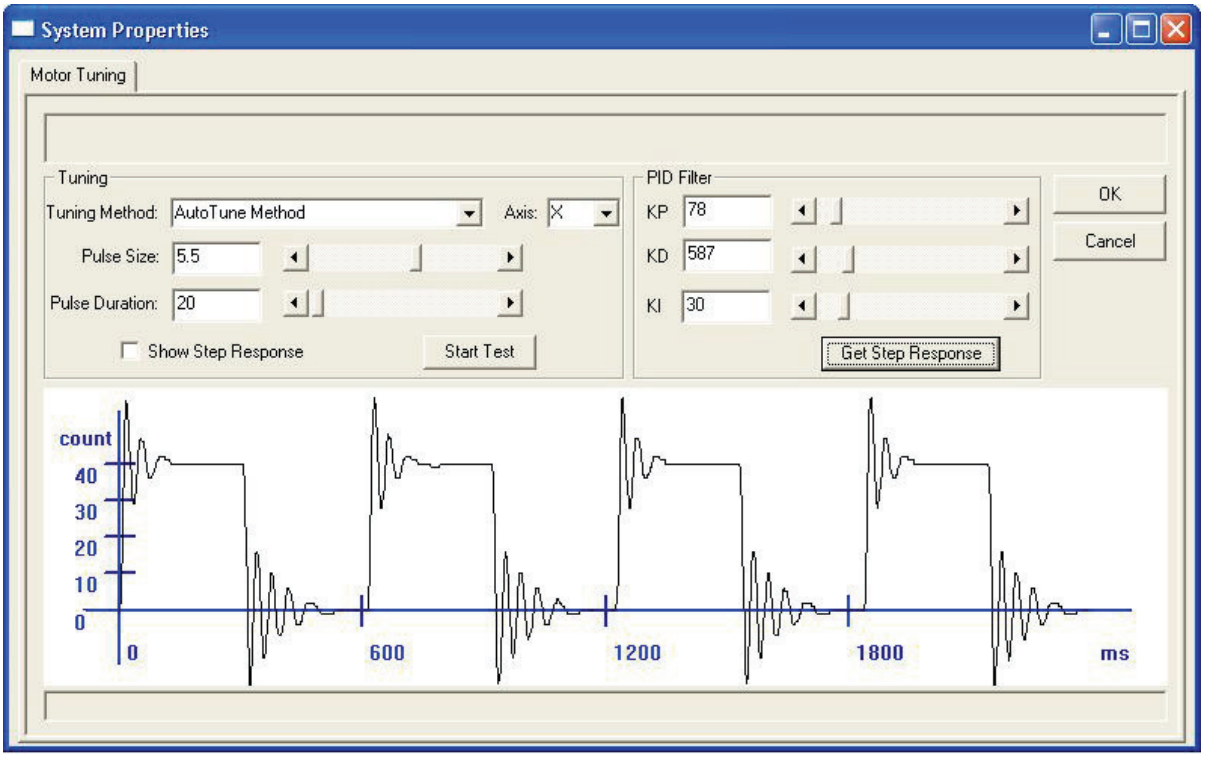

Figure 32: System Properties Dialog

The System Properties Dialog is used to tune the proportional-integration-derivative (PID) control loop for each of the motors. There are two automatic tuning methods in addition to the manual method. The dialog provides a *Get Step Response* button that will perform a step response on the motor and graphically show the results. This provides immediate feedback on the validity of the current control parameters.

Generally, the motor should attain the input position as quick as possible with no undershoot and as little over shoot as possible. It should maintain that position without error before commanded to return back. On returning back to the start position, it should do so in the exact same manner as it did for the step target. Figure 32 shows a motor that consistently overshoots the target and exhibits ringing but does ultimately stop at the correct value. This system would benefit from additional tuning.

Two methods of automatic tuning are available: *General Tuning Method* and *AutoTune Method.* Both methods employ the built in automatic tuning algorithms provided by the Galil controller card driver itself (Galil, 2006). The first method steps the motor back and forth while increasing the values of the PID until it becomes unstable, then the values are backed off to a final value that

may be appropriate. This is the most flexible method of tuning but it is not appropriate for the Physik Instrumente motors on the BAMBI 8-axis amplifier system. The *AutoTune Method* works well with the BAMBI 8-axis system. It operates by putting the motor through a series of pulses of a varying pulse and duration. The optimal cross over frequency is determined and the PID values are adjusted accordingly.

Sometimes it may be required to fine-tune the parameters after running one of the automatic methods for a satisfactory response. Various methods of manual tuning are available in the literature (Astrom *et al*., 1995; Lewis *et al*., 1997; Ziegler *et al*., 1942). A straightforward method to tune the PID values specific to the BAMBI 8-axis system is presented below:

1. Set KP to 50 -100.
2. Set KI to 0.
3. Set KD to an arbitrary value between 200 and 400 (Approximately four times KP).
4. Increase KP until the system just meets the target position on the step response curve
5. Gradually increase both KD and KP if necessary until a quick response time is seen.
6. If there is some steady state error, gradually increase KI until the final position error is zero and desired response time is met without too much ringing.

5.3.3 Camera Window

The camera window provides a real time display of the Sony CCD cameras allowing the user to change camera settings and view the current image on the screen. The user can independently adjust the view's brightness and contrast without changing settings on the camera itself. This helps to preserve the original dynamic range of intensity values for the image being collected. The user can choose between the available resolutions for the camera and the frame capture rate. While in operation the user can dynamically adjust the gain and shutter speed of the camera

hardware for the best performance as needed. The origin of the image, upper left corner on the screen, is mapped to motor units from the actual position of the 3-axis stage. The coordinates are displayed in the status bar at the bottom of the camera window. The position values are updated with the appropriate offsets as the user moves the mouse anywhere within the window view. Single image captures and movie captures can be saved to file as needed. The movie capture mode is useful for saving a video record of a manually controlled robotic procedure such as pick-and-place operations with the micropipette.

5.3.4 Mosaic Builder

The Mosaic Builder is the GUI that allows the user to set up automatic time courses. Time courses composed of one or more mosaic blocks. Each mosaic block contains a set of waypoints, illumination rules, and camera parameters (see Figure 33). The complexity of a mosaic block can range from a single DIC illuminated field-of-view captured through time to a set of fields-of-view in a 3-D volume with DIC and fluorescent illumination through time. Mosaic blocks are displayed in a recursive tree view to make viewing and modification of block settings very efficient and user friendly.

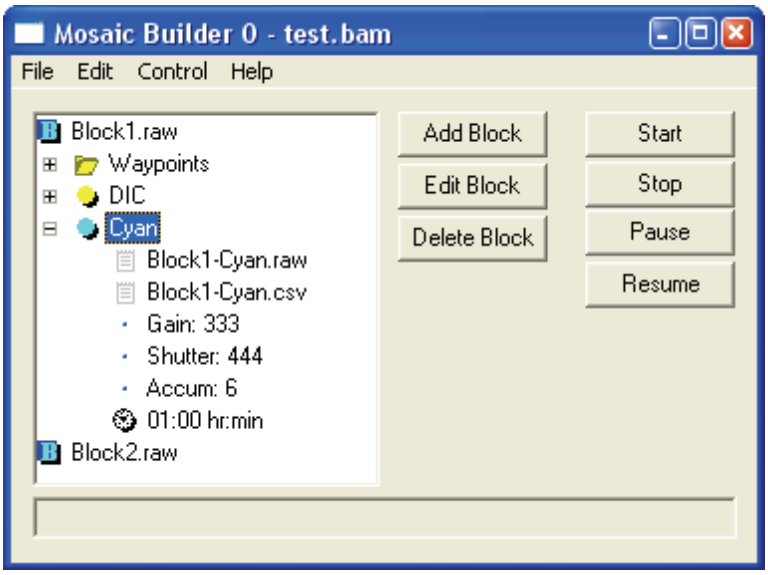

Figure 33: Mosaic Builder Dialog

The Mosaic Builder window is shown to illustrate the GUI design for the setup, control, and storage of long-term live cell imaging experiments. Mosaic blocks are displayed in a recursive tree view.

Each mosaic block with all of its respective properties is displayed in a recursive tree list format. This allows the user to select the level of detail as needed. It also provides a user friendly and intuitive interface for viewing and changing parameters on the fly. The ability to stop a time course and change the settings for a mosaic block after a live run has started is a boon to the success of the experiment. Allowing blocks to grow, shrink, and follow the ROI as needed greatly increases the amount of valid information captured.

5.4 Code Considerations

BAMBI has been developed entirely in C++ using Windows Visual Studio 2005 MFC. The camera control drivers were adapted from Chris Baker and Iwan Ulrich's version 6.3 CMU 1394 camera driver from Carnegie Melon University (Baker & Ulrich, 2004). Galil provided the motor control drivers and library files for use with Visual C++ 2005. Originally, the early versions of BAMBI employed Windows NT drivers and software developed in-house to support Physik Instrumente C-812 (Karlsruhe, Germany) motor control card but this code became obsolete when the new motors and controller cards were purchased. Throughout the development of BAMBI, different devices and applications were implemented to support the new specifications of experiments and assays within the lab. Designs were implemented and tested; redesigned and retested as needed; resulting in numerous changes to the existing software. Some of these additions were kept and some abandoned in favor of final approaches presented herein. In order to minimize the effort required on the programmer to implement these changes the underlying code had to be easy to change and swap in or out different code sections. To this end, BAMBI was developed within an object-orientated framework from the very beginning.

5.4.1 The Windows Programming Model

5.4.1.1 Microsoft's Foundation Classes (MFC)

Since the introduction of Windows in 1987, Microsoft had created an object-based Application Interface (Windows API) that allowed programmers to interact with system objects. As Windows and the Windows API developed further an object orientated wrapper for C++ was created called Application Frameworks (AFX) that later evolved into the Microsoft Foundation Classes (MFC) that is in use today. MFC is a set of object-orientated C++ classes that affords programmers all the advantages of object orientated code design. Object orientated code design depends on three guiding concepts: encapsulation, inheritance, and polymorphism. (1)

Encapsulation: hides the system objects such as windows, graphic cards, and hard drives and represents them as a simple handle or pointer. (2) Inheritance: grants the programmer the ability to inherit all the code from an existing class and even expand on it. (3) Polymorphism: is the ability to change the way an existing block of code from an inherited class is implemented (White *et al*., 1999).

5.4.1.2 Windows Message Loop

Every Microsoft Windows application has a message loop that allows it to handle local and system events in a queued manner. System events can be passed from one program or application to another and used to communicate between them. Local events are passed between windows, dialogs and threads within a single application. Every Windows program begins execution with a WinMain() function that provides an entry point for all the subsequent processes such as windows, dialogs, and views for the application. The WinMain() function is the equivalent windows version of the Run() function found in MS-DOS applications and there can be only one.

The WinMain() function illustrated in Figure 34 implements a continuous message loop that grabs the topmost message from the local event cue, translates, and dispatches it to the appropriate message handler. In this case, the message handler is the WinProc() for the window shown in the diagram.

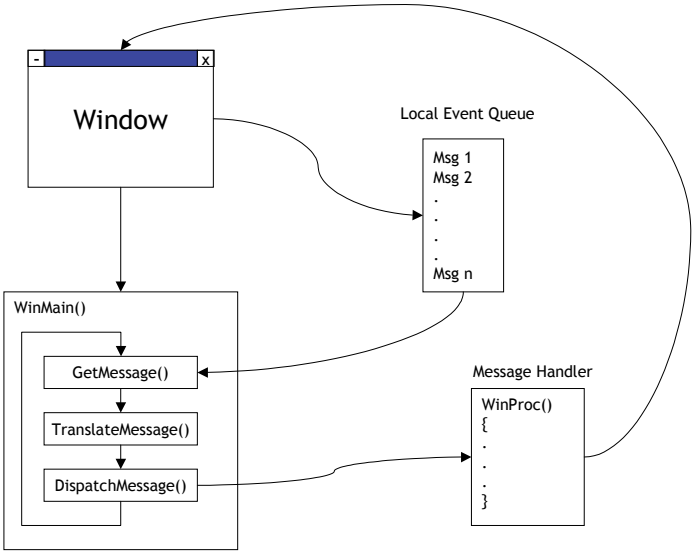

Figure 34: Windows Message Loop Event Handling

This figure shows the Windows main message loop event handling. Each instanced window communicates with the rest of the program via the Winmain() function. This diagram was adapted from (LaMothe, 2003).

5.4.1.3 Multithreading in MFC

In order to take direct advantage of multiple central processing units (CPUs) a solution must implement multiple threads. However, a single processor can still benefit from multi-threading as well by allowing applications to better control the concurrency of operations by the CPU. A thread is defined as a single unit of executing code within a process or application (White *et al*., 1999). In MFC there are two major types of threads: Worker Threads and User Interface Threads. A worker thread can complete tasks that do not require windows event processing or GUIs such as windows or dialogs. User interface threads have access to the event queue and can create and destroy GUIs as needed. Each Windows application has at least one thread object called CWinApp which is a subclass of the user interface thread.

Assigning worker threads is relatively straightforward and requires very little code to create and destroy them. Worker threads are useful to perform lengthy calculations that would otherwise tie up the main window thread. This is not ideal, as it will cause the window or dialog to lock until the required calculations have been completed. User interface threads on the other hand, require much more code to create and destroy them properly. However, they can instance user interface classes such as more windows and dialogs which the worker threads cannot.

5.4.2 BAMBI Class Structure

BAMBI has been designed in a modular fashion in an effort to keep the code groups within their own context as much as possible. In other words, if a module were removed from the code, the rest of the code should still be able to function normally. Obviously the jobs that the module may have performed would not be accessible, but the program would nevertheless be able to run and continue to perform the unaffected operations. Figure 35 illustrates how the classes of BAMBI are related to each other through ownership. The parent or owner of all BAMBI classes is the CBAMBIApp. It can create two graphical user interface threads: CMosaicBuilderThread and CNavpanelThread. It can also create a single instance of four classes: CRobotControl, CCameraFrame, CCameraFrame, CBAMBIDlg, and CChooseDlg. It can also create as many instances of the class CImageFrame as needed. Each one of these classes, except for the CChooseDlg, may in turn create other class instances as needed by the program.

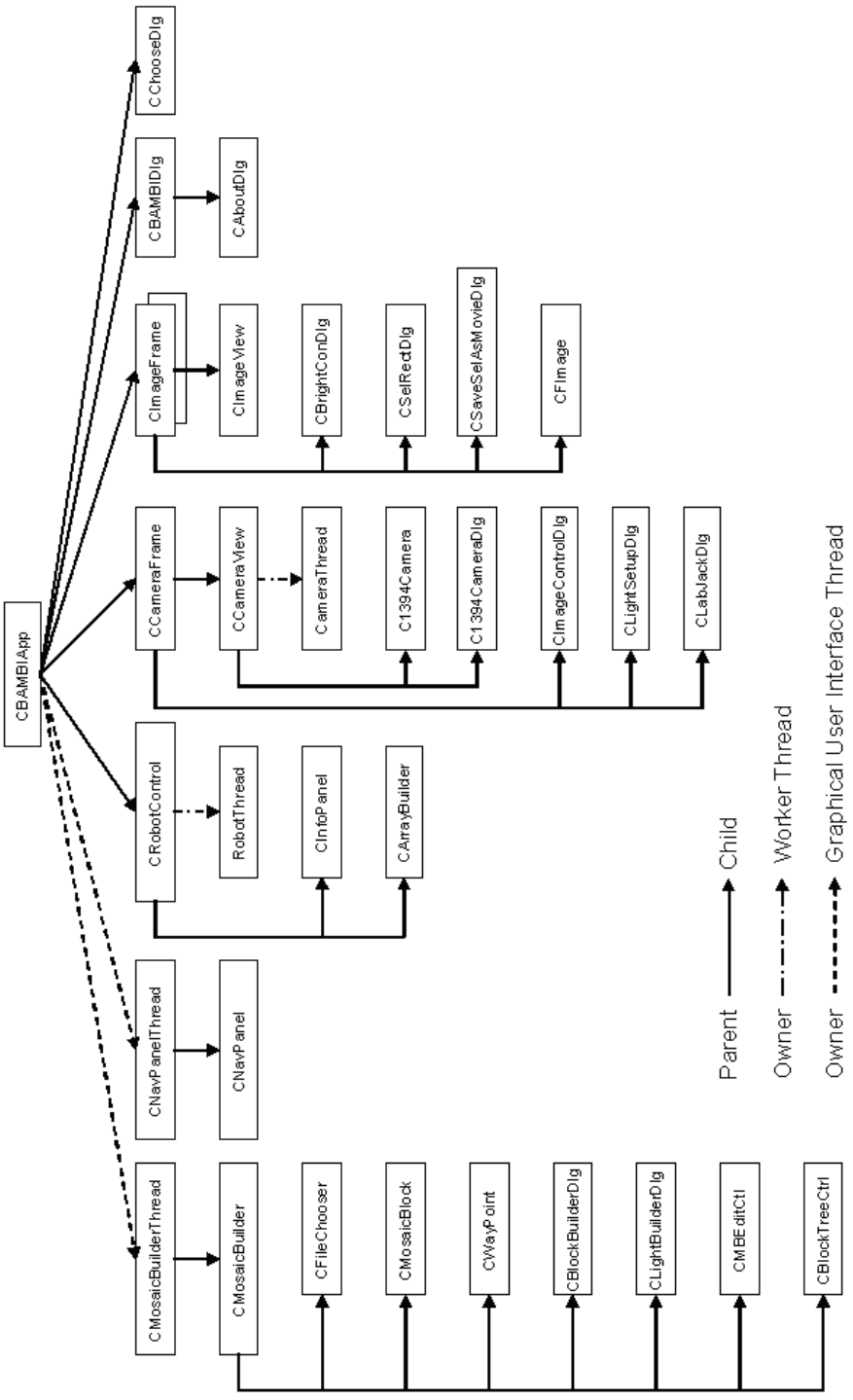

Figure 35: Class Ownership Diagram

This figure illustrates the class creation and ownership in BAMBI. Dotted lines represent new user interface thread objects instanced from the calling class and dash-dot lines represent worker threads.

5.4.2.1 CBAMBIApp

CBAMBIApp is inherited from CWinApp, the main user interface thread in this Windows application. Its job is to create the first GUI, in this case the CBAMBIDlg, and any subsequent windows or user interface threads as needed. It retains pointers and handles to the objects created, allowing them to be used by other classes, and in the event of a shutdown it can destroy them in a safe manner. It can also create the CImageFrame, CRobotControl, CChooseDlg, CCameraFrame, and CImageFrame windows in addition to two graphical user interface threads called the CMosaicBuilderThread and CNavPanelThread. Because the CImageFrame does not have limits on how many instances are allowed to run, CBAMBIApp can create more than one instance as needed. This allows the user to have multiple images or mosaic blocks open and displayed simultaneously on the screen at the same time.

5.4.2.2 CBAMBIDlg

CBAMBIDlg is the first GUI that opens and is the main user dialog interface through which the user is able to call on CBAMBIApp indirectly to perform desired actions. There is no visible window for CBAMBIApp other than the CBAMBIDlg dialog. CBAMBIDlg coordinates the actions of CBAMBIApp by providing the user with a menu dialog from where choices can be entered to instance the appropriate classes needed. Therefore, CBAMBIDlg remains available throughout the entire duration of the program. In most Windows applications the CWinApp is usually accessed through a main window interface instead of a dialog interface. A window interface supports a document view in addition to the menu options where as a dialog only has menu items. This is similar to opening Microsoft Word and having a blank document page show up ready to be filled with text. Since BAMBI does not have this need, in fact it is not even certain what kind of job the user has in mind, it is better to start with a list of choices before assuming a window view will even be needed.

5.4.2.3 CAboutDlg

The CAboutDlg is created by the CBAMBIDlg interface to display general information about the BAMBI program. This includes the currently running code version, copyright information, and a general dialog about the BAMBI and its creators.

5.4.2.4 CChooseDlg

The CChooseDlg is a dialog created by the CBAMBIApp to force the user to choose which microscope is to be used if it detects the 8-axis version of the Galil controller. The choice will be either M1 corresponding to axes 1-4, or M2 corresponding to axes 5-8. This allows CBAMBIApp to access the correct registry values for the servos, shutter, and LED array being used.

5.4.2.5 CMosaicBuilderThread

CBAMBIApp is responsible for the creation of CMosaicBuilderThread, a user interface thread. This thread manages the entire mosaic capture process by allowing all the mosaic builder related GUIs to run in a separate thread from the main user interface. The first task of CMosaicBuilderThread is to create a CMosaicBuilder dialog box from which the user can interact with. The decision to place the mosaic builder application in a separate thread was to avoid lock ups between the CBAMBIApp and the CMosaicBuilder classes. During automated image capture, the CBAMBIApp thread will wait on events from the DMC Controller card that would cause a single threaded process to become blocked or locked.

5.4.2.6 CMosaicBuilder

The CMosaicBuilder class is the main dialog GUI used for the creation and management of mosaic blocks for long-term live cell imaging. It displays the tree list view of the mosaic blocks and contains all the algorithms for running a time course. It also contains the code to load and export the "bam" files.

5.4.2.7 CFileChooser

The CFileChooser dialog is a subclass of the MFC CFileDialog. Its purpose is to provide a GUI dialog to allow the user to create, save, and load files from computer system. Sub classing CFileDialog allowed BAMBI to access to private variables in CFileDialog that were needed to separate file names from the file paths during saving and retrieval.

5.4.2.8 CMosaicBlock

A CMosaicBlock class contains all the parameters that define a BAMBI Mosaic Block. It is created by CMosaicBuilder and inserted into the CObject list of CMosaicBlocks for the current

time course. The structure and function of each parameter of CMosaicBlock is fully defined in Appendix C.2.

5.4.2.9 CWayPoint

Each CMosaicBlock class contains a CObject list of CWayPoints that are created when the mosaic array is calculated. CWayPoint is a subclass of CObject and contains the ID, (x, y, z) coordinates, and state of the enable for the waypoint.

5.4.2.10 CBlockBuilderDlg

The CBlockBuilder class is a dialog GUI created by CMosaicBuilder to enable the user to create a mosaic block. It also allows the user to easily generate waypoints from defined coordinates and parameters.

5.4.2.11 CLightBuilderDlg

The CLightBuilderDlg class is a dialog GUI created by CMosaicBuilder to enable the user to setup the illumination settings for the mosaic block. This includes DIC and multi-channel fluorescence.

5.4.2.12 CBMEditCtl

The CBMEdtCtl is a small dialog GUI created by CMosaicBuilder to allow the user to easily navigate to the waypoints in a mosaic block. Once at a waypoint, the coordinates can be adjusted if needed and the results saved. CMBEditCtl also allows the user to enable or disable the waypoint from being captured.

5.4.2.13 CBlockTreeCtrl

CBlockTreeCtrl is sub classed from CTreeCtrl and is created by CMosaicBuilder. This class implements the mosaic block tree view that is displayed in the CMosaicBuilder dialog.

5.4.2.14 CNavPanelThread

CBAMBIApp is the parent for the CNavPanelThread, a user interface thread. Upon creation, this thread instances the CNavPanel dialog. Like the CmosaicBuilderThread, a user interface thread

is required to display the Navigation Panel to avoid lock ups when the main user thread is waiting on a robot move.

5.4.2.15 CNavPanel

The CNavPanel class is a dialog created by CNavPanelThread to allow the user to interact with and control the 3-axis stage and micromanipulator. It is a Friend Class of CRobotControl. The friend status allows CNavPanel to access all the private members and functions of CRobotControl. However, since CNavPanel can access the private functions of CRobotControl, great care must be taken to ensure that it takes into account any offsets that may have been imposed by CRobotControl. Otherwise, it is possible to unintentionally access the control of the wrong four axes that may have been granted to possible concurrent instance of the BAMBI program.

5.4.2.16 CRobotControl

CRobotControl is inherited from CWnd and serves as the main interface and interpreter to the Galil DMC Controller card. It is created by CBAMBIApp directly and runs within the same thread as CBAMBIApp. Technically, CRobotCotnrol is an instance of a window interface, but it is never made visible. There are several reasons for this: In order for a class to respond to system event messages like user configured interrupts they must be able to access the WinMain() message loop which is available to classes derived from CWnd. In addition, CRobotControl serves as the parent window for CInfoPanel and CArrayBuilder dialogs. Because dialogs minimize whenever a parent window is minimized it was not appropriate to attach these dialogs to any parent window that could be inadvertently closed or minimized. Since the CRobotControl is a window class, but it has not been made visible, these child dialogs can remain (on top) when needed and are never minimized due to the parent window being minimized.

The CRobotControl class marshals the 3-axis stage, 1-axis micromanipulator, LED panel, and electromechanical shutter. This class is made available to the other windows, dialogs, and threads by making it a global object. It operates as a gatekeeper, exposing all the functions necessary to operate the DMC controller in public functions. By forcing the classes to use the public methods exposed by CRobotControl it becomes straightforward to make changes to the way the controller is used because the code only needs to be modified in one class. This encapsulation allows the code to adapt to changes such as replacing the controller with a new

design or manufacture very quickly. This encapsulation also has the benefit of being able to providing translations or offsets globally in one place. This is important when the program is started on an eight axis-controller card because the CRobotControl class must know which four of the eight axes are to be used but the calling function does not. Therefore, it can simply add an offset of 0 or 4 to all the internal commands without having to involve every part of the program that needs to operate the controller.

5.4.2.17 CRobotThread

During CRobotControl creation, a new worker thread called RobotThread is started with a handle to the DMC Controller Card. This worker threads sole task is to pole the controller for any errors in communication. It was implemented as a work around for a problem found when running two instances of the BAMBI program on the same controller card. When one application terminates its HANDLE to the DMC Controller Card, the driver issues a card command that shuts down any communication with the buffer. This is not a problem unless you have another application using the card at the same time, as it will lose communication with the update buffer as well. The worker thread poles the card's buffer count, if it should ever receive the same value twice in a row, it will issue a command to reinstate communication with the buffer. Galil Inc. has been informed of this issue with the "Accelera" models, but to date has not yet published a fix for it.

5.4.2.18 CInfoPanel

The CInfoPanel is a dialog GUI created by CRobotControl to display and edit the current state and configuration settings for each motor.

5.4.2.19 CArrayBuilder

The CArrayBuilder is a dialog GUI created by CRobotControl for semi-automated construction of microwell plates.

5.4.2.20 CCameraFrame

The CCameraFrame is inherited from CMainFrame and contains a single CView object, the CCameraView. The CCameraView is responsible for the display of the video images captured by the Sony 1394 Firewire camera. It creates a C1894Camera object and passes its handle to a new worker thread called the CameraThread. This thread is responsible for the continual update

of the display image buffer located in memory. The CCameraView also exposes access to its settings with a GUI dialog, the C1394CameraDlg, whenever it is required. The CCameraFrame is also the parent window for CImageControlDlg, CLightSetupDlg, and CLabJackDlg. CImageControlDlg is a GUI panel that allows the user to change the hardware gain and shutter speed settings for the camera. The CLightSetupDlg allows the user to configure the LED panel lights and CLabJackDlg allows the user to setup the LabJack hardware settings.

5.4.2.21 CCameraView

The CCameraView is inherited from CView and is the parent of C1394Camera and C1394CameraDlg. CCameraView implements the CameraThread as well as all the functions necessary for the control of the C1394Camera class.

5.4.2.22 CameraThread

The CameraThread is a worker thread created by CCameraView. Its purpose is to continually capture the current image from the CCD camera buffer and write it into the memory buffer. It is the job of the CCameraView to continually access the memory buffer and display the image as needed.

5.4.2.23 C1394Camera

The C1394Camera is a class that encapsulates a selected 1394 Firewire CCD device to be used by the program. This class is made available by the C1394Camera driver as a header only. The source code resides inside the driver "dll" file.

5.4.2.24 C1394CameraDlg

The C1394CameraDlg is a GUI dialog used to change the settings for various features for the CCD camera. This includes parameters like brightness, contrast, gain and shutter speed. This functionality is provided by the C1394Camera driver.

5.4.2.25 CImageControlDlg

The CImageControlDlg is a GUI dialog created by the CCameraFrame class to evaluate the fluorescence illumination settings. It allows the user to try out various gain, shutter, and

accumulates and see the results immediately. The accumulated images are summed and the resulting image is displayed in the Mosaic Editor Window.

5.4.2.26 CLightSetupDlg

The CLightSetupDlg is a dialog GUI that is used to setup and configure the light sources that are availible for illumination. This includes the DIC and LED channels. Information such as wavelength, color, and a short name can be saved in the registry for each of the channels. It also has buttons to turn the channels *on* or *off* for testing.

5.4.2.27 CLabJackDlg

The CLabJackDlg is a dialog GUI that is used to configure any devices that are attached to the Labjack controller. Like the CLightSetupDlg, it has buttons to allow the user to turn *on* or *off* the channels for testing.

5.4.2.28 CImageFrame

CBAMBIApp creates the CImageFrame, which inherits from CMainFrame, to display and edit images, mosaics, or time courses. BAMBI supports more than one CImageFrame at a time in case the user wants to have several files open.

5.4.2.29 CImageView

The CImageView is an implementation of the CView class and is used to display an image inside the CImageFrame. Each CImageFrame has one CImageView object.

5.4.2.30 CBrightConDlg

The CBrightConDlg is a GUI dialog used to adjust the brightness and contrast settings for the current CImageView.

5.4.2.31 CSelRectDlg

The CSelRectDlg is a small GUI dialog used to help the user select a rectangular area on the current CImageView image. This is used for extracting parts of a time course into a separate file as a movie or an image.

5.4.2.32 CSaveSelAsMovieDlg

This GUI dialog is used to save a rectangular selection of a mosaic block opened in the Mosaic Editor as a movie.

5.4.2.33 CFImage

A CFImage is a CObject class that contains all the information to extract an image from a raw file. The CFImage class contains a pointer to a location in a "raw" file, the number of bytes to read, and the coordinate placement of that image within a mosaic block. When Mosaic Editor opens a "raw" image file of a mosaic block, it creates a CFimage object for each image in the file and places them in a linked list. Mosaic Editor is then able to quickly access any image needed by using the CFImage class to grab the data as needed.

Chapter 6
Applications of BAMBI

Much of the work presented in the present chapter is the result of the combined effort of several students whose work spans the last four to five years. My involvement started in the summer of 2003 while working as a co-op student working in the Lab for Single Cell Bioengineering at the University of Waterloo. At that time, I was given the task of writing software to interface a 3-axis stage to a microscope and visualize data captured via an attached digital camera. I managed to finish this task in the four months allotted. Upon graduating, I decided to return to the lab to build upon my prior work as fulfillment towards my Masters of Applied Science degree.

The result of this work has lead to the development of a completely new automated microscopy system entitled Bio-Assembly, Mosaic Building, and Informatics (BAMBI). The process of its development and iterative testing was tied directly to the requirements of the studies that were being run by other students in the lab at the time. I was directly involved in many of the experiments providing direct support for the electronics and even performed some of the cell culture protocols for the 5-day CFU Hill colony assay. These studies have shaped the requirements and final outcome of BAMBI.

6.1 Monolayer Cell Cultures

Previous work introduced a novel cell culture chamber, herein referred to as the "gap chamber", which could be used to image cell aggregates as a true monolayer (Ramunas *et al*. 2007). The design effectively restricted the growth of cell aggregates to a single layer rather than a multilayer thus avoiding light from other cells on top and below obscuring the focused image. This successfully facilitated the imaging and lineage analysis of individual cells within an aggregate while allowing high resolution "confocal like" DIC contrasting. Originally developed to view murine neural stem cell neurospheres (Ramunas *et al*. 2007), it has also been used to image primary rabbit blood cells (unpublished work), murine embryo bodies (unpublished work), murine hematopoietic stem cells (Dykstra *et al*. 2006), and human islets of Langerhans (Moogk *et al*. 2007). The use of the gap chamber allowed many of the 2-D time course experiments that have been captured by BAMBI to be conducted. Its introduction also served as the starting point for BAMBI research and development.

The success of the first murine neural stem cell assay showed that long-term live cell imaging could be achieved and the results revealed relationships between the lineage, phenotype and microenvironment. However, since neurodisks formed only from a neural stem cell progenitor, it was a rare event. This restricted the imaging to be done at a low resolution of 5x until a cell colony was observed to form. Only then could one of these colonies was selected to be imaged at the higher resolution of 40x. This made high-resolution movies of the initial stage of neurodisk formation difficult to impossible to capture. In order to capture these early events we needed to implement an automated stage to capture as much of the area of the gap chamber as possible at high-resolution. This motivated the design of BAMBI and its requirement to construct 2-D time course images for future cell culture work.

6.2 Hematopoietic Stem Cell Assay

Time lapse video imaging offers unique opportunities to determine how specific physical properties of individual living cells change with respect to each other over time and under different conditions. Here we wanted to know if time-lapse video imaging could be used to identify previously unidentified behavioral traits of hematopoietic stem cells (HSCs) with functionally validated long-term multilineage repopulating activity *in-vivo*. In other words, could long-term image tracking be used to identify behavioral traits that could be used in the future to uniquely identify HSCs. The complete details of this work can be found in the original published work (Dykstra *et al*. 2006).

6.2.1 Method

To search for new indicators of self-renewing hematopoietic stem cells, highly purified populations were isolated from adult mouse marrow, micromanipulated into a specially designed microscopic array, and cultured for 4 days. During this period, each cell and its progeny were imaged at 3-min intervals. Individual clones were then harvested and assayed for HSCs in mice by using a 4-month multilineage repopulation endpoint.

Cells were cultured in custom fabricated microwell chambers. These microwell arrays were constructed by applying silicone gel to a glass coverslip to form a film approximately 20 μm thick. Before the gel was allowed to set, the slide was attached to the microscope stage and a 100 μm wide glass scraper tool was attached to the BAMBI 3-axis micromanipulator. BAMBI was then used to machine sets of perpendicular rows to form the array of microwells (see Figure 36.A

and B). A short glass tube was then affixed around the array to form a reservoir to contain the culture medium.

To deposit the cells within the array, the entire reservoir was filled with 1 ml of medium containing approximately 50 cells that were then allowed to settle. After settling, each of the 40 microwells was then loaded with a single cell by repositioning the cells using a glass micropipette held stationary with the tip end at the focal plane of the microscope. The cell chamber itself was translated in x, y by the BAMBI 3-axis stage for cell pick-and-place operations. The micropipettes were made from capillary tubes (3-000-203-G/X; Drummond) by using a vertical pipette puller (Model 720; Kopf) and cut with a single-crystal diamond tipped glass etcher to give an opening 15–30 μm wide. Images were obtained on a Zeiss Axiovert 200 microscope equipped with phase-contrast optics and a Sony XCD-SX900 digital camera. Cells were exposed to light only during imaging. A single stationary field-of-view was captured over time at 3 minute intervals for approximately 4 days. Each cell in each image of the 1850-image time course was scored for morphological characteristics, location, and parentage by using human-assisted custom cell-tracking software that generated pedigree diagrams with other data superimposed on them for visualization. Data from these diagrams were then imported into standard analysis programs (EXCEL, MATLAB, and PRISM) to test correlations between candidate biomarkers and HSC activity.

6.2.2 Results

The results of the experiment showed that there were indeed characteristics of the HSCs that could be used to predict an HCS with an efficiency of 63%, an increase in previous discrimination methods of 2 to 3 fold. The discrimination attributes were reduced cell cycle times and lack of uropodia during the 12 hours immediately preceding injection of the cells into the recipient mice. Figure 36 presents a summary of the results.

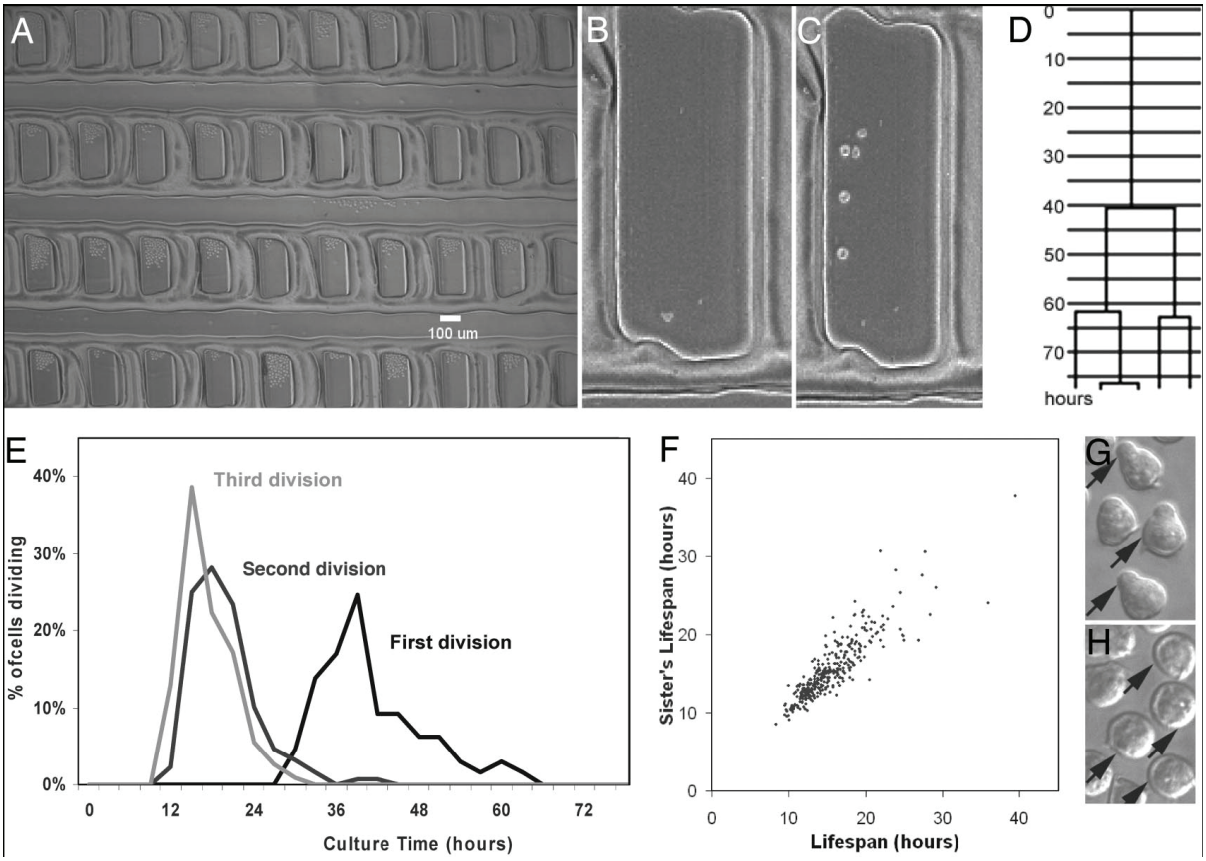

Figure 36: Microfabricated array and representative culture results

(A) A digital image of an array showing 40 silicone microwells, each capable of holding up to approximately 150 cells that can be tracked simultaneously. (B) Higher-power view of a representative well containing one cell suspended in medium. (C) Close-up of the well shown in B after 4 days. (D) The pedigree diagram of the clone that developed in the well shown in C, illustrating the precision with which sequential cell divisions could be timed. (E) Cell-cycle time histogram of 67 individually cultured cells. A delayed initial cell cycle was observed, followed by synchronously maintained subsequent divisions. Cells that did not complete the corresponding cell cycle were excluded from this histogram. (F) Comparison of the cell-cycle times of individual progeny pairs, demonstrating the pronounced synchrony retained between such ‘‘sister’’ cells, despite the wide range of cycle times observed. Cells whose sisters did not complete the corresponding cell cycle were not included in the plot. (G) Example of part of a clone in which many cells have large trailing projections (uropodia). Arrows indicate cells with uropodia. (H) Example of part of a clone in which very few cells have uropodia.

6.2.3 Discussion

The use of BAMBI was a critical factor in the micro fabrication of the multiwell arrays. However, the first arrays were made by manual command instructions to control the end effector movement that soon became tedious to perform. This laid the groundwork for an automated array

creation add-on module that would simply create the complete array given a relatively few set of inputs.

Although BAMBI lacked a separate axis for the micropipette movement the x-y stage movement enabled researchers to pick and place the cells in to and out of the microwells with great precision. The need for another axis to control vertical pipette motion was clear as it was quite difficult to do this by hand and wasted a lot of precious time. The latest design of BAMBI has incorporated a 4th axis to automate this motion and cell seeding and sorting times have been drastically reduced. Additional micropipette designs such as the miniaturization of the pipette inner diameter and use of a digital pressure transducer to provide feedback on the fluid pressure and direction inside the micropipette has also improved performance.

Use of the micropipette for the cell repositioning while viewing through the eyepiece indicated that it would be preferable to have the keyboard controller inside the flow hood for right-handed operation. The current version of BAMBI has a radio-controlled numeric keypad inside the hood that can be used to control movement.

The level of detail obtained in the 5x magnification time course provided enough information to track and identify uropodia, but much of the inner cell was not resolvable. At this time BAMBI could not yet capture multiple fields-of-view and only a stationary time course could be conducted. This magnification limited the pixel count from 5 to 6 pixels per cell which is far less that what is needed to observe inner cell contents. The pictures shown in Figure 36.G and H are representative of cells that were captured with a higher power objective. This shows the level of detail that could be attained if automatic panning had been available.

This early work was confounded by the limitations of the hardware. The 4-axis controller card, C-812 (Physik Instrumente, Germany), was obsolete in that it was originally developed to work on Windows 3.14. To allow it to function on Windows XP a custom memory access driver was developed. However, an intermittent problem with the communication buffer would cause unintended insertions and deletions in the command buffer that could have unpredictable effects on stage movements. This made long term live cell imaging frustrating as the micropipette tip was inadvertently shattered multiple times and 2-D time courses were unreliably captured. The final solution was to replace the hardware with a completely new state of the art system.

6.3 CFU-Hill Formation Assay

The process of vasculogenesis (blood vessel development following the differentiation of endothelial progenitor cells (EPC) or angioblasts) is believed to persist into adulthood. This has generated interest in the use of the putative EPC for neovascularization of ischemic or injured tissue and for the clinical assessment of risk factors for various diseases. Although this cell has not been characterized as yet, a number of groups have reported the ability to culture a unique colony type containing a central core of round cells with radiating spindle shaped cells at the periphery. We have termed these unique colonies Colony Forming Unit-Hill or CFU-Hill, and their assay the 5-Day CFU-Hill assay. Quantification of colonies correlated with various clinical disorders with reduced colony number associated with cardiovascular risk and function, chronic obstructive pulmonary disease and rheumatoid arthritis. In an attempt to understand the origin and behaviors of the cell population(s) responsible for colony formation, we used long-term live cell imaging to characterize and track the development of individual colonies over the culture period.

6.3.1 Method

Whole blood was collected from 30 normal donors (age range 24-55 years), peripheral blood mononuclear cells (PBMC) were isolated and the 5-Day CFU-Hill assay was performed. The CFU-Hill assay is performed using EndoCult® media (StemCell Technologies Inc.) and human fibronectin coated multi-well plates. On day 2 of the assay, non-adherent cells were collected plated on three fibronectin coated glass coverslips in 24 well dishes. The dishes were imaged for the remaining 3 days on three 200 Axiovert (Zeiss, Germany) microscopes. One of the microscopes was fitted with a BAMBI 3-axis stage controller and was used to image a single well of a 24 well plate. A 10 x 10 field-of-view time course was collected every 7 minutes.

6.3.2 Results

Long-term live cell imaging showed that plated cells immediately began to display very different morphologies. The four distinct morphologies were classified as small round cells (SRC), small podiated cells (SPC), large round cells (LRC), and spindle like cells (SLC) shown in Figure 37.

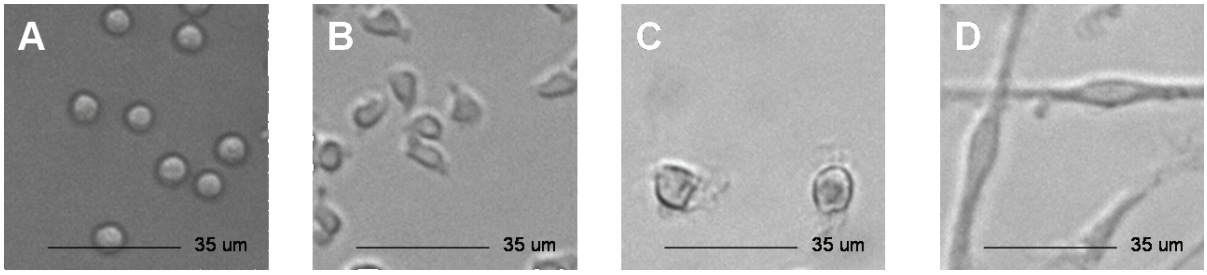

Figure 37: Four sub-populations of morphologically distinct cells contribute to CFU-Hill formation

A. Small round cells. B. Podiated cells. Irregular shaped cells with protruding podia. C. Large round cells, cobblestone appearance with tiny protruding cilia. D. Spindle like cells.

A novel discovery of an event that took place on day 4 of the CFU-Hill assay was made possible only though time course imaging (see Figure 38). This sequence demonstrates the plasticity of the LRC phenotype as they can transform into a SLC and back again in as little as 7 hours. Without time course imaging these would be scored as separate cell types when in fact they are the same cell with different morphologies.

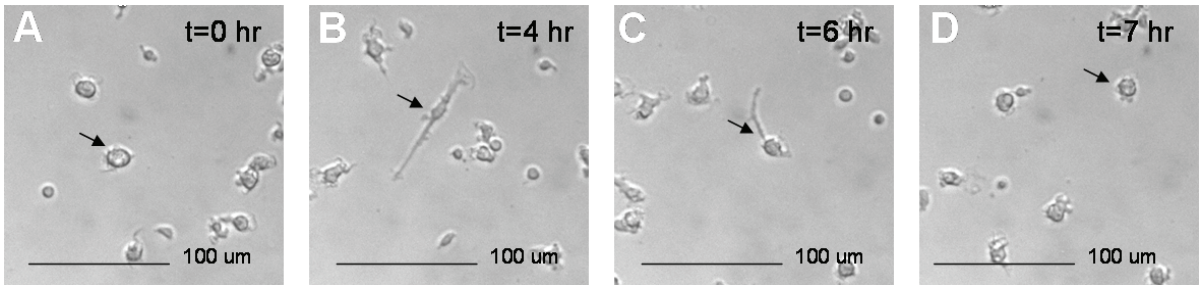

Figure 38: Plasticity of large round cell phenotype

A. Large round cell at t=0 hr. B. Same cell has transformed into spindle like phenotype at t=4 hr. C. The same cell is in the process of returning to the large round phenotype at t=6 hr. D. The same cell has returned to the large round phenotype and has begun to move away from the region at t=7 hr.

Results of large field imaging showed that the most important cell in CFU-Hill formation was the LRC phenotype. Not only was it identified as the source of all the spindle-like cells, it was also shown to be primarily responsible for the CFU-Hill formation itself. This result could only be shown clearly by tilting the microscope stage by 5º. Preliminary results had confirmed that this approach yielded a similar number of CFU-Hill without the high numbers of SRC. The tilt ensured that senescent or non-adherent cells and debris would gradually leave the region of interest allowing for a much clearer picture of CFU-Hill formation. In Figure 38.C, a picture of a

CFU-Hill produced by this method shows that the most dominant cell type present is the LRC and SLC. A second CFU-Hill can be seen in the lower right section of inset B. This CFU-Hill formed near a piece of debris that appeared to nucleate colony formation.

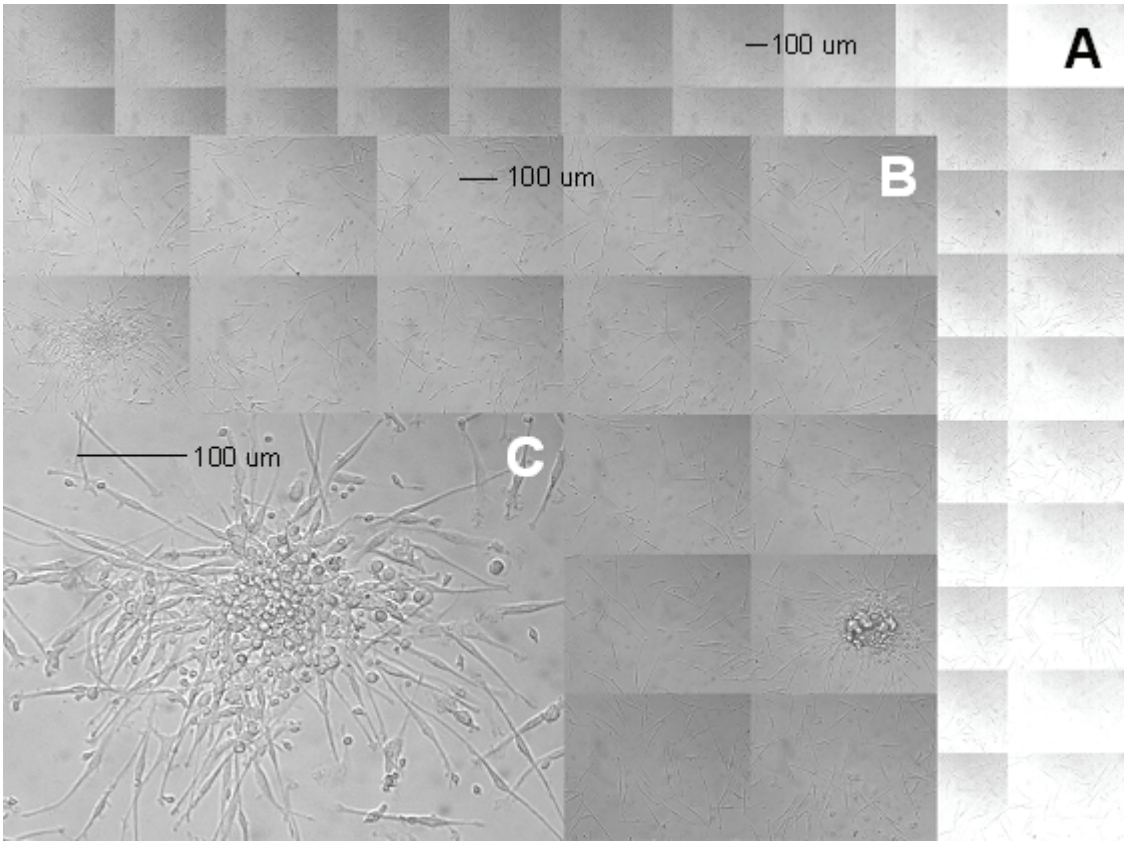

Figure 39: Multi-scale large field mosaic of the CFU Hill assay on day 5

A. Original 10x10 microscope image mosaic B. Zoom of 6x6 section at 150% C. Zoom of single image frame at 500% showing a typical CFU-Hill.

Additionally, it was shown that CFU-Hill formation was a rare event. This is evident in Figure 39, wherein only 2 hill colonies formed within a region of approximately 5 millimeters square.

Morphologically distinct cell populations can also mobilize to resemble CFU-Hill formations with varying levels of similarity throughout the five day experiment (see Figure 40).

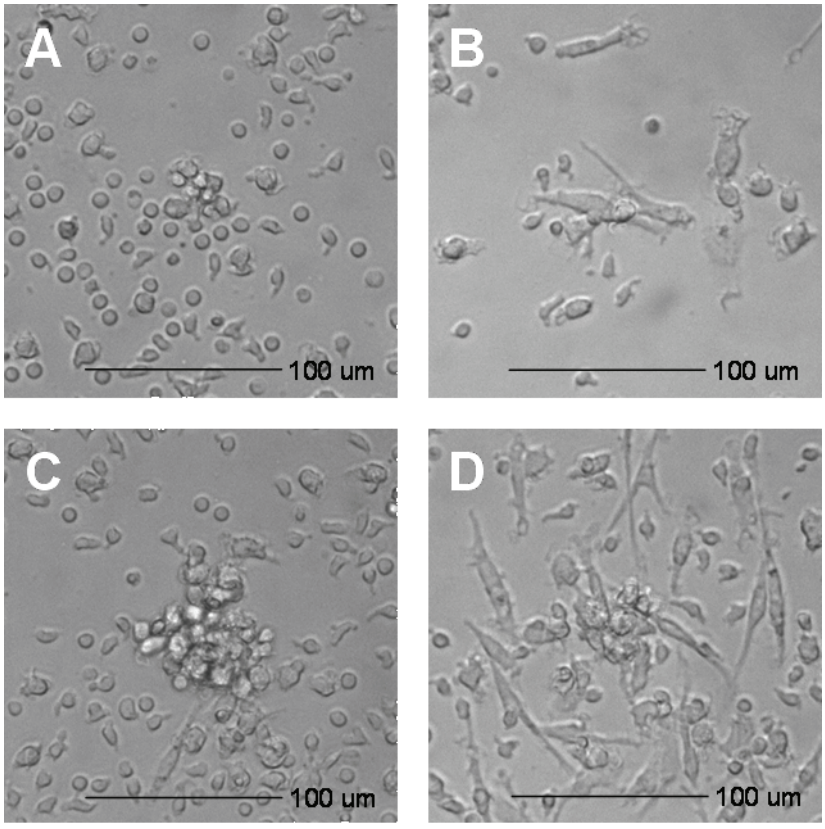

Figure 40: Stages of CFU-Hill Formation

A. Proto-Clusters. B. Proto-Clusters with Spindles. C. Clusters. D. Clusters with Spindles.

The Proto-Clusters in Figure 40.A are characterized as aggregates of three or more cells that are transient, but maintain a cohesion and similar travel path for at least 20 minutes. They may be composed of one or more cell phenotypes, large round cells (LRC), spindle like cells (SPC), and small podiated cells (SPC). Figure 40.B shows Proto-Clusters with Spindles characterized by having at least one SLC and two or more cells of any other phenotype. They are transient in nature as the round cells can leave almost as fast as they arrive. These SLC clusters typically start to form after day 4. A cluster is shown in Figure 40.C. Clusters are aggregates of fifteen or more cells that last more than several hours. They may be composed of one or more cell phenotypes LRC, SPC, and SLC. The final stage of CFU-Hill formation is characterized as clusters of which some of the cells have started to undergo spindle transformation (see Figure 40.D). Once spindle formation has started it will continue until many more of the large round cell members have transformed into the spindle like phenotype at which point the central mass of the cluster will almost disappear.

6.3.3 Discussion

CFU-Hill colonies are the result of the aggregation of cells and are not clonal as originally believed. Endothelial precursor cells in the CFU-Hill colony assay are composed of a heterogeneous sub-population that require further classification. The source of the spindle like cell phenotype is the result of the large round cell phenotype changing morphologically into the spindle like cells.

Large field-of-view long-term live cell imaging can provide new information and answer questions about low frequency events at single cell resolution. CFU-Hill colony formation requires multiple coordinated cellular behaviors including morphological changes and cell migration, likely in response to a chemokine gradient. Characterization of the cell types and regulatory molecules that support the formation of CFU-Hill colonies may increase our understanding of clinical disease. The probability of forming a CFU-Hill colony is quite low (.025 per image) compared with the number of proto-clusters and proto-clusters with spindles (~4 per image). Cluster formation has a probability at a peak value of about 0.5 per image, 40 X greater than the count of CFU-Hill formed.

We have demonstrated that using large-field long-term live cell imaging dynamic events and cell activities can be recorded and classified even for low frequency events such as CFU-Hill formation. Future work will focus on using these observations to identify and classify progenitors with a potential to go on to form a CFU-Hill. If this work is successful, we will recover cells for further molecular characterization. This project is an example of the application of behavior activated cell selection (BACS) and lineage/cell culture informatics.

6.4 Imaging Human Islets of Langerhans

Type I and II diabetes are associated with the autoimmune destruction of insulin producing beta cells or impaired beta cell function. Islets are composed of tens of hundreds of cells consisting of an outer shell of alpha cells shrouding an inner mass of beta cells. Recent evidence has shown that there is a possibility for insulin therapy through islet transplantation. As donor islets are of limited availability, there is a need to be able to expand islet cell mass *in-vitro*. Long-term live cell imaging has the potential to identify the specific cells and processes involved in islet transformation. Using a novel imaging chamber, it was shown that it is possible to construct a high-resolution three-dimensional time course of a human islet while maintaining the structure of the islet cells and the intercellular matrix (Moogk *et al*. 2007).

6.4.1 Method

Imaging chambers were constructed with a gap chamber to ensure the cells would not grow more than 4 cells in height. A 2 x 8 millimeter glass slide was glued at the short ends to a coverslip with silicon adhesive glue. A short 12 mm inside diameter glass tube was glued to the coverslip to form a watertight well around the gap. Human islets were isolated from cadaveric donor organs at the Montreal General Hospital.

To load the islets under the imaging chamber the top surface was lifted from the bottom cover slip using tweezers and 5-10 μL of the suspension was pipetted onto the coverslip at the opening of the imaging chamber, which was then drawn into the gap space by capillary action. The top surface was gently lowered to minimize ejection of the loaded islets and microspheres.

Islets were imaged on an inverted microscope (Axiovert 200, Zeiss Germany) with a stationary stage and a single z-axis focus control motor. Chambers were maintained at 37oC in a 5% CO2 humidified air atmosphere. To minimize phototoxicity, an electromechanical shutter was used to ensure incident light from the microscopes only reached samples while images were being acquired. Images were captured at a 3 minute interval using a digital camera (XCD-SX910, Sony Japan). The islets were manually focused on an optical section deemed to be near the center of the islet. The focus was locked, but readjusted from time to time to account for slight focal plane drift.

6.4.2 Results

The imaging chamber successfully restricted the z-axis thickness of the culture and kept the islets within the focal range for high-resolution DIC imaging. The gap within the chamber allowed the islets to exist in an *in-vivo* state while limiting the islet thickness to 2-4 cells in height. This facilitated the successful z-axis optical sectioning as shown in Figure 41 and subsequent tracking of each cell history within the islet.

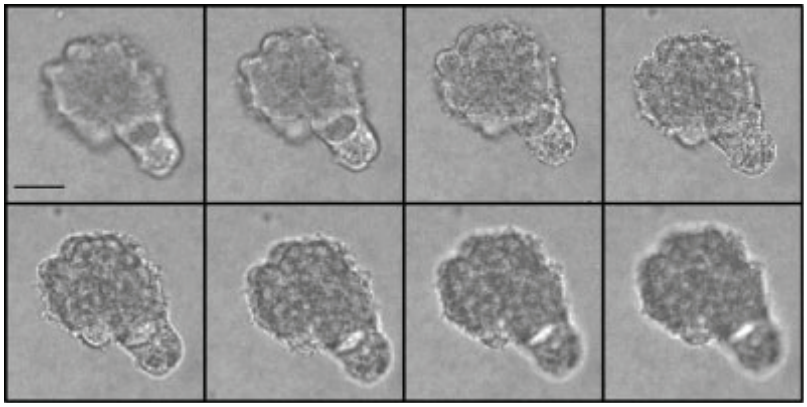

Figure 41: Eight optical sections of a human islet of Langerhans

Z-axis optical sections of a human islet in a 25 mm gap chamber using DIC illumination. The optical sections are 5 µm apart and include an extra section above and below the islet to ensure the entire islet was imaged. The scale bar equals 25 µm.

At the end point of the experiment, 5 days, the islets were fixed and stained with fluorescent markers for the islet hormones insulin, glucagon, and somatostatin. The Islets cells identified with fluorescent imaging could be related to the final time point of the DIC time course which allowed for movies to be observed with the knowledge of cell phenotype.

6.4.3 Discussion

This study showed that 3-D time course imaging was useful in the analysis and characterization of cellular activities in cellular aggregates for transplant. As Islets are a gift from human donors and only some (less than 10) from one donor are amenable for imaging, care must be taken to insure that as many of these events as possible are captured. This means that BAMBI must be able to simultaneously capture several different islet locations for long-term live cell imaging. At the time of this study there was only one field-of-view available with only motion of travel (z-axis) automated. The current BAMBI design allows for multiple locations or blocks to be imaged simultaneously via the automated 3-axis stage.

Focal drift and the gradual settling of the islets within the collagen matrix required that multiple adjustments were necessary to keep the islet centered within the z-stack. To account for this, extra optical sections were taken above and below the islet. However, focus was still manually adjusted to keep the islet centered within the stack to avoid the task of having to apply a drift correction to the data at the end of the experiment.

In the fluorescent modality rat kidney cells have been successfully tracked in 3-D by finding the center of mass of the fluorescence intensity each time the image stack was collected (Rabut *et al*. 2004). Here, the figure-of-merit to maximize is light intensity, which can be collected directly from the raw image data. In the human islet experiment, DIC illumination also provides light intensity values but they are not well correlated with the center of mass of an aggregate. To accurately use DIC illumination for an autofocus algorithm requires more work. The latest version of BAMBI provides a measure of focus by determining a figure-of-merit based on normalized variance between each slice. By constantly maximizing this figure-of-merit and repositioning the cell within the center of the focal stack it should be possible to maintain focus for long term studies without the need for user intervention.

At the time of this experiment only one field-of-view could be optically sectioned for a single time course. Although the islet selected for long-term imaging was small enough to fit into a single field-of-view, there were other islets observed under the gap that would have required up to four fields of view at the current magnification. This can now be achieved with the latest version of BAMBI using mosaic blocks.

Chapter 7
Discussion

The realization of the BAMBI system was only possible by adopting a transdisciplinary approach. BAMBI was designed using mechatronic engineering principles to work on a chemical engineering problem that fell within the context of cell biology and photonics. The problem was: "Can we identify stem cells in culture and expand them *in-vitro*?" This required a fully integrated imaging system with life support for long-term live cell assays that could be manipulated on a single cell level.

The original functional design goals for BAMBI started out as this simple need to image more than one field-of-view over time under various conditions. Starting in 2005, new live cell experiments required additional features to be implemented and, in turn, these features enabled experimenters to ask more questions and to push the limits of BAMBI. This again required additional enhancements to be added until the final system was developed. The end result was a system that could capture multiple fields-of-view, capture contiguous images in a ROI that may represent a 2-D or 3-D region of space in time. The addition of dynamic mosaic blocks allowed the ROIs to be created or destroyed, to grow or shrink as needed to capture the live cell dynamics of the experiment. 3-D mosaic blocks can also be used to optically section cells or aggregates of cells when used with DIC illumination. Five additional fluorescent LED wavelengths are available for fluorophore imaging. BAMBI provides a micropipette manipulator to pick-and-place single cells within the microenvironment that enables researchers to set up conditions found *in-vivo* and experiment on a single cell level *ex-vivo*. All these features are made available and managed within a single multithreaded software application.

The task of implementing the mosaic capture algorithms and autofocus were the two of most challenging tasks faced. The most difficult task to implement on BAMBI was the mosaic capture algorithm itself. This was mainly due to the fact that a concurrent algorithm had to work with multiple threads, including user interface threads which are much harder to manage. Multithreading was a necessary addition to the program. It allows the mosaic capture algorithm to wait on feedback from the robot or video capture device before continuing. This is essential in maintaining safe concurrent operations that depend on actions being completed at the right time. It also allows the user to interact with GUIs in a "real-time" way that is, being able to interrupt a process while it is currently running. The problem of having a robust algorithm was confounded

by the fact that there could be more than one mosaic block and each mosaic block has up to six possible illumination modes all to be captured at different intervals.

The second most difficult challenge to implement was robust autofocus. Even an autofocus function that works 99% of the time is not robust when one considers the effect that 1% could have on the time course. Focus functions must operate very quickly when the assay demands fast cycle times. It is simply not feasible to collect images through the entire depth of field; only a limited number of images can be gathered above and below the last focal plane to determine the correction for the new image given the time constraints of cell tracking over multiple ROIs. Indeed, if the 1% focus result were to place the incorrect "in-focus" image at the edge of the correct focus range, the next focus check may not find the true peak of the focus curve. Other factors such as the high amount of noise present in images due to low illumination conditions used to maintain the health of the cells, multimodal focus curves, and the dynamic nature of the experiment where the background substrate is not constant from one experiment to another, all factor into how well an autofocus function performs. For now, one must be vicarious when employing the autofocus features of BAMBI, but for the future there is promise that a robust autofocus solution is still attainable with artificial intelligence, fuzzy systems, or Bayesian approaches.

The success of BAMBI can be measured by its robustness, the use of dynamic mosaic blocks, and the ease at which endpoint software can integrate with the system. One of the most important design criteria was that BAMBI maintain stable operation over hundreds of hours - the system must be robust, as an interruption in time course imaging at any point will result in an experiment failure. If a system were to crash during a time course it can be costly both financially and ethically. Financially, the cost of reagents used and number of man-hours spent preparing for the run are not recoverable after an experiment fails. Ethically, the type of cells used in the experiment could come from human or animal donors. In the case of animal donors, they are usually sacrificed just before the experiment to harvest the cells of interest. When a study like this fails, it often brings into question the cost versus benefit of live animal studies.

The process of “validating” BAMBI against failure required a considerable amount of debugging and practice test runs, often using polyurethane beads or mouse cell lines. In the end, the process of testing, performing practice runs, and getting feedback from actual experiments lead to the creation of a stable software and hardware platform that met the (evolved) design criteria. Since the last iteration of BAMBI released in December 2006, the system has been running

experiments simultaneously on three microscopes, almost continually without failure. The successful implementation of dynamic mosaic blocks truly sets BAMBI apart from other automated microscopy systems to date. The ability to pause an experiment once it has started and dynamically add more regions of coverage, grow or shrink existing regions is just not available in the systems surveyed to date. However, most automated microscopy software providers are aware of this deficit and it is only a matter of time before they implement their own dynamic solution. Finally, BAMBI has been successfully mated with a number of off-line endpoint programs such as Microscoft Excel, Microsoft Access, NIH ImageJ, CellTracker™, and CellHunter™. The purpose of these programs is to perform post-capture image processing, pattern recognitions, and informatics on the data gathered by BAMBI.

Although BAMBI has achieved its original primary objectives it should still be considered a work in progress. The number of cell based assays and imaging techniques are always growing. This is partly due to the fertile nature of the field of cell biology and is partly due to the ongoing advances in computer technology. As these fields advance, so will the applications for a BAMBI-approach to cell culture analysis and manipulation. The most relevant advancements that could be considered for the next version BAMBI would be: robust autofocus, online image processing, and autonomous single-cell handling. Robust autofocus would allow the experimenter to walk away from long-term live cell time courses with confidence that the images will be kept in focus. As yet, autofocus is roughly 80% reliable but can be improved by focusing on only a small portion of the image containing a single focal curve. Online image processing might include the ability to track cells in "real-time", either under DIC or fluorescent illumination, for the purposes of automatically growing, moving, and shrinking mosaic blocks as needed. Online image processing would occur at the same time as the experiment to allow closed loop feedback of the system. Autonomous single-cell handling could work with online processing to allow BAMBI to automatically pick-and-place cells. Currently, BAMBI can be controlled robotically for this purpose, but the task is usually very tedious as experiments can require manual placement of several hundred cells.

BAMBI is a new facet in the field of automated high content and high throughput live cell imaging. It is unique in that it can provide a wide range of features compared with other available commercial systems. It can operate at speeds that can attain more than 50,000 fields-of-view a day which places it in the high throughput category according to Gough and Johnston (e.g. Molecular Devices, ImageXpress ULTRA, and Evotecs Opera). Most importantly, it is a seamless add-on to a conventional microscope and allows it to be used for work at the research

level. That is, if a microscope itself employs a unique illumination technology such as multi-photon excitation, BAMBI would be able to take advantage of that. At the time of this writing there are no other systems that feature single-cell pick-and-place operation with automated microscopy. Usually, commercially available systems leave the robotic manipulation of cells to entirely different systems. A comprehensive group of features like BAMBI would require commercial systems to either develop their own technology for cell manipulation in-house or support the plethora of currently available systems. Providing support for an entirely different product is very costly and requires a significant amount of redundant coding. Currently BAMBI is proprietary software and is not yet available to the general public. Therefore the degree of customization BAMBI offers the end user is a matter of perspective. Within the Jervis Laboratory it allows for the limitless customization of BAMBI provided the user understands Windows Visual C++ and MFC. Without access to the source code, it would not be possible to add additional functionality. There are solutions to this problem, such as implementing a script language that would enable the user to add functionality that was not already there. The most obvious choice would be to allow for script based image processing algorithms to be added as needed. Generally, the BAMBI software is very flexible in this regard and lends itself easily to new code modules and modification of existing ones.

Accumulating more images increases the number of events scored and thereby imparts more statistical significance to the assay. As systems like BAMBI approach the theoretical limits of the current technology for image collection rates, a new bottleneck is reached where the pace of data collection far exceeds the pace of data extraction and mining. Although data mining is usually an off-line process and thereby not under time constraints, feasibility limits can be imposed by the nature of the data being extracted. At least in the bright field modality, identification of cells, cell types, various morphologies, and tracking of cell lineages still requires a human to sit down and actually do it. Computer algorithms are still in the developmental stages when it comes to tracking cells robustly without fluorescent markers for guidance. BAMBI has changed the problem from "Can we gather sufficient data with available imaging infrastructure?" to "Do we have sufficient human resources to process data offline?" Therefore, care should be taken to acquire the least amount of data necessary to achieve the goals of the experiment. Through the course of many live cell experiments with BAMBI it was found that the upper limit to the viable amount of data captured depended on maintaining an imaging cycle time of no less than three minutes to enable cell tracking. If the time course is less than three minutes, the cells become overexposed to light and there are no appreciable gains in temporal information.

However, if the time course takes longer than three minutes, there may be no guarantee that the cells can be individually tracked between time points.

Chapter 8
Conclusions and Recommendations

8.1 Conclusions

Although challenging to implement, multithreaded design was essential for managing concurrent operations required to efficiently automate large field high throughput long-term image captures. In the automated system there is variability in the time it takes for some events to occur such as opening a shutter, collecting an image, performing a backlash correction, or writing to a file. Multithreading frees BAMBI from having to wait on each event to finish before starting the next one. Provided the events are handled in a thread safe manner, the efficiency of image capture has been enhanced to sub-second intervals between adjacent fields-of-view in some cases.

Using backlash correction with the ultra high-resolution servomotors (Galil Inc., USA) proved to be very precise over long periods of time and wide ranges of motion. The repeated collection of images gathered from multiple fields-of-view through time showed very little drift after the system reached temperature equilibrium. Additionally, the accuracy of the servomotors enables the display of image mosaics to be stitched together without the need to perform lengthy corrections; corrections for position overlap discrepancies can require minutes to hours to process depending on the size of the mosaic.

The implementation of dynamic mosaic blocks allows researchers to modify the scope of a currently running live cell experiment without having to restart the time course. Dynamic mosaic blocks can be grown or shrunk, and created or destroyed, in order to capture the regions of interest as cell colonies grow and move. This is beneficial to researcher; as they are not locked into a single image capture protocol.

BAMBI has proven itself to be a robust software application that is not prone to crashes that would otherwise compromise the outcome of live cell experiments. Since the last iteration compiled on December 2006, BAMBI has been running experiments on three different microscopes on a daily basis without failure. This success is the result of using an iterative design methodology wherein the development, test, feedback, development cycle was performed on a near continuous basis while actual experiments were in progress.

The ability to work at a single cell level on a cell-by-cell basis paired with long-term live cell imaging allows researchers to answer a completely new set of questions related to cell behavior. Cells are not insensitive to their surroundings; scientists are discovering that a change in a cell's neighboring environment has a significant impact on its behavior or phenotype. BAMBI enables researchers to create these environments *in-vitro* to learn about these effects.

8.2 Recommendations

8.2.1 Enhanced Sony Drivers

When the original BAMBI software was written, drivers for the Sony XCD-XS710/910 CCD cameras did not exist and an open source generic 1394 Firewire version had to be used. This is the 1394Camera v.63 driver provided by Carnegie Mellon University. Unfortunately, this driver does not support camera binning for the Sony cameras used on M1, M2, and M3. Recently, Sony has released a version of their driver that supports camera binning. It is recommended that these new drivers be incorporated into the BAMBI software program to take advantage of camera binning. Binning will greatly increase the cameras sensitivity to the very faint emissions experienced under fluorescent illumination conditions.

8.2.2 Data Compression

Given that experiments have been running almost continually on microscopes M1, M2, and M3 for the past seven months, there will come a point where the data storage capacity of the hard drives will be exceeded. Rather than purchase more storage, data compression techniques could be used to compress the raw image files. A lossless image compression algorithm such as LZW (Gonzales *et al*., 2002) has an average compression ratio of 1:5 that could be employed to shrink the finalized raw files.

8.2.3 Autofocus

Although autofocus has been implemented on BAMBI, it has not yet stable enough state to be used for long-term live cell operations. It is recommended that research continue on this application with the following suggestions. Other studies have shown success focusing on a fluorescent marker (Burglin, 2000). It may be possible to place a fluorescently coated polyurethane bead in the cell culture media as a reference. By performing fluorescently illuminated autofocus on the bead it may be easier and more robust allowing for a general

correction for focal drift. Another possibility is to perform a cross correlation between the previous in-focus image and the stack of images acquired to generate the current focal score. The correlation coefficients could be used to weight the focal scores generated from each image.

8.2.4 Autonomous Cell Sorting

The first step in developing a fully automated cell pick-and-place capability for BAMBI was to develop the robotics necessary for manual control. With the exception of pressure control BAMBI has successfully been used to move hundreds of living cells from one location to another in the microenvironment. The downside is that the process has been slow and tedious for the user to perform. The process of transferring cells between different environments such as from one dish to another is very stressful on the cells and they can only be exposed to these conditions for a short time before cell death occurs. Automation of this process or part of this process would relive stress on the cells and the experimenter. It is recommended that the next step to automating this process is to close the control loop with computer vision. Using pattern recognition techniques, it should be possible to provide feedback as to where the end effector is located with respect to the environment and the cells.

8.2.5 Fog-Light Warning System

BAMBI has been designed with built in safety features like the amplifier enable signal that must be logic high to provide power to the motors or the shut down states that occur when a limit switch is tripped. These precautions are fairly effective for most application but in the case of long-term live cell imaging, they can also cause the unwanted loss of data from a current unattended run. (i.e. If a motor is turned off because it encountered an unexpected resistance to motion it remain off until the experimenter arrives the following morning and resolves the issue and re-enables the motor.) To avoid these situations it is recommended that a "fog-light" or "watch dog" warning system be implemented that can notify the appropriate person or persons that a fault has occurred. The system can provide notification by any number of communication methods such as cell phone text messaging, email, or pager.

Appendix A

Mechanical

A.1. Micromanipulator

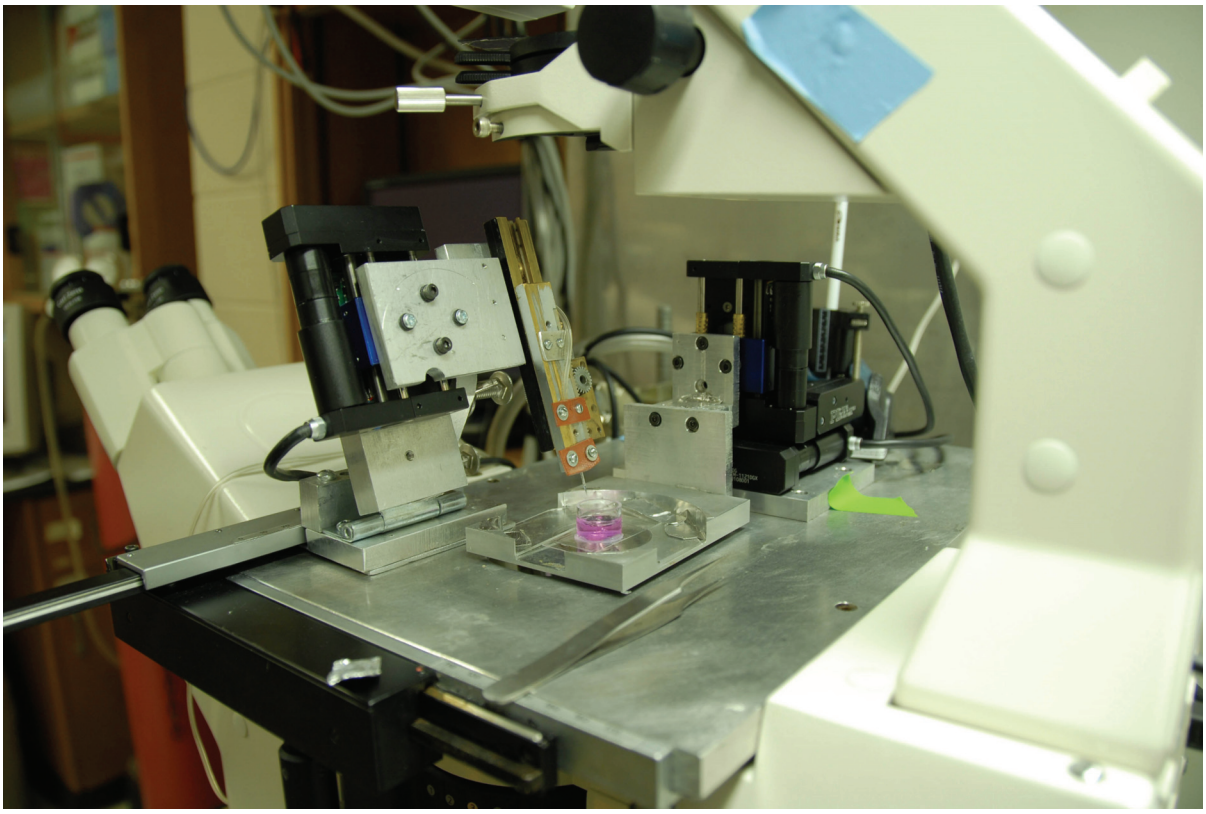

The BAMBI Micromanipulator with Micropipette Attached

A.2. 8-Axis Control Module Assembly

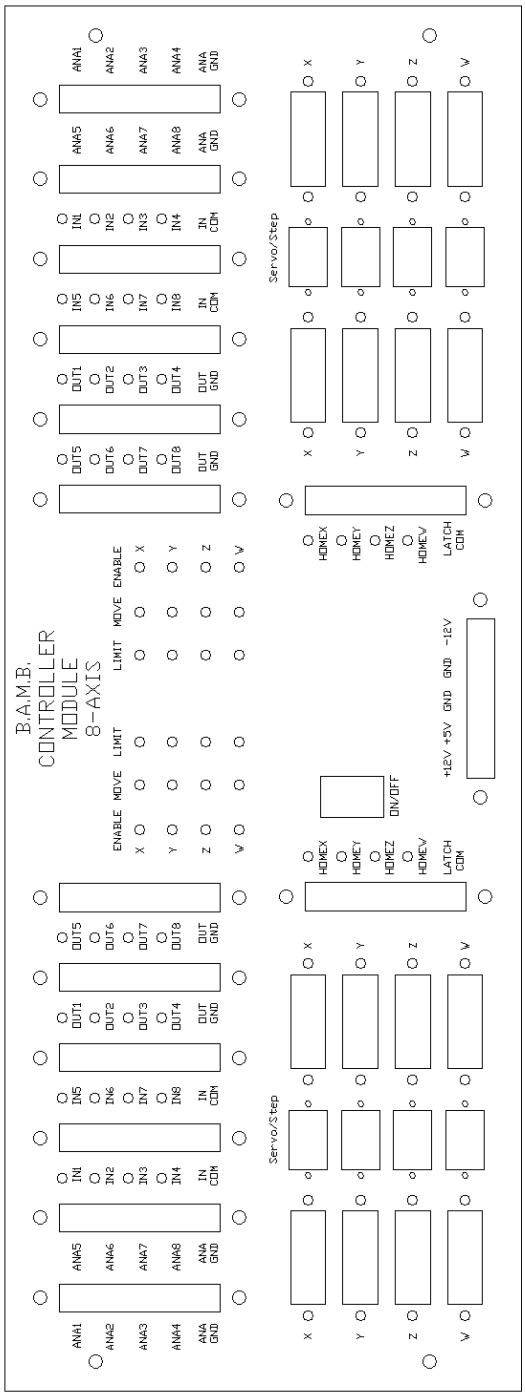

BAMBI 8-Axis Front Panel

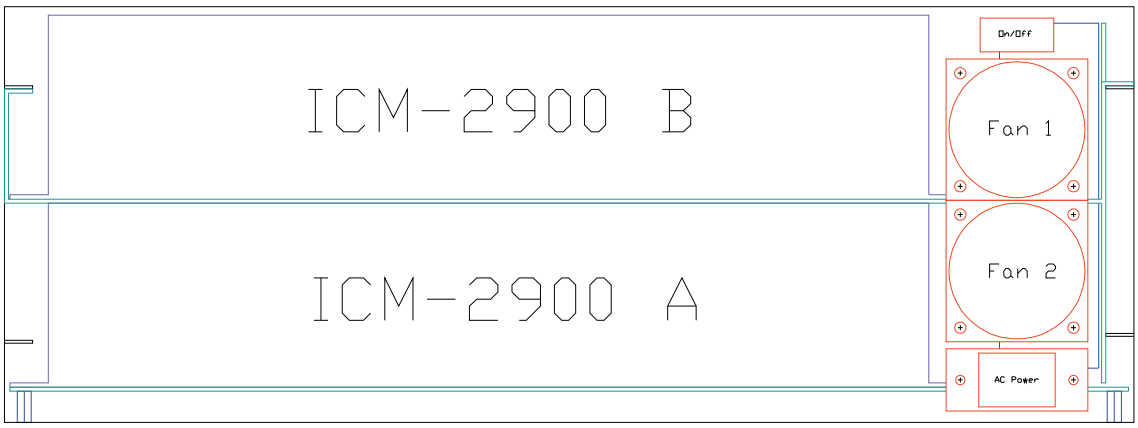

BAMBI 8-Axis Module Layout: Rear View

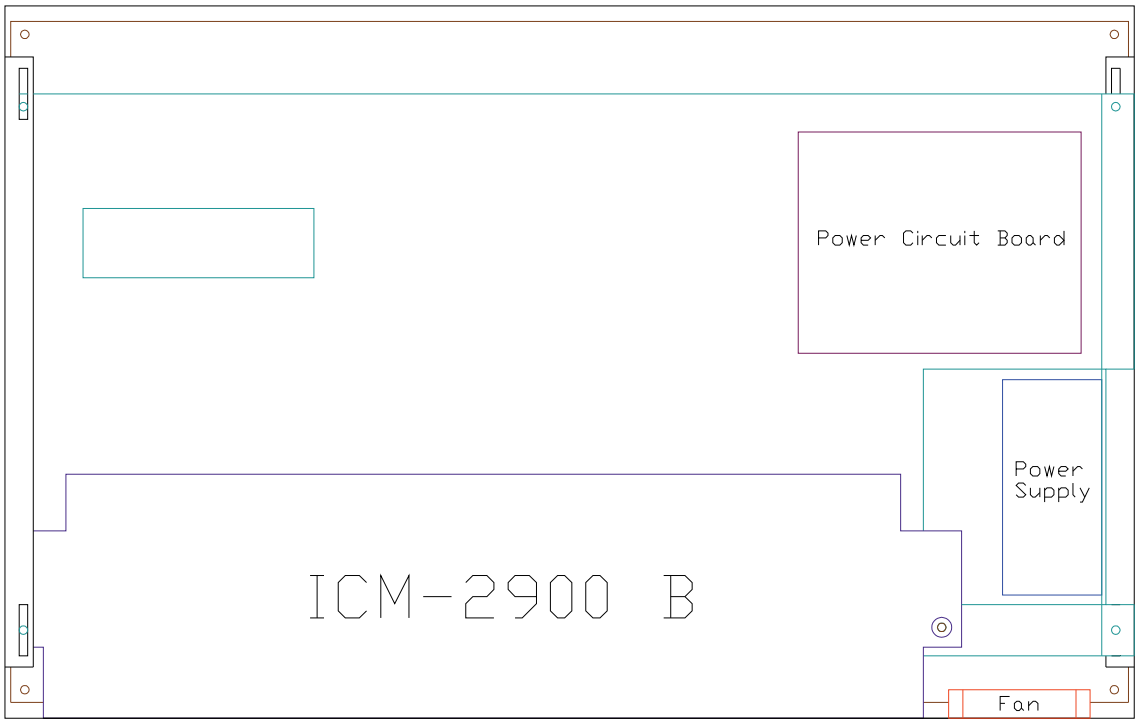

BAMBI 8-Axis Module Layout: Top Level View

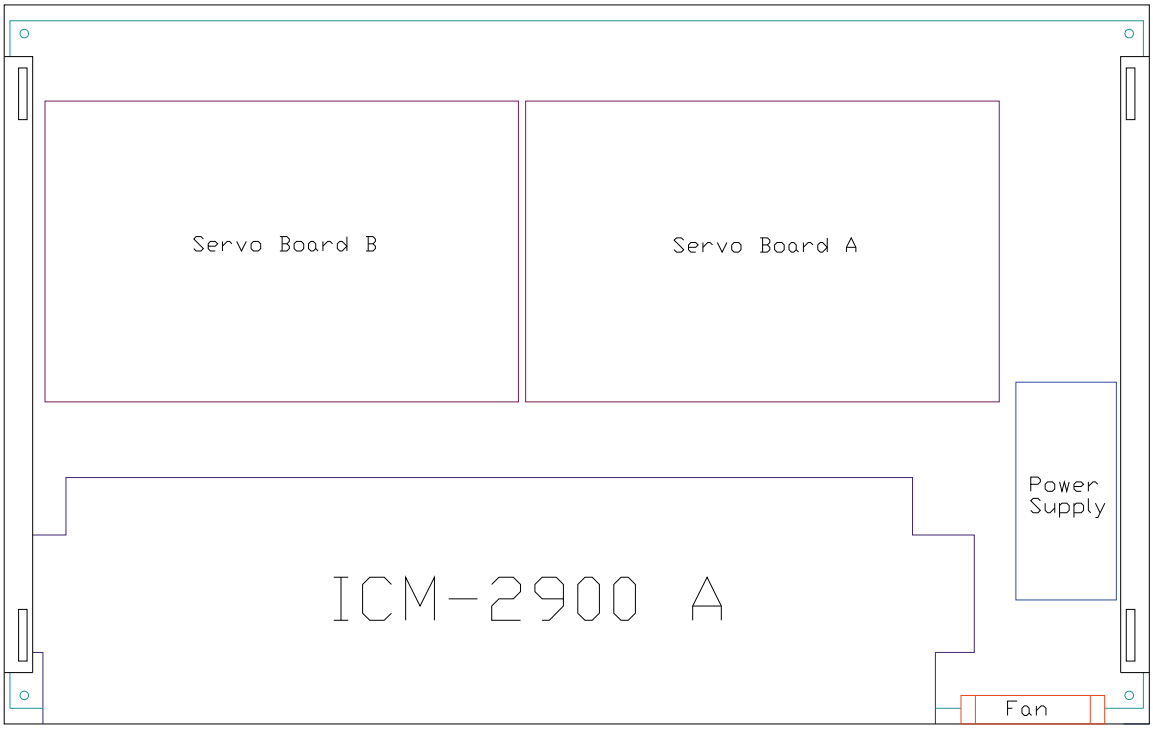

BAMBI 8-Axis Module Layout: Bottom Level View

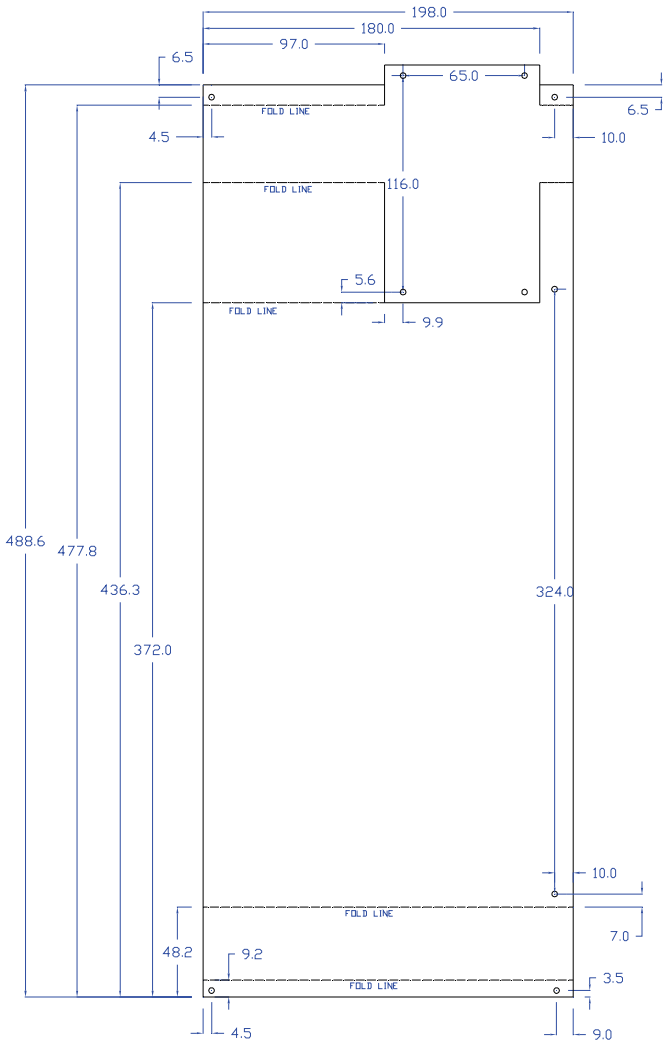

Notes: All dimensions are in mm.		Material: 1/16" Aluminum
DWG Name: 8-Axis Module Top Shelf Cut/Fold Layout		Rev. A
File Name: Shelf Assembly Top Folding View.dwg		Drawing not to scale.
Date: 04/09/06	Designed by: April Blaylock	Sheet: 1/3

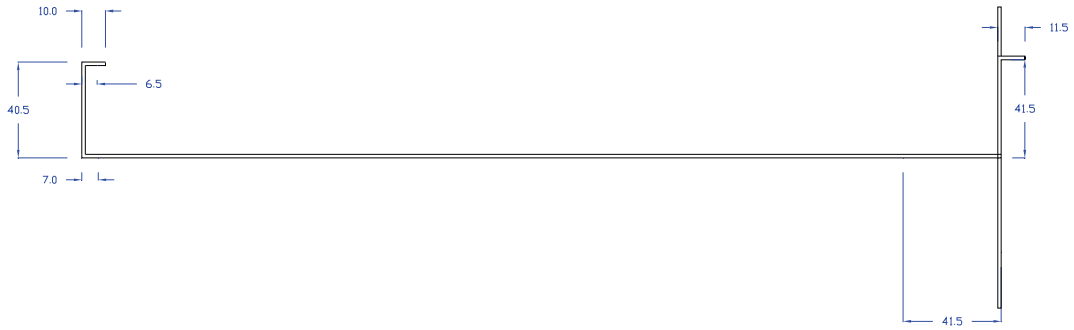

Notes: All dimensions are in mm.		Material: 1/16" Aluminum
DWG Name: 8-Axis Module Top Shelf Cut/Fold Layout (SideView)		Rev. A
File Name: Stage Modifications.dwg		Drawing not to scale.
Date: 04/09/06	Designed by: April Blaylock	Sheet: 2/3

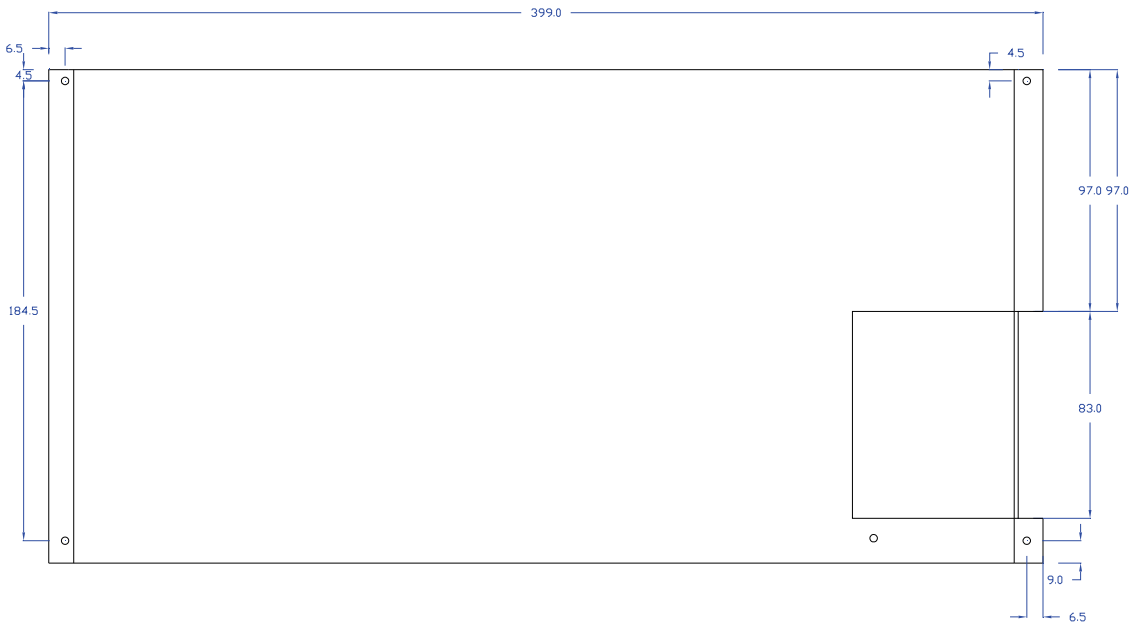

Notes: All dimensions are in mm.		Material: 1/16" Aluminum
DWG Name: 8-Axis Module Top Shelf Layout (Top View)		Rev. A
File Name: Stage Modifications.dwg		Drawing not to scale.
Date: 04/09/06	Designed by: April Blaylock	Sheet: 3/3

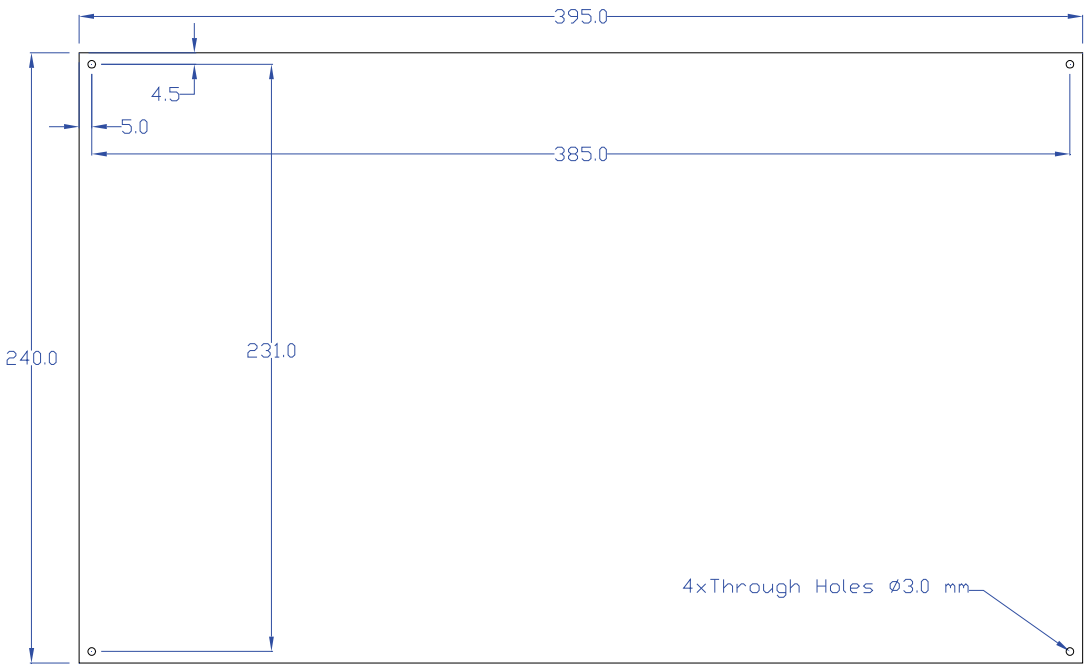

Notes: All dimensions are in mm.		Material:1/16" Aluminum
DWG Name: : 8-Axis Module Bottom Shelf Layout (Top View)		Rev. A
File Name: Stage Modifications.dwg		Drawing not to scale.
Date: 04/09/06	Designed by: April Blaylock	Sheet: 1/1

A.3. Axiovert 200 Stage Modifications

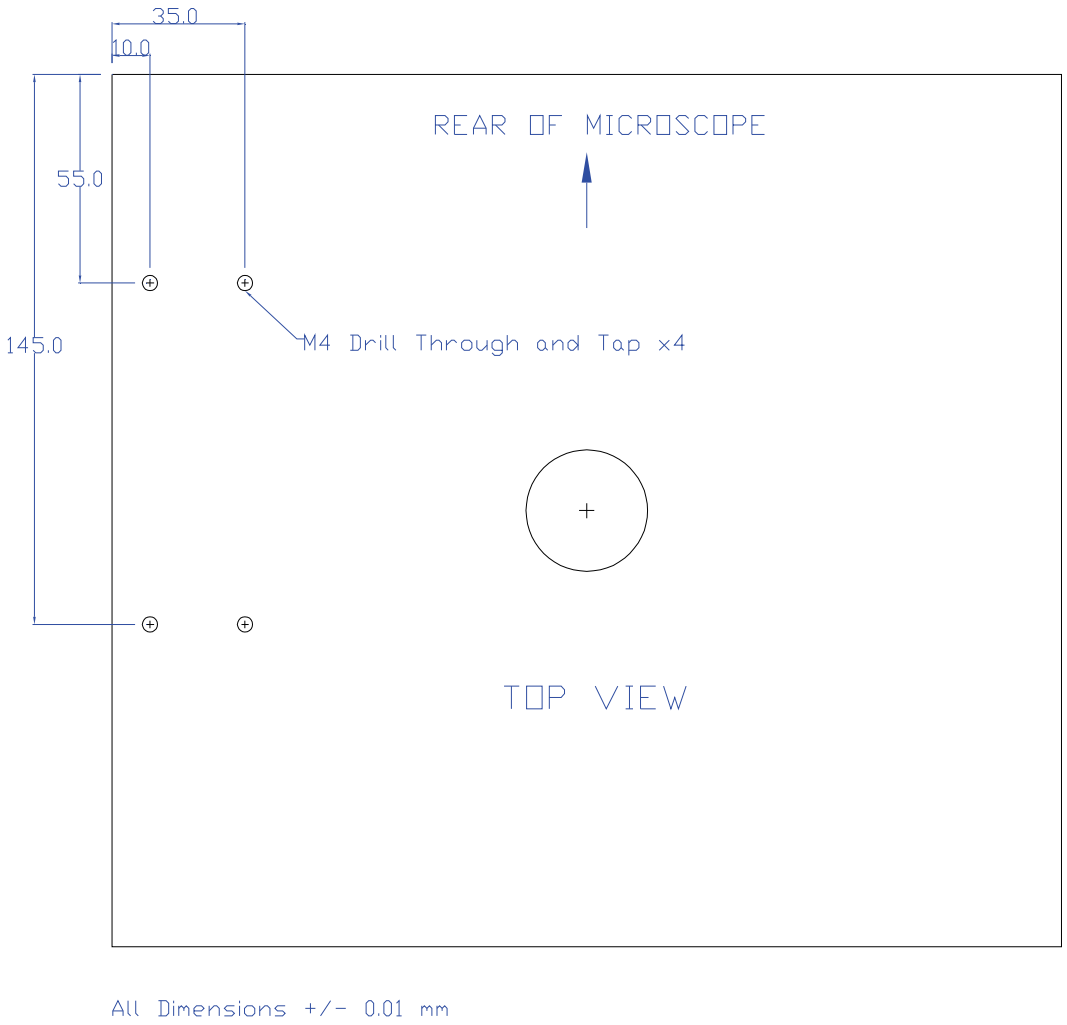

Notes: All dimensions are in mm.		Material: Aluminum
DWG Name: Axiovert 200 Stage Modifications		Rev. A
File Name: Stage Modifications.dwg		Drawing not to scale.
Date: 04/09/06	Designed by: April Blaylock	Sheet: 1/1

A.4. Cell Culture Plate

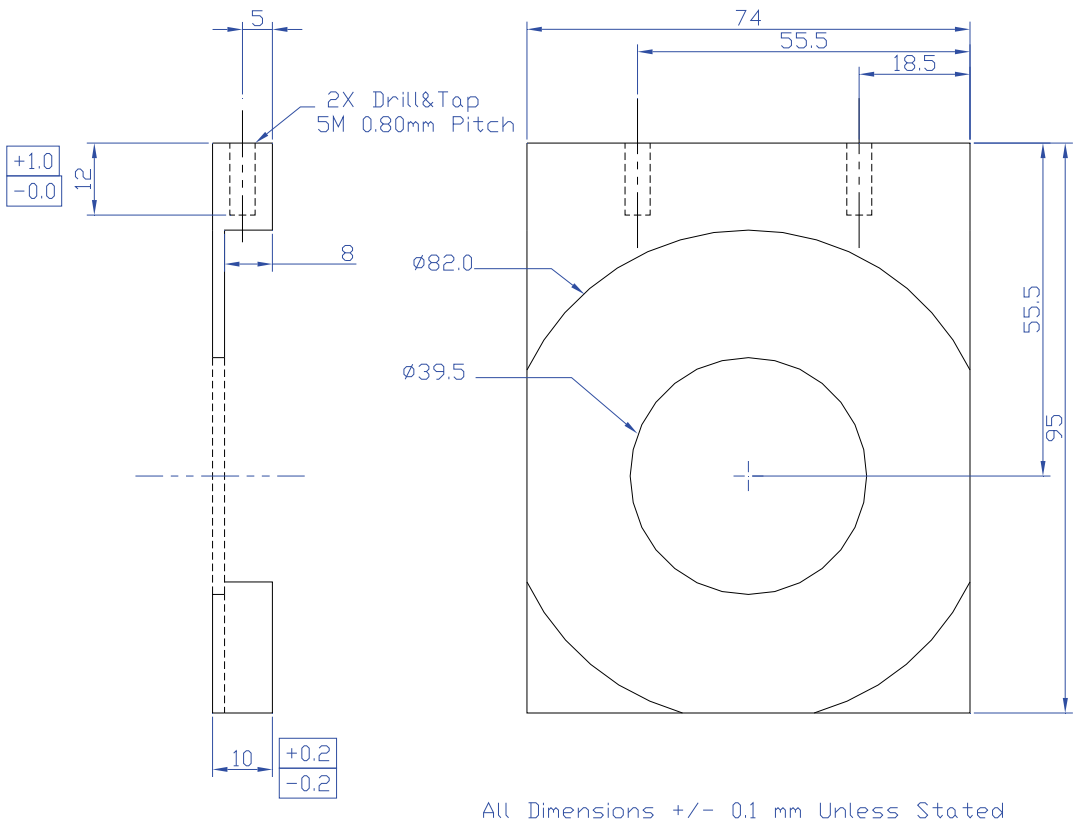

Notes: All dimensions are in mm.		Material: Aluminum
DWG Name: Cell Culture Plate		Rev. A
File Name: Cell Culture Plate Revision A.dwg		Drawing not to scale.
Date: 04/09/06	Designed by: April Blaylock	Sheet: 1/1

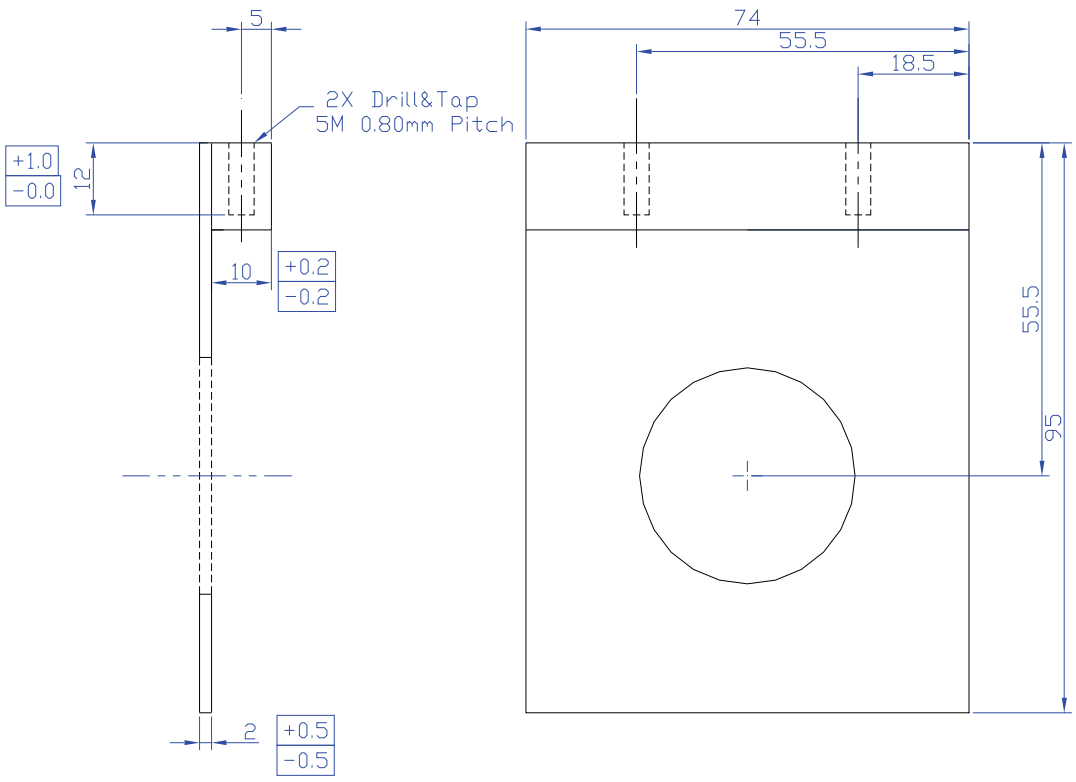

Notes: All dimensions are in mm.		Material: Aluminum
DWG Name: Cell Culture Plate		Rev. B
File Name: Cell Culture Plate Rev B.dwg		Drawing not to scale.
Date: 04/09/06	Designed by: April Blaylock	Sheet: 1/1

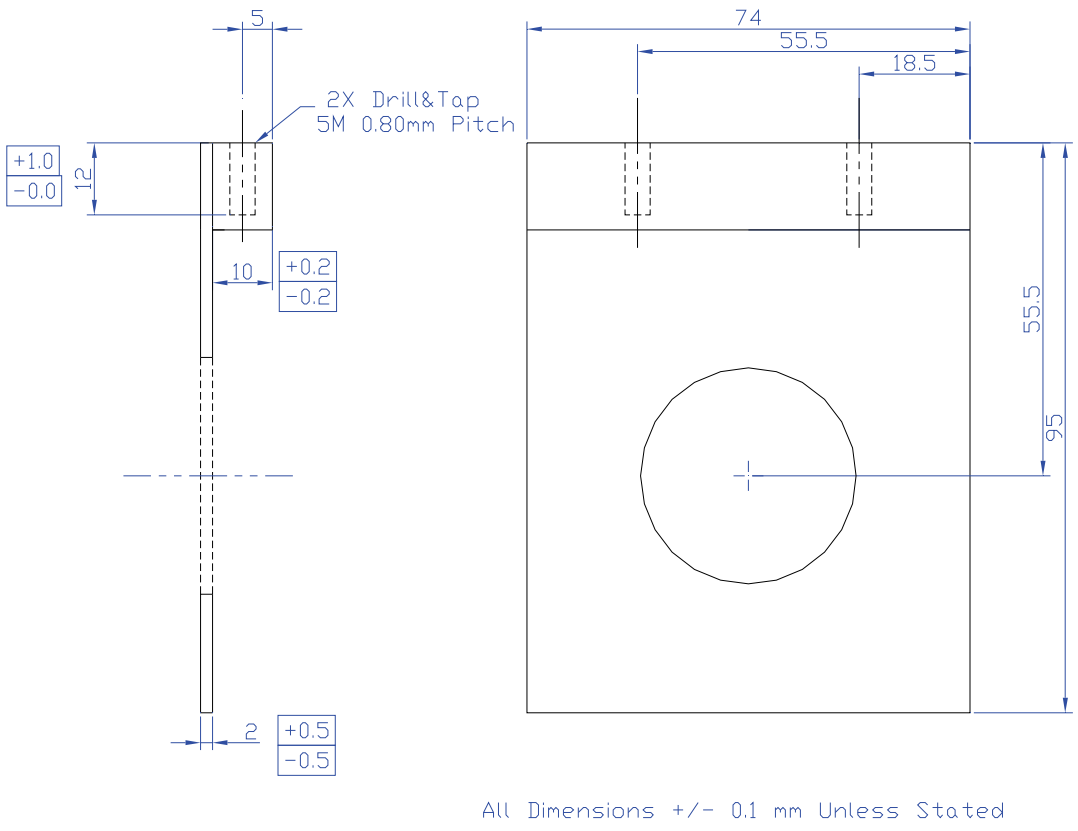

Notes: All dimensions are in mm.	Material: Aluminum	
DWG Name: Cell Culture Plate		Rev. C
File Name: Cell Culture Plate Rev C.dwg		Drawing not to scale.
Date: 04/09/06	Designed by: April Blaylock	Sheet: 1/1

A.5. 3-Axis Stage Mounting Plate

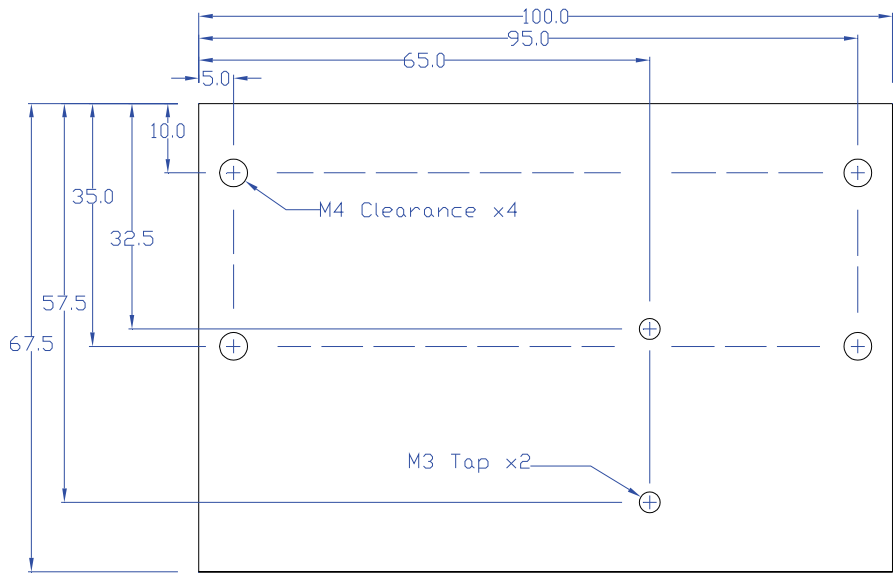

All Dimensions are +/- 0.01 mm

Notes: All dimensions are in mm.		Material: 1/2"Aluminum
DWG Name: 3-Axis Stage Mounting Plate		Rev. A
File Name: 3-Axis Stage Mounting Plate.dwg		Drawing not to scale.
Date: 04/09/06	Designed by: April Blaylock	Sheet: 1/1

A.6. 3-Axis Stage Assembly

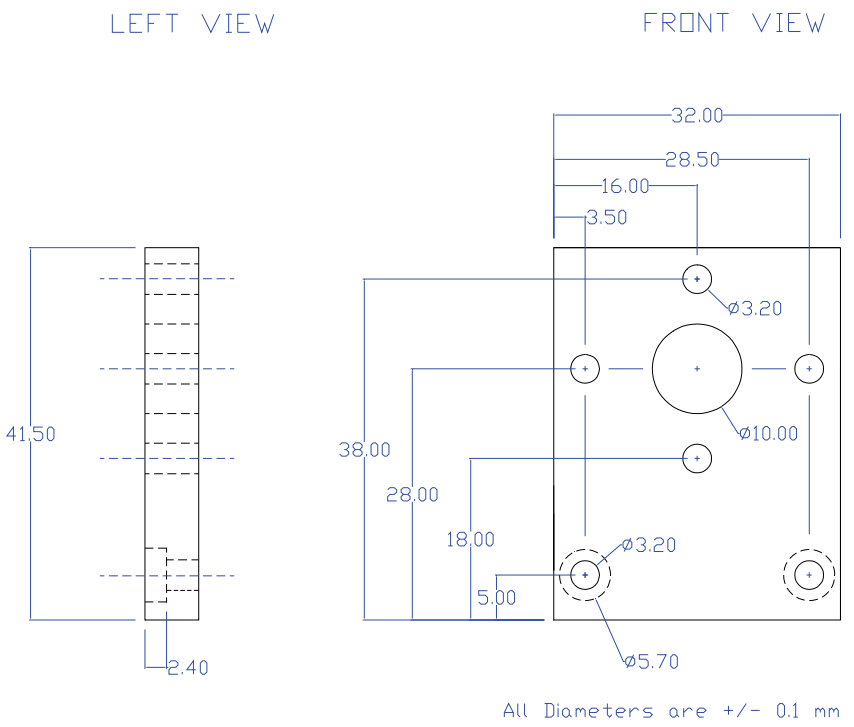

Notes: All dimensions are in mm.		Material: 1/4" Aluminum
DWG Name: 3-Axis Stage Assembly		Rev. A
File Name: 3-Axis Stage Part 1 Rev A.dwg		Drawing not to scale.
Date: 04/09/06	Designed by: April Blaylock	Sheet: 1/3

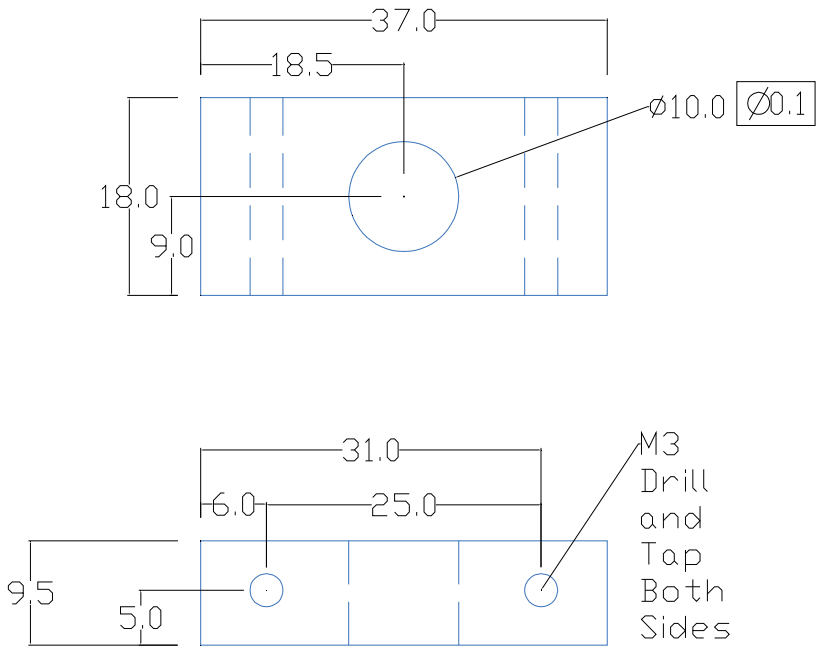

All Dimensions +/- 0.01 mm Unless Stated

Notes: All dimensions are in mm.		Material: 1/4" Aluminum
DWG Name: 3-Axis Stage Assembly		Rev. A
File Name: 3-Axis Stage Part 2 Rev A.dwg		Drawing not to scale.
Date: 04/09/06	Designed by: April Blaylock	Sheet: 2/3

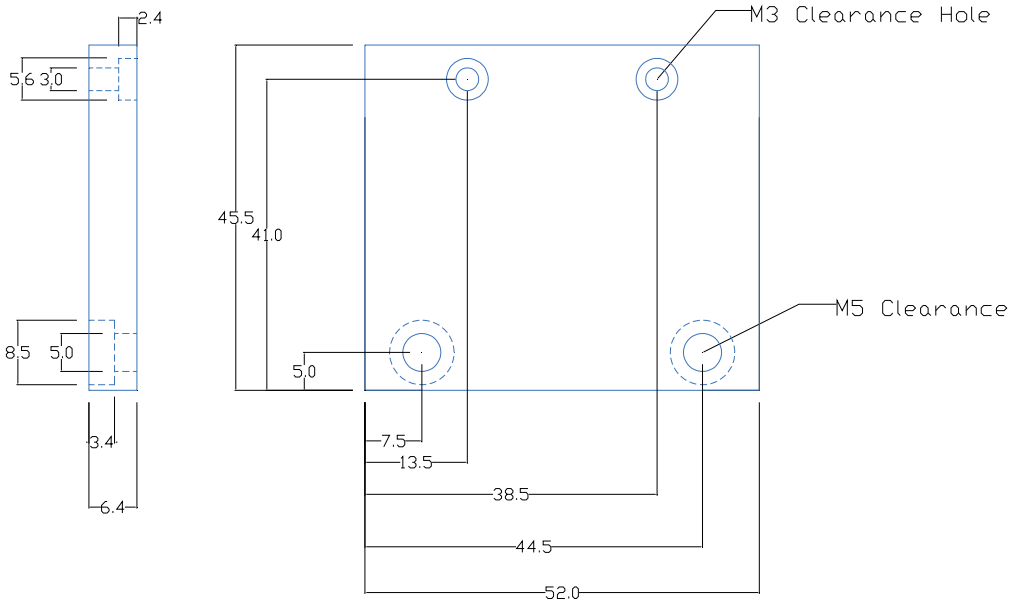

All Dimensions +/- 0.01 mm Unless Stated

Notes: All dimensions are in mm.		Material: 1/4" Aluminum
DWG Name: 3-Axis Stage Assembly		Rev. A
File Name: 3-Axis Stage Part 3 Rev A.dwg		Drawing not to scale.
Date: 04/09/06	Designed by: April Blaylock	Sheet: 3/3

A.7. DMC-2900 Interconnect Module

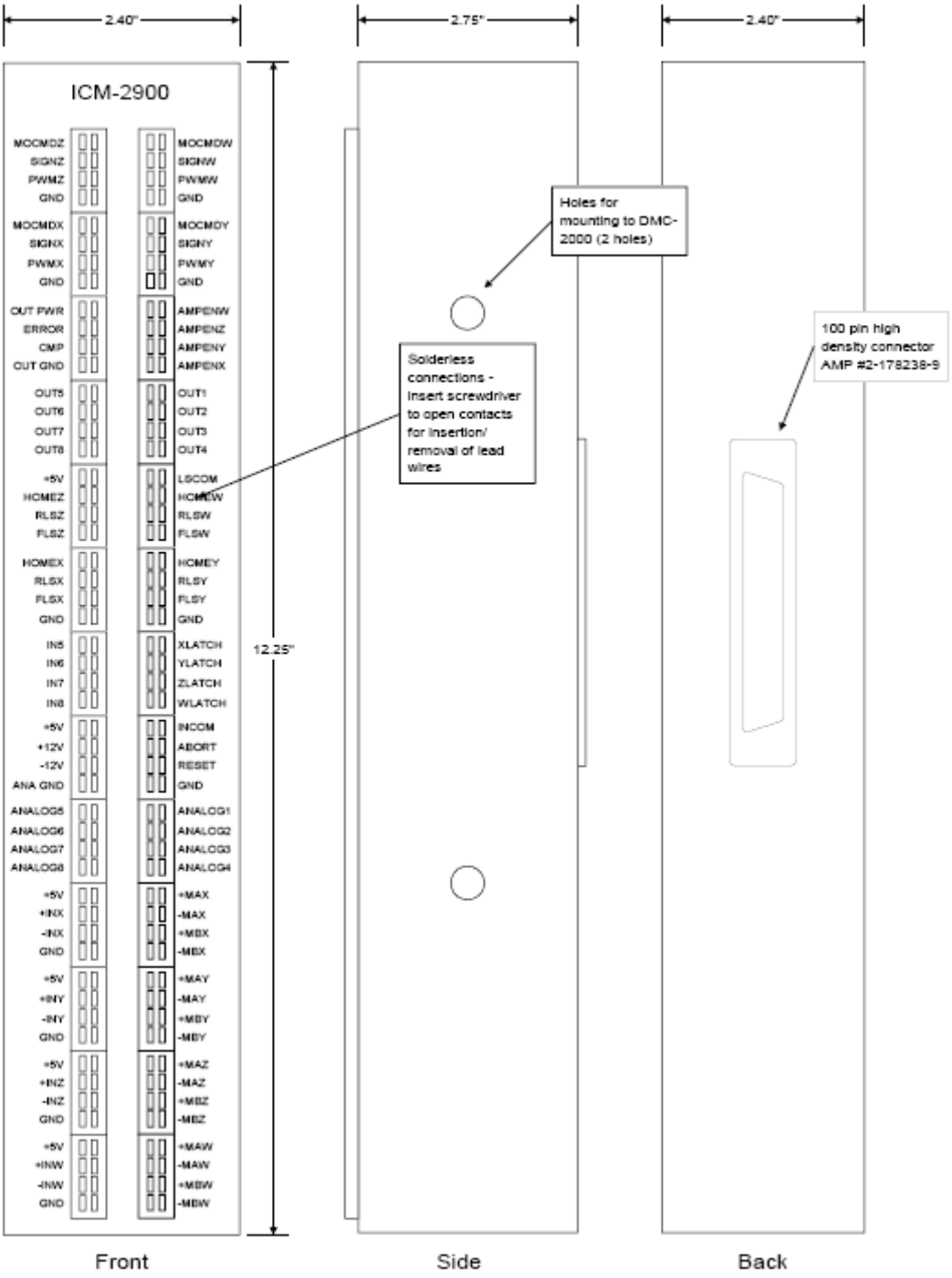

Drawing taken from "Application Note #1424" by Galil Motion Control Inc. (www.galilmc.com).

Appendix B
Electrical

B.1. DMC-2900 Interconnect Module

DMC-2900 Interconnect Module Pin I/O Table

Block (4 PIN)	Label	I/O	Description
1	MOCMDZ	O	Z axis motor command to amp input (w / respect to ground)
1	SIGNZ	O	Z axis sign output for input to stepper motor amp
1	PWMZ	O	Z axis pulse output for input to stepper motor amp
1	GND	O	Signal Ground
2	MOCMDW	O	W axis motor command to amp input (w / respect to ground)
2	SIGNW	O	W axis sign output for input to stepper motor amp
2	PWMW	O	W axis pulse output for input to stepper motor amp
2	GND	O	Signal Ground
3	MOCMDX	O	X axis motor command to amp input (w / respect to ground)
3	SIGNX	O	X axis sign output for input to stepper motor amp
3	PWMX	O	X axis pulse output for input to stepper motor amp
3	GND	O	Signal Ground
4	MOCMDY	O	Y axis motor command to amp input (w / respect to ground)
4	SIGNY	O	Y axis sign output for input to stepper motor amp
4	PWMY	O	Y axis pulse output for input to stepper motor amp
4	GND	O	Signal Ground
5	OUT PWR	I	Isolated Power In for Opto-Isolation Option
5	ERROR	O	Error output
5	CMP	O	Circular Compare Output
5	OUT GND	O	Isolated Ground for Opto-Isolation Option
6	AMPENW	O	W axis amplifier enable
6	AMPENZ	O	Z axis amplifier enable
6	AMPENY	O	Y axis amplifier enable
6	AMPENX	O	X axis amplifier enable
7	OUT5	O	General Output 5
7	OUT6	O	General Output 6
7	OUT7	O	General Output 7
7	OUT8	O	General Output 8
8	OUT1	O	General Output 1
8	OUT2	O	General Output 2
8	OUT3	O	General Output 3
8	OUT4	O	General Output 4
9	+5V	O	+ 5 Volts

9	HOMEZ	I	Z axis home input
9	RLSZ	I	Z axis reverse limit switch input
9	FLSZ	I	Z axis forward limit switch input
10	LSCOM	I	Limit Switch Common Input , No Connection @
10	HOMEW	I	W axis home input
10	RLSW	I	W axis reverse limit switch input
10	FLSW	I	W axis forward limit switch input
11	HOMEX	I	X axis home input
11	RLSX	I	X axis reverse limit switch input
11	FLSX	I	X axis forward limit switch input
11	GND	O	Signal Ground
12	HOMEY	I	Y axis home input
12	RLSY	I	Y axis reverse limit switch input
12	FLSY	I	Y axis forward limit switch input
12	GND	O	Signal Ground
13	IN5	I	Input 5
13	IN6	I	Input 6
13	IN7	I	Input 7
13	IN8	I	Input 8
14	XLATCH	I	Input 1 (Used for X axis latch input)
14	YLATCH	I	Input 2 (Used for Y axis latch input)
14	ZLATCH	I	Input 3 (Used for Z axis latch input)
14	WLATCH	I	Input 4 (Used for W axis latch input)
15	+5V	O	+ 5 Volts
15	+12V	O	+12 Volts
15	-12V	O	-12 Volts
15	ANA GND	O	Isolated Analog Ground for Use with Analog Inputs
16	INCOM	I	Input Common For General Use Inputs @
16	ABORT	I	Abort Input
16	RESET	I	Reset Input
16	GND	O	Signal Ground
17	ANALOG5	I	Analog Input 5 , No Connection @
17	ANALOG6	I	Analog Input 6 , No Connection @
17	ANALOG7	I	Analog Input 7 , No Connection @
17	ANALOG8	I	Analog Input 8 , No Connection @
18	ANALOG1	I	Analog Input 1 , No Connection @
18	ANALOG2	I	Analog Input 2 , No Connection @
18	ANALOG3	I	Analog Input 3 , No Connection @

18	ANALOG4	I	Analog Input 4 , No Connection @
19	+5V	O	+ 5Volts
19	+INX	I	X Main encoder Index +
19	-INX	I	X Main encoder Index -
19	GND	O	Signal Ground
20	+MAX	I	X Main encoder A+
20	-MAX	I	X Main encoder A-
20	+MBX	I	X Main encoder B+
20	-MBX	I	X Main encoder B-
21	+5V	O	+ 5Volts
21	+INY	I	X Main encoder Index +
21	-INY	I	X Main encoder Index -
21	GND	O	Signal Ground
22	+MAY	I	X Main encoder A+
22	-MAY	I	X Main encoder A-
22	+MBY	I	X Main encoder B+
22	-MBY	I	X Main encoder B-
23	+5V	O	+ 5Volts
23	+INZ	I	X Main encoder Index +
23	-INZ	I	X Main encoder Index -
23	GND	O	Signal Ground
24	+MAZ	I	X Main encoder A+
24	-MAZ	I	X Main encoder A-
24	+MBZ	I	X Main encoder B+
24	-MBZ	I	X Main encoder B-
25	+5V	O	+ 5Volts
25	+INW	I	X Main encoder Index +
25	-INW	I	X Main encoder Index -
25	GND	O	Signal Ground
26	+MAW	I	X Main encoder A+
26	-MAW	I	X Main encoder A-
26	+MBW	I	X Main encoder B+
26	-MBW	I	X Main encoder B-

This table is adapted from the DMC-18x2 User Manual (rev. 1.0f) by Galil Motion Control Inc. (2003).
@ Connection not available for the DMC-1842 Econo Series controller card.

B.2. BAMBI 4-Axis Electrical Assembly

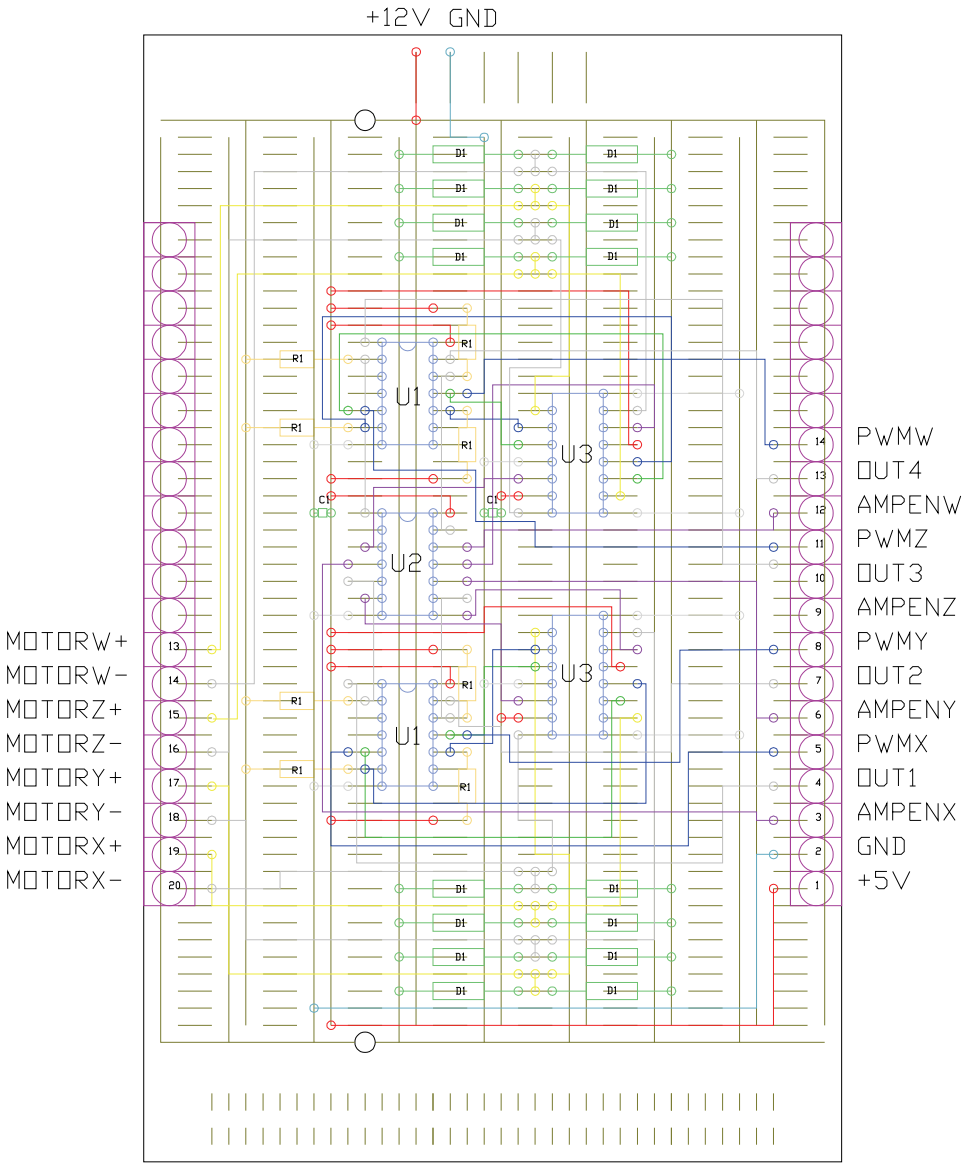

4-Axis PWM Driver Board Rev. A

Notes: This circuit was implemented on a proto-board with the traces shown in gold. A hole was drilled at the top and bottom traces to break the circuit path for high and low voltages.

Parts List for 4-Axis PWM Driver Assembly

Description	Name	Item	Qty.	Unit	Cost
Dual H-Bridge	U3	L298N	4	$5.40	$21.60
Universal Solder Board			2	$6.00	$12.00
20 pin Terminal Block			4	$7.20	$28.80
450W Power Supply /w Fan			1	$29.70	$29.70
SATA Power Cable (5.25)			1	$3.59	$3.59
Diff Green LEDs			10	$0.40	$3.96
Wire Solid, 22 gauge, 7 color, 5ft			2	$3.15	$6.30
2.75x3.75 Universal Solder Board			2	$2.25	$4.50
Capacitor mono 0.1 uF	C1		5	$0.18	$0.90
Diode (Fast Switching)	D1	1N4934	16	$0.15	$2.40
Spacer hex 2-56 11 mm			30	$0.32	$9.72
Strain Gromet			1	$0.90	$0.90
Nut 2-56 Hex			100	$0.03	$2.97
Lock Washer #2			100	$0.03	$2.97
Screw 2-56 1/4in Phillips			100	$0.02	$2.16
14 Pin IC Socket			4	$1.26	$5.04
Aluminum Case			1	$30.00	$30.00
LED holder and ring set 5mm			2	$1.35	$2.70
Hex Inverter	U1	45LS05N	2	$0.52	$1.03
20 Pin IC Socket			2	$2.40	$4.80
Quad AND GATE	U2	74ALS08	2	$0.45	$0.90
10 pin Key Female			4	$2.50	$10.00
10 pin Key Male with Ears			4	$2.50	$10.00
10 pin Key Connector			4	$2.50	$10.00
1K Resistors package of 10	R1		1	$0.90	$0.90
Tax (15%):					$31.18
Total					**$239.02**

B.3. BAMBI 8-Axis Electrical Assembly

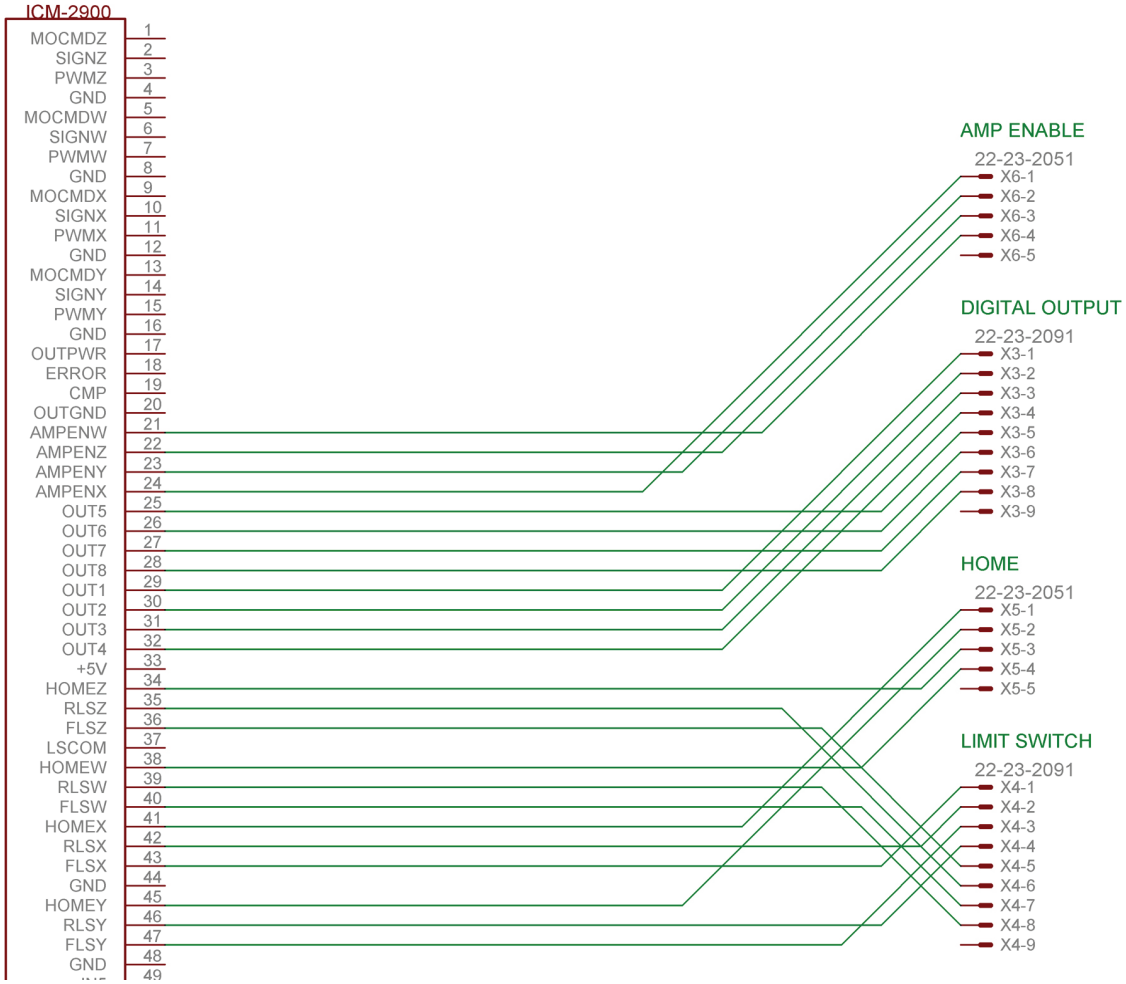

ICM-2900 Breakout I/O Electrical Connection Diagram (Page 1 of 2)

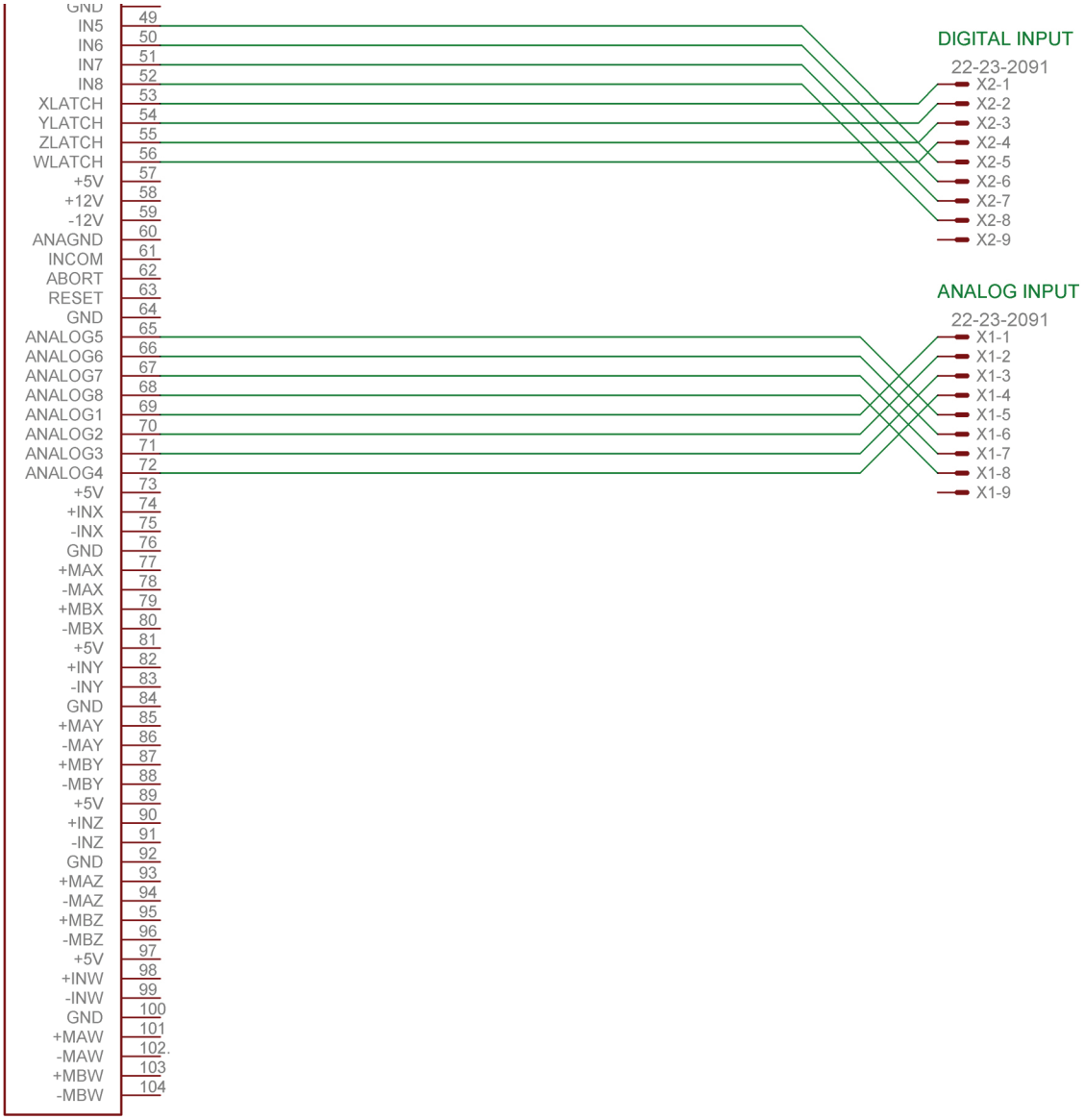

ICM-2900 Breakout I/O Electrical Connection Diagram (Page 2 of 2)

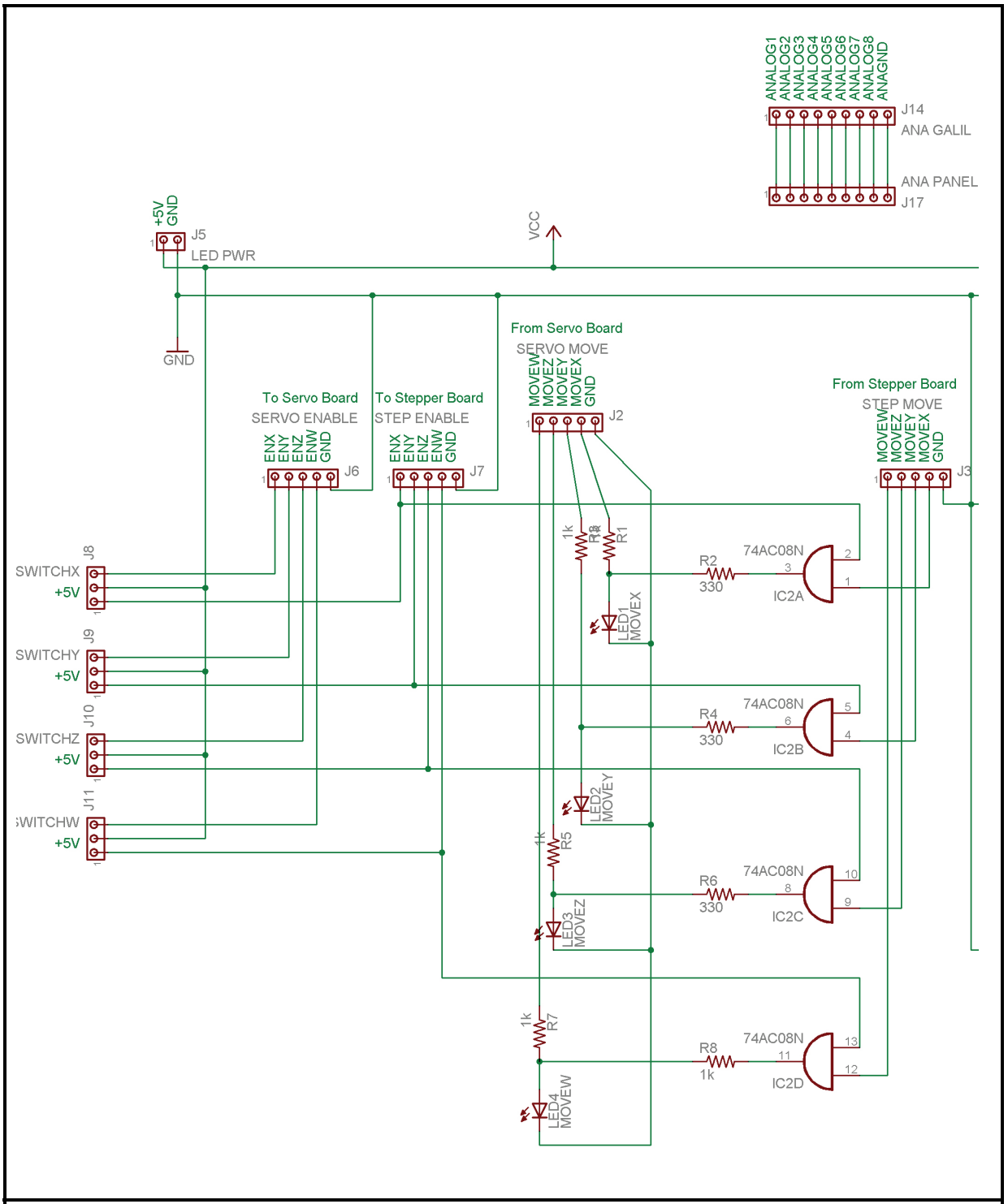

Front Panel Electrical Circuit Diagram Rev. B (Page 1 of 5)

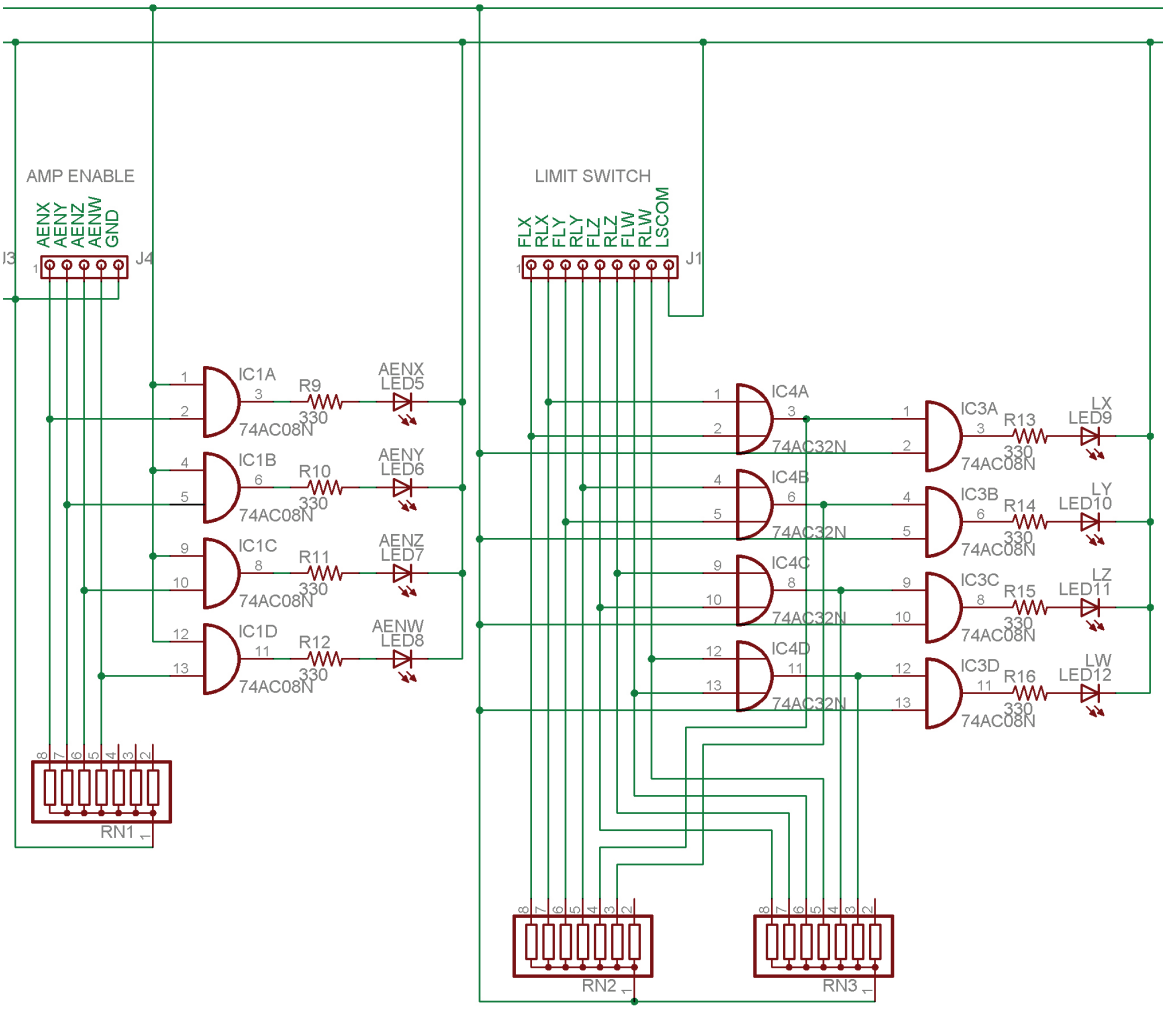

Front Panel Electrical Circuit Diagram Rev. B (Page 2 of 5)

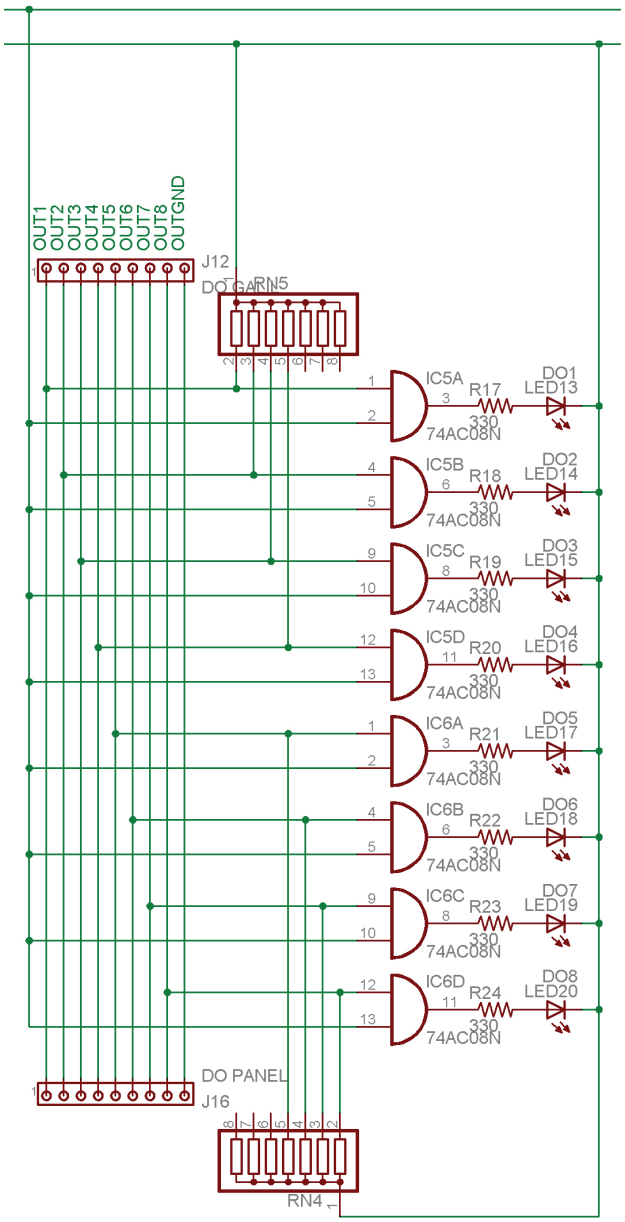

Front Panel Electrical Circuit Diagram Rev. B (Page 3 of 5)

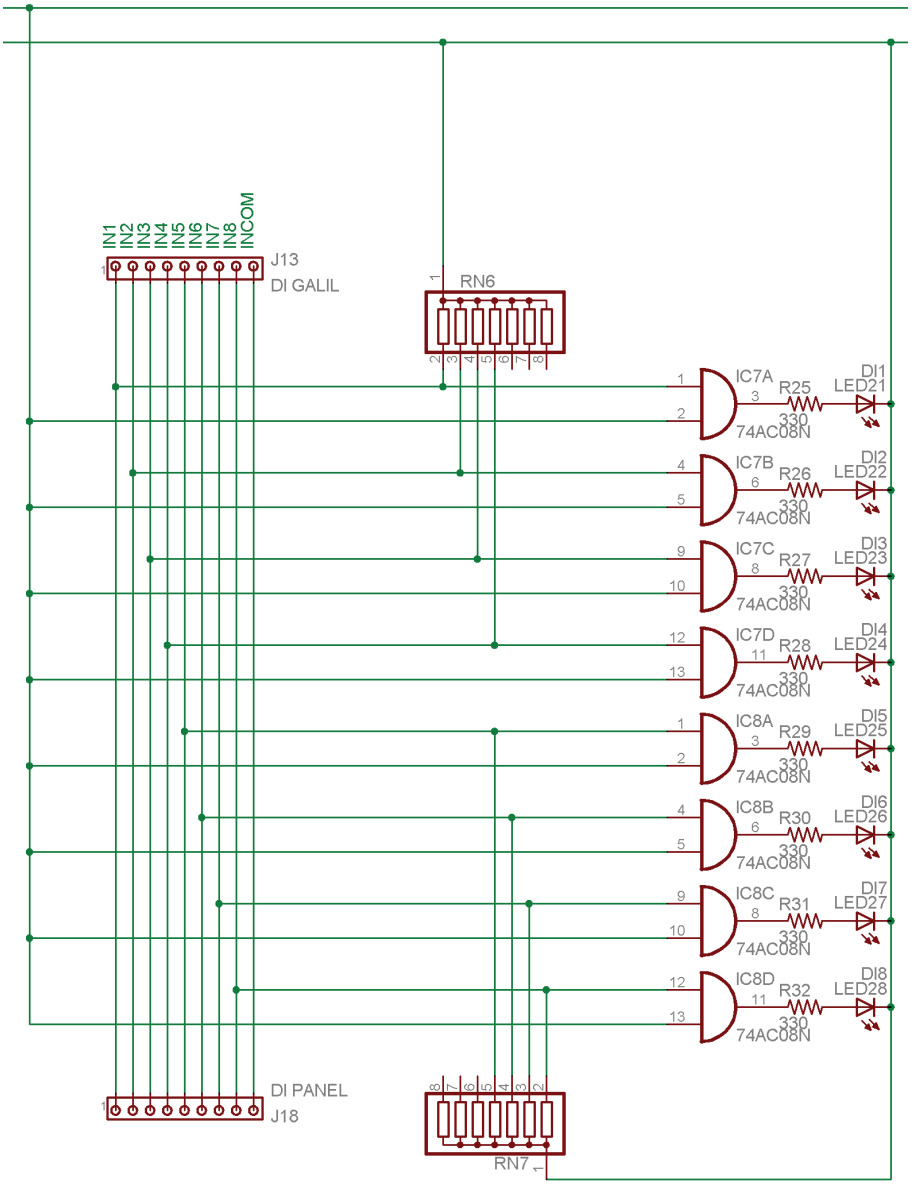

Front Panel Electrical Circuit Diagram Rev. B (Page 4 of 5)

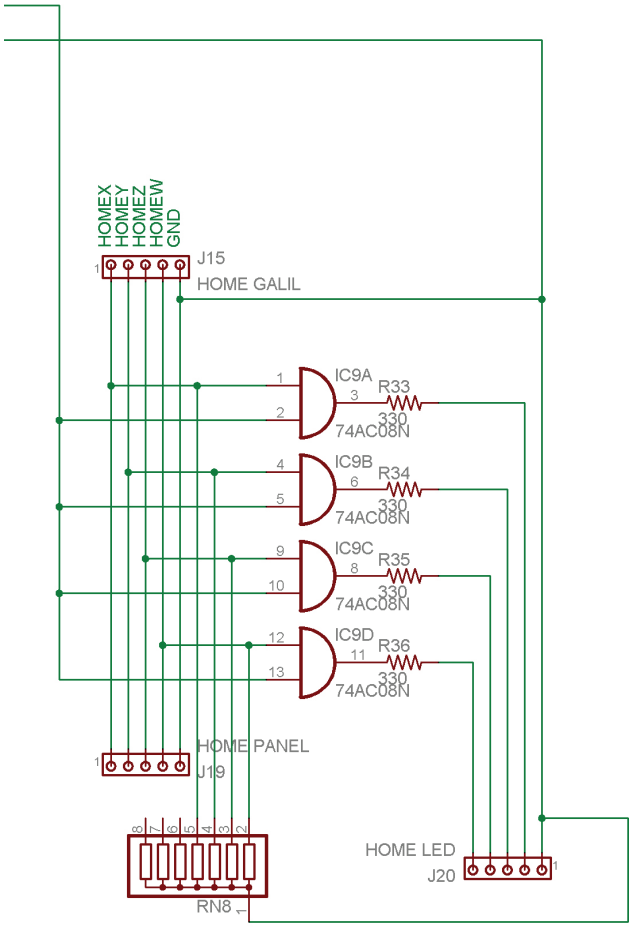

Front Panel Electrical Circuit Diagram Rev. B (Page 5 of 5)

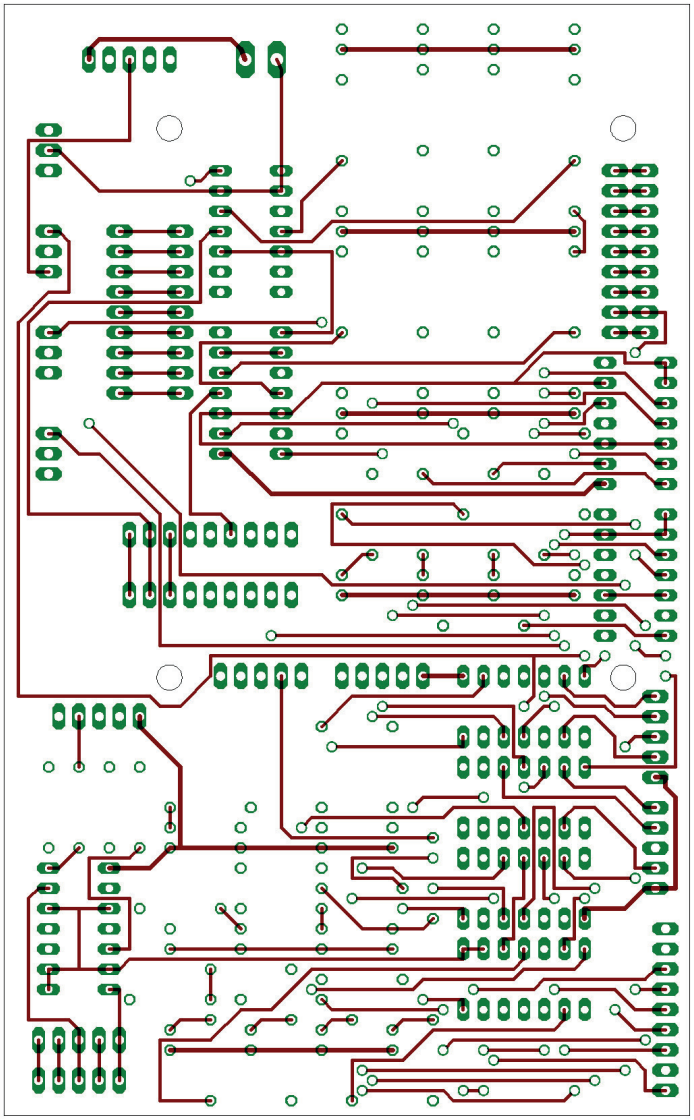

Panel Board Top Trace Rev. A

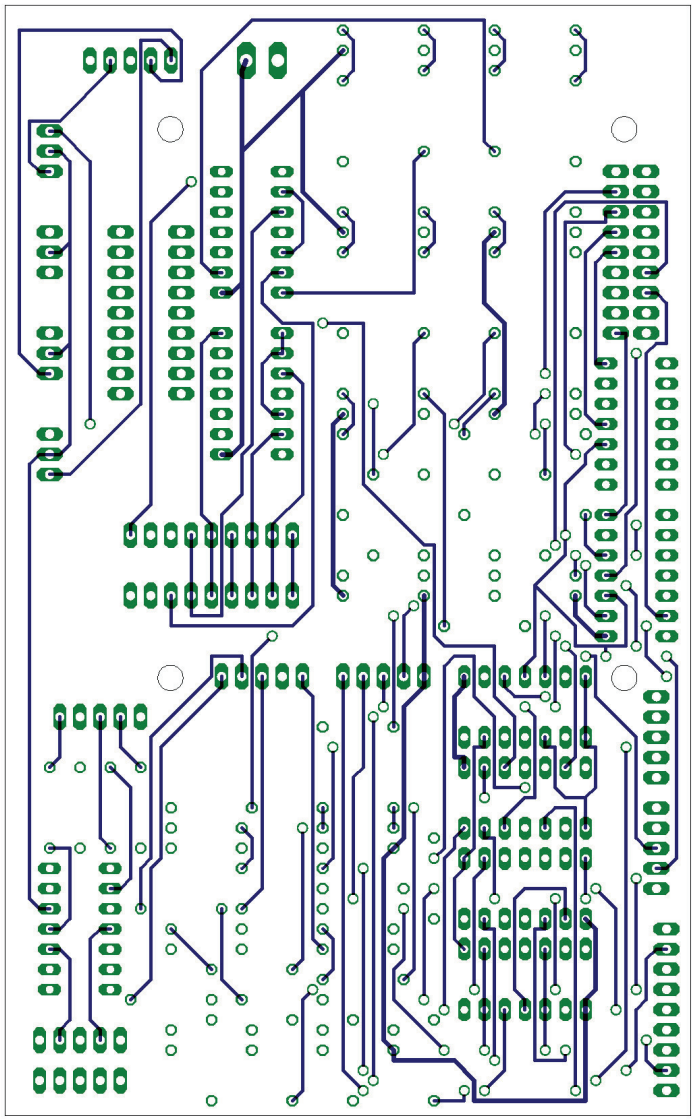

Panel Board Bottom Trace Rev. A

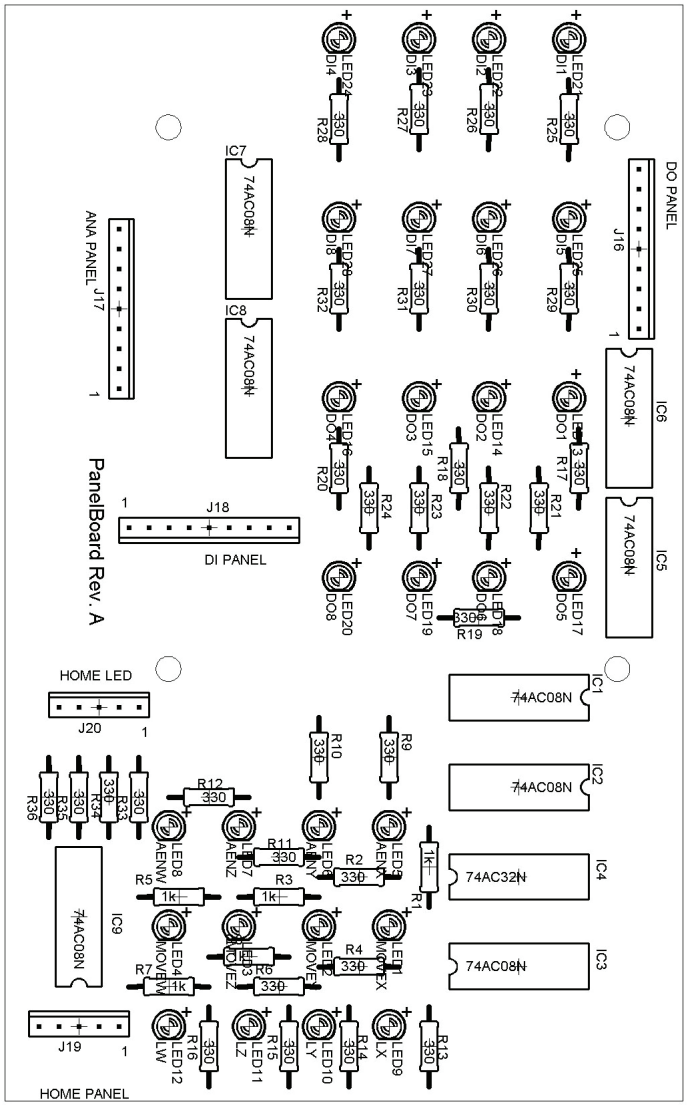

Panel Board Component Placement Rev. A

Parts List for Panel Board Assembly Rev. A

Part	Value	Device	Package	Library
IC1	74AC08N	74AC08N	DIL14	74xx-eu
IC2	74AC08N	74AC08N	DIL14	74xx-eu
IC3	74AC08N	74AC08N	DIL14	74xx-eu
IC4	74AC32N	74AC32N	DIL14	74xx-eu
IC5	74AC08N	74AC08N	DIL14	74xx-eu
IC6	74AC08N	74AC08N	DIL14	74xx-eu
IC7	74AC08N	74AC08N	DIL14	74xx-eu
IC8	74AC08N	74AC08N	DIL14	74xx-eu
IC9	74AC08N	74AC08N	DIL14	74xx-eu
J1	LIMIT SWITCH	MTA09-100	10X09MTA	con-amp
J2	SERVO MOVE	MTA05-100	10X05MTA	con-amp
J3	STEP MOVE	MTA05-100	10X05MTA	con-amp
J4	AMP ENABLE	MTA05-100	10X05MTA	con-amp
J5	LED PWR	MTA02-156	1X2MTA	con-amp
J6	SERVO ENABLE	MTA05-100	10X05MTA	con-amp
J7	STEP ENABLE	MTA05-100	10X05MTA	con-amp
J8	SWITCH 1	MTA03-100	10X03MTA	con-amp
J9	SWITCH 2	MTA03-100	10X03MTA	con-amp
J10	SWITCH 3	MTA03-100	10X03MTA	con-amp
J11	SWITCH 4	MTA03-100	10X03MTA	con-amp
J12	DO GALIL	MTA09-100	10X09MTA	con-amp
J13	DI GALIL	MTA09-100	10X09MTA	con-amp
J14	ANA GALIL	MTA09-100	10X09MTA	con-amp
J15	HOME GALIL	MTA05-100	10X05MTA	con-amp
J16	DO PANEL	MTA09-100	10X09MTA	con-amp
J17	ANA PANEL	MTA09-100	10X09MTA	con-amp
J18	DI PANEL	MTA09-100	10X09MTA	con-amp
J19	HOME PANEL	MTA05-100	10X05MTA	con-amp
J20	HOME LED	MTA05-100	10X05MTA	con-amp
LED1	MOVEX	LED3MM	LED3MM	led
LED2	MOVEY	LED3MM	LED3MM	led
LED3	MOVEZ	LED3MM	LED3MM	led
LED4	G/Y	LED3MM	LED3MM	led
LED5	AENX	LED3MM	LED3MM	led
LED6	AENY	LED3MM	LED3MM	led
LED7	AENZ	LED3MM	LED3MM	led
LED8	Green	LED3MM	LED3MM	led
LED9	LX	LED3MM	LED3MM	led
LED10	LY	LED3MM	LED3MM	led
LED11	LZ	LED3MM	LED3MM	led
LED12	Red	LED3MM	LED3MM	led
LED13	DO1	LED3MM	LED3MM	led
LED14	DO2	LED3MM	LED3MM	led

LED15	DO3	LED3MM	LED3MM		led
LED16	DO4	LED3MM	LED3MM		led
LED17	DO5	LED3MM	LED3MM		led
LED18	DO6	LED3MM	LED3MM		led
LED19	DO7	LED3MM	LED3MM		led
LED20	DO8	LED3MM	LED3MM		led
LED21	Green	LED3MM	LED3MM		led
LED22	DI2	LED3MM	LED3MM		led
LED23	DI3	LED3MM	LED3MM		led
LED24	DI4	LED3MM	LED3MM		led
LED25	DI5	LED3MM	LED3MM		led
LED26	DI6	LED3MM	LED3MM		led
LED27	DI7	LED3MM	LED3MM		led
LED28	DI8	LED3MM	LED3MM		led
R1	1k	R-US_0207/	30	7/10	rcl
R2	1k	R-US_0207/	30	7/10	rcl
R3	1k	R-US_0207/	30	7/10	rcl
R4	1k	R-US_0207/	30	7/10	rcl
R5	1k	R-US_0207/	30	7/10	rcl
R6	1k	R-US_0207/	30	7/10	rcl
R7	1k	R-US_0207/	30	7/10	rcl
R8	1k	R-US_0207/	30	7/10	rcl
R9	1k	R-US_0207/	30	7/10	rcl
R10	1k	R-US_0207/	30	7/10	rcl
R11	1k	R-US_0207/	30	7/10	rcl
R12	1k	R-US_0207/	30	7/10	rcl
R13	1k	R-US_0207/	30	7/10	rcl
R14	1k	R-US_0207/	30	7/10	rcl
R15	1k	R-US_0207/	30	7/10	rcl
R16	1k	R-US_0207/	30	7/10	rcl
R17	1k	R-US_0207/	30	7/10	rcl
R18	1k	R-US_0207/	30	7/10	rcl
R19	1k	R-US_0207/	30	7/10	rcl
R20	1k	R-US_0207/	30	7/10	rcl
R21	1k	R-US_0207/	30	7/10	rcl
R22	1k	R-US_0207/	30	7/10	rcl
R23	1k	R-US_0207/	30	7/10	rcl
R24	1k	R-US_0207/	30	7/10	rcl
R25	1k	R-US_0207/	30	7/10	rcl
R26	1k	R-US_0207/	30	7/10	rcl
R27	1k	R-US_0207/	30	7/10	rcl
R28	1k	R-US_0207/	30	7/10	rcl
R29	1k	R-US_0207/	30	7/10	rcl
R30	1k	R-US_0207/	30	7/10	rcl
R31	1k	R-US_0207/	30	7/10	rcl
R32	1k	R-US_0207/	30	7/10	rcl
R33	1k	R-US_0207/	30	7/10	rcl

R34	1k	R-US_0207/	30	7/10	rcl
R35	1k	R-US_0207/	30	7/10	rcl
R36	1k	R-US_0207/	30	7/10	rcl

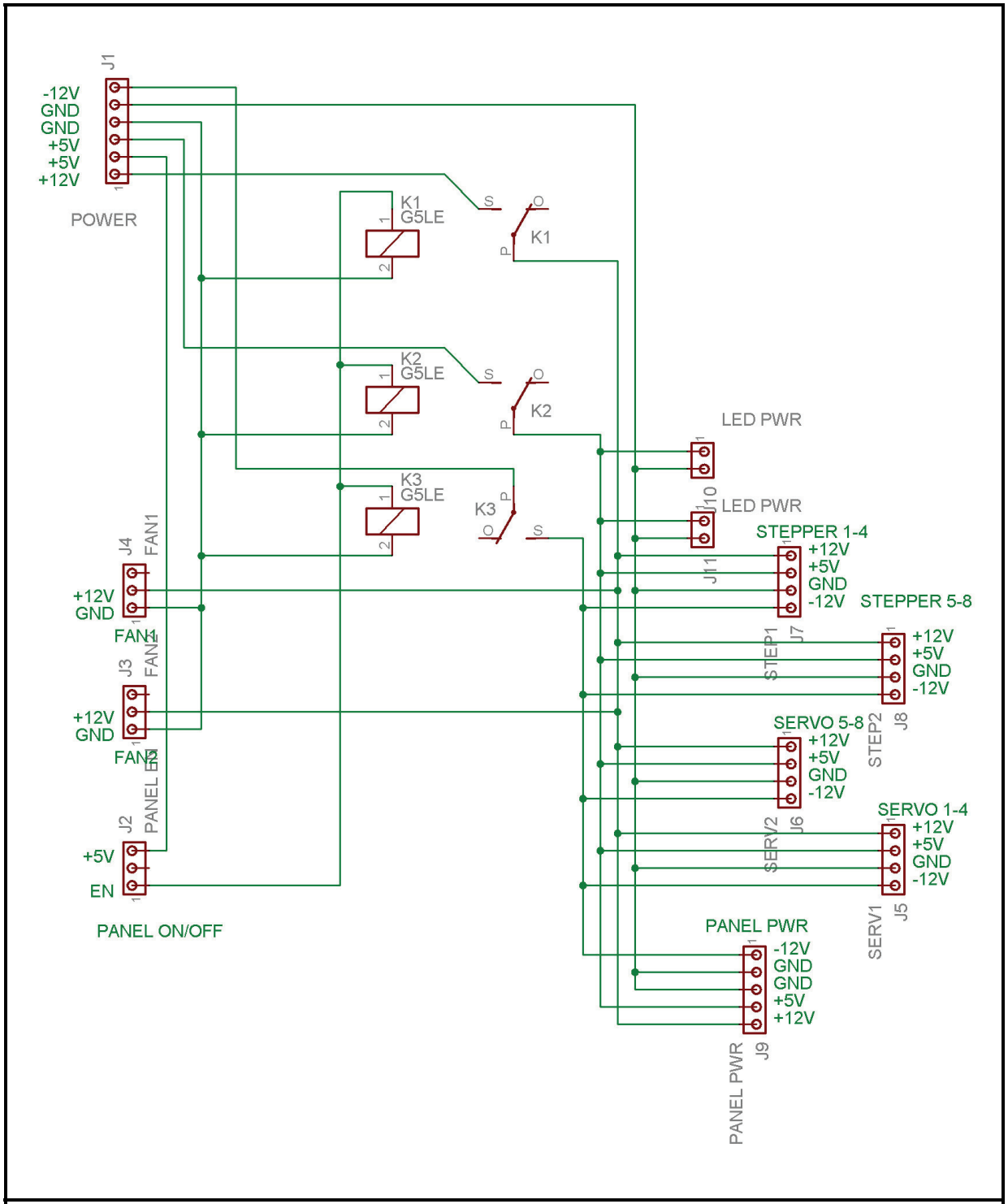

Power Board Schematic Diagram Rev. B

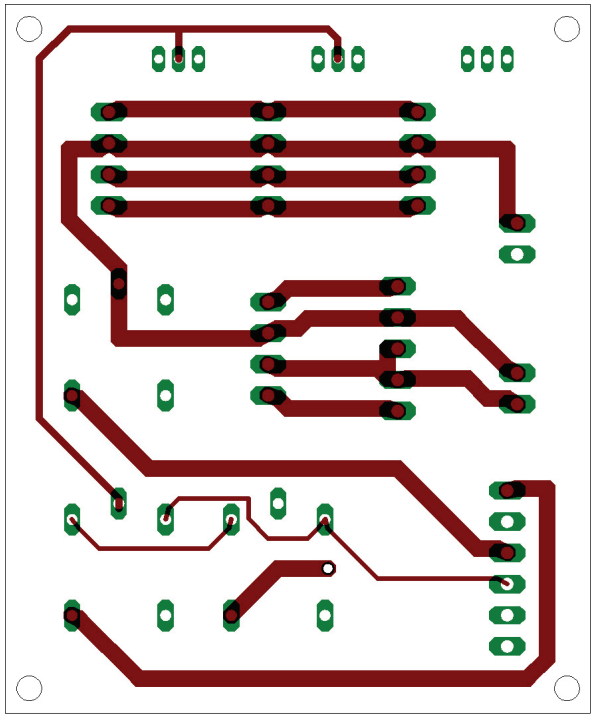

Power Board Top Trace Rev. A

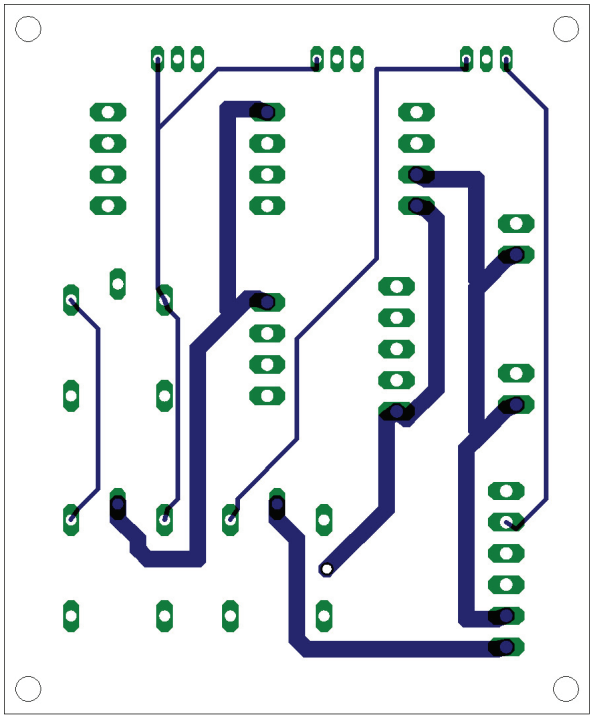

Power Board Bottom Trace Rev. A

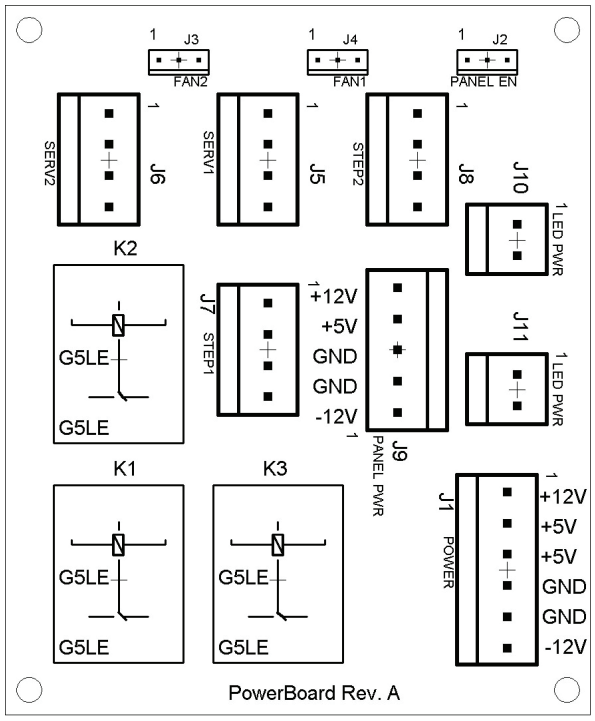

Power Board Component Placement Rev. A

Parts List for Power Board Assembly Rev. A

Part	Value	Device	Package	Library
J1	POWER	MTA06-156	1X6MTA	con-amp
J2	PANEL EN	MTA03-100	10X03MTA	con-amp
J3	FAN2	MTA03-100	10X03MTA	con-amp
J4	FAN1	MTA03-100	10X03MTA	con-amp
J5	SERV1	MTA04-156	1X4MTA	con-amp
J6	SERV2	MTA04-156	1X4MTA	con-amp
J7	STEP1	MTA04-156	1X4MTA	con-amp
J8	STEP2	MTA04-156	1X4MTA	con-amp
J9	PANEL PWR	MTA05-156	1X5MTA	con-amp
J10	LED PWR	MTA02-156	1X2MTA	con-amp
J11	LED PWR	MTA02-156	1X2MTA	con-amp
K1	G5LE	G5LE	G5LE	relay
K2	G5LE	G5LE	G5LE	relay
K3	G5LE	G5LE	G5LE	relay

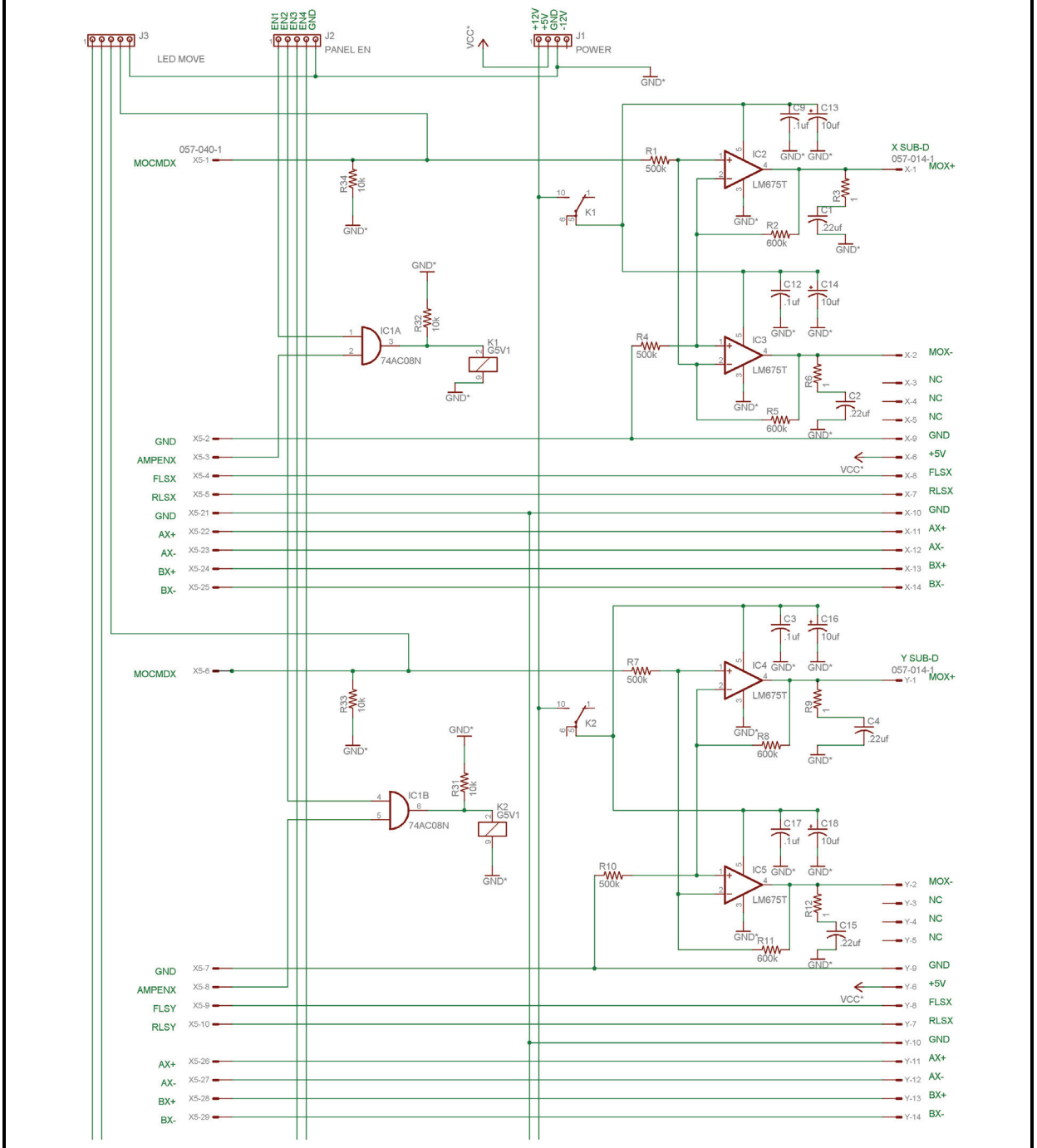

Servo Board Schematic Diagram Rev. B (Page 1 of 2)

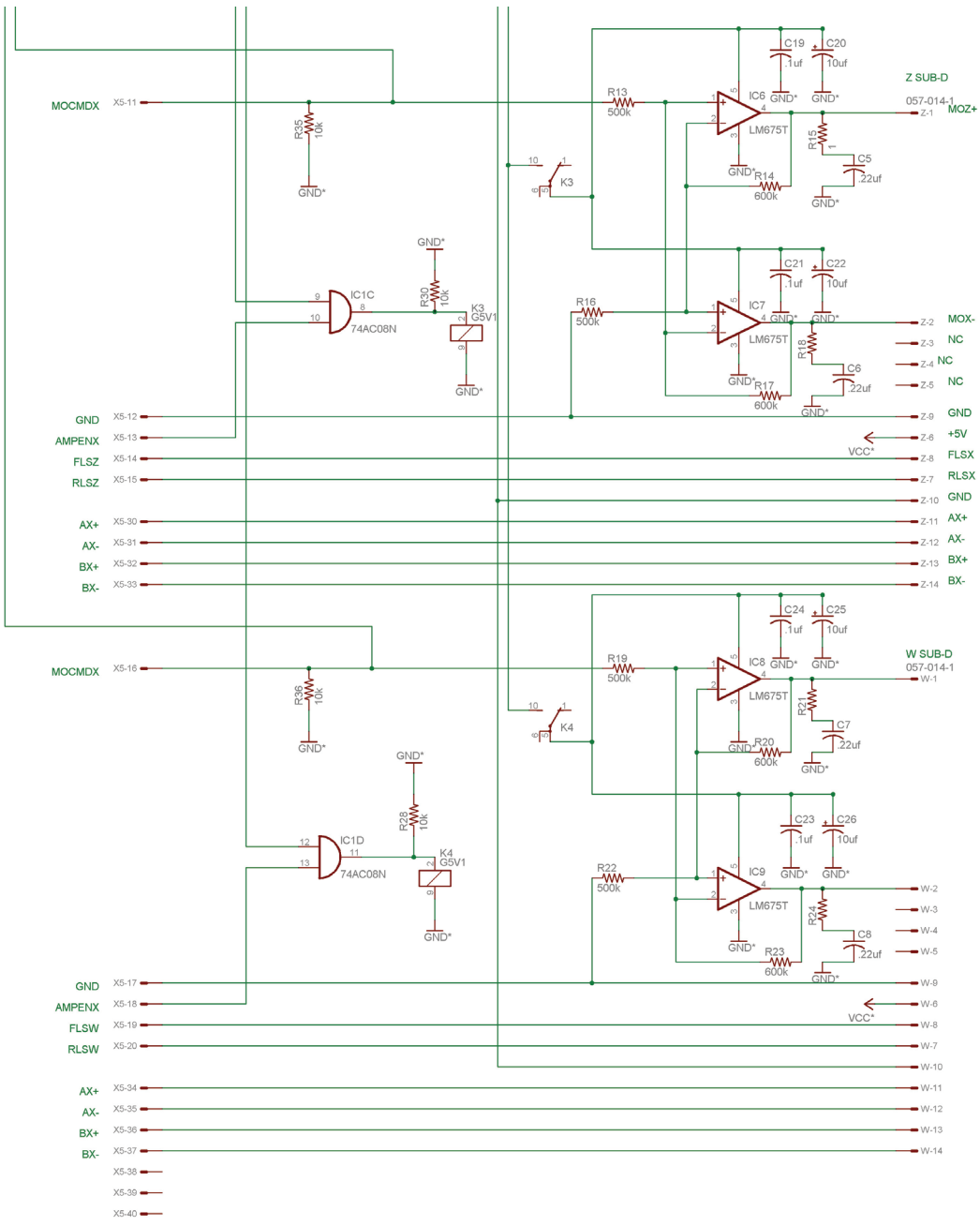

Servo Board Schematic Diagram Rev. B (Page 2 of 2)

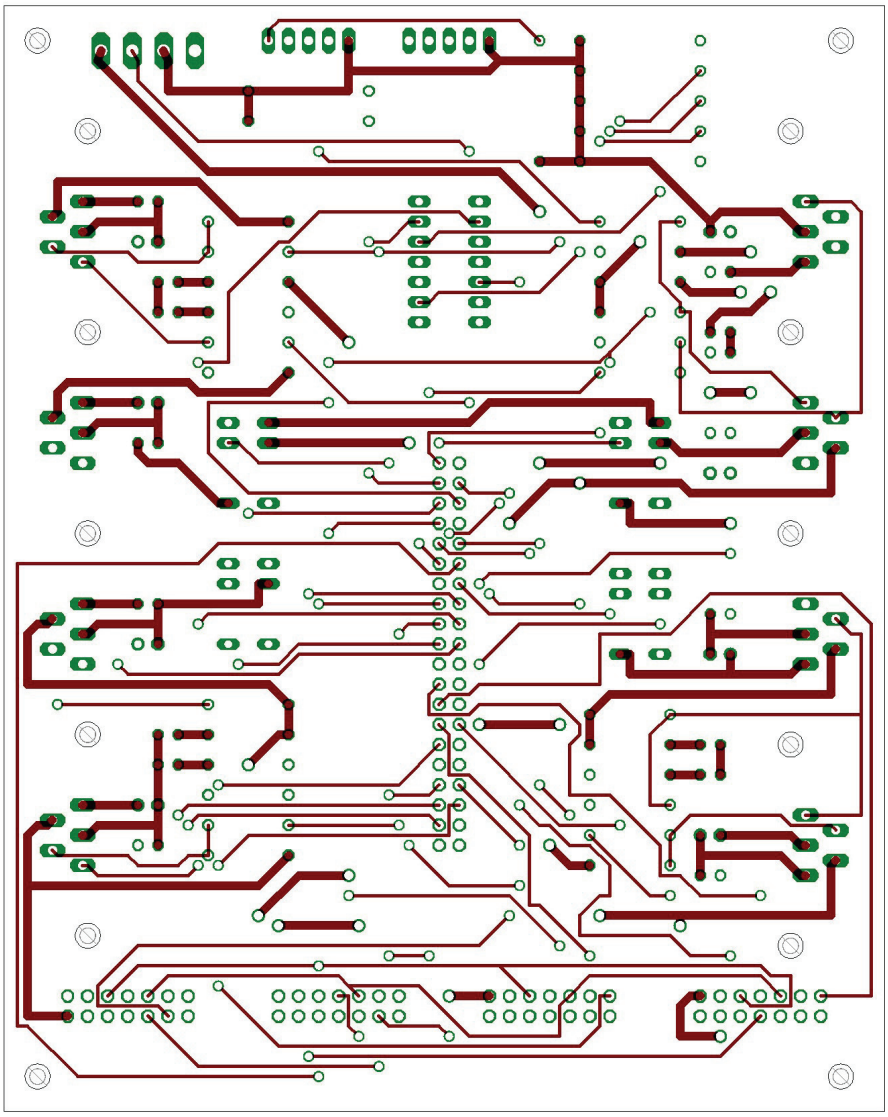

Servo Board Top Trace Rev. A

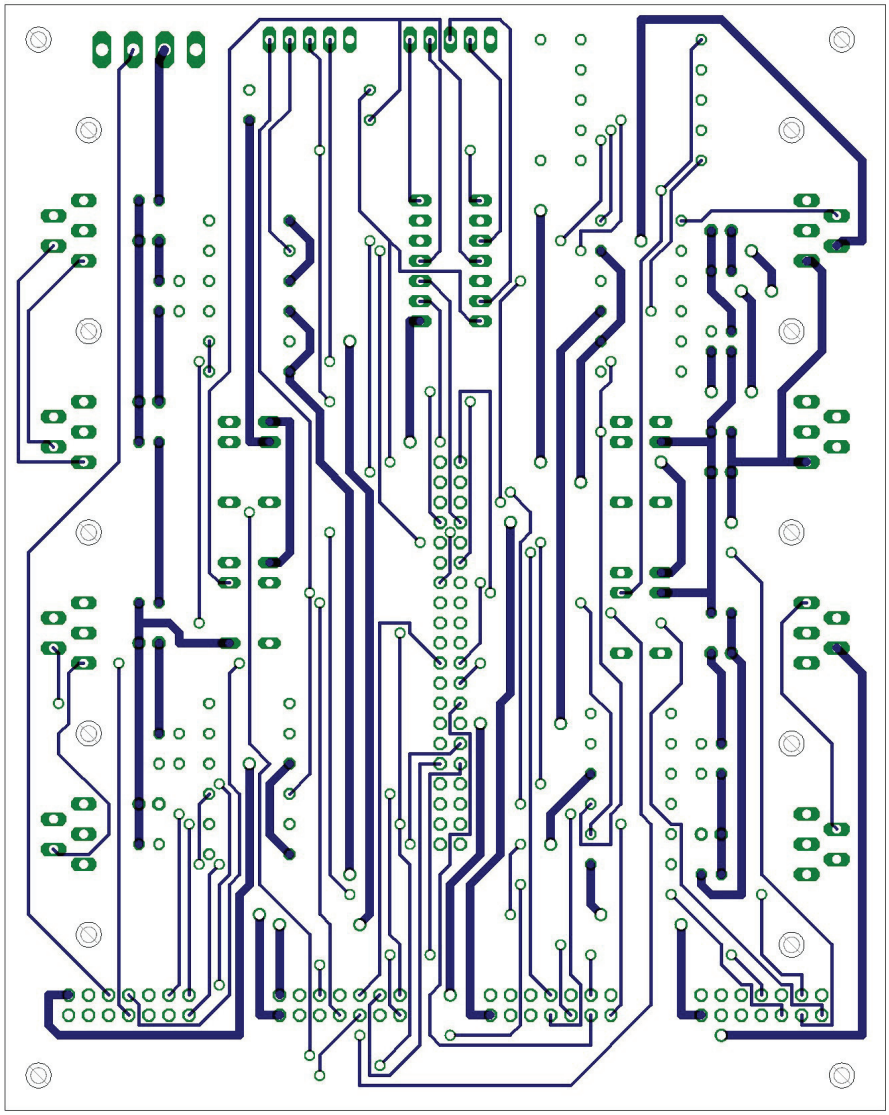

Servo Board Bottom Trace Rev. A

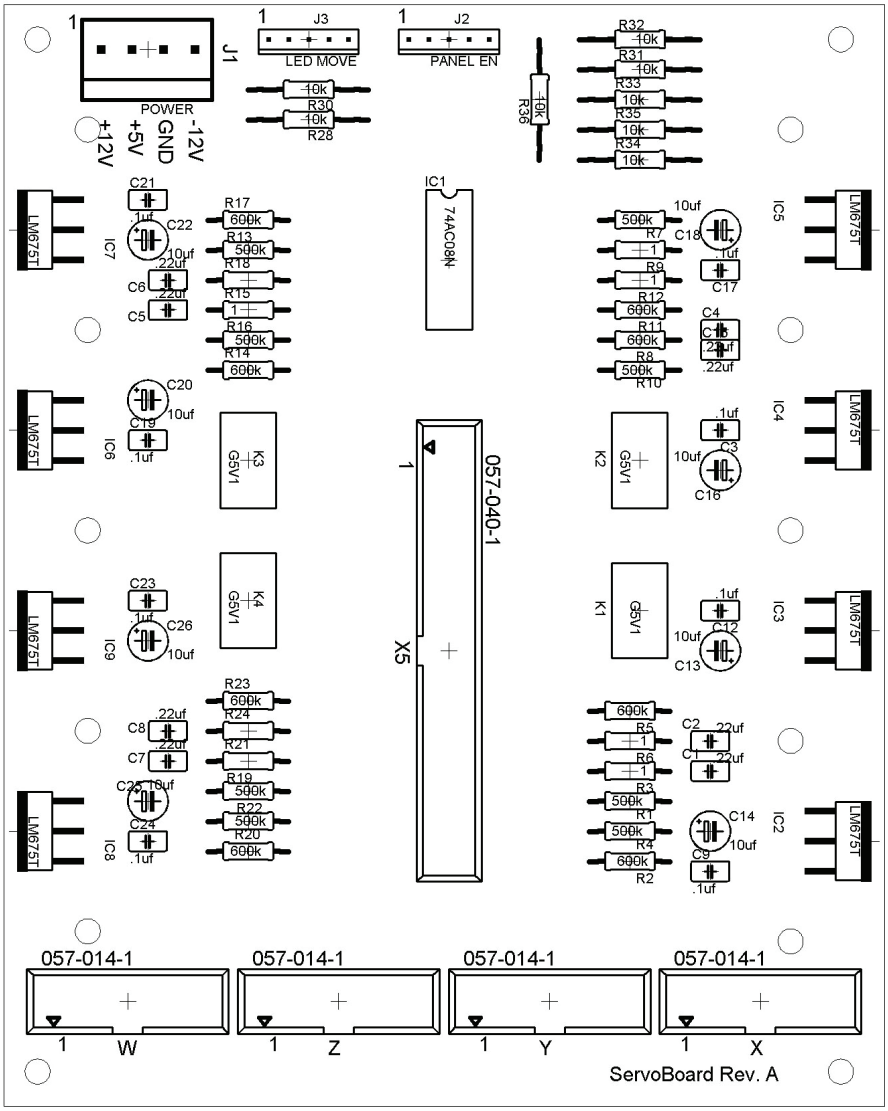

Servo Board Component Placement Rev. A

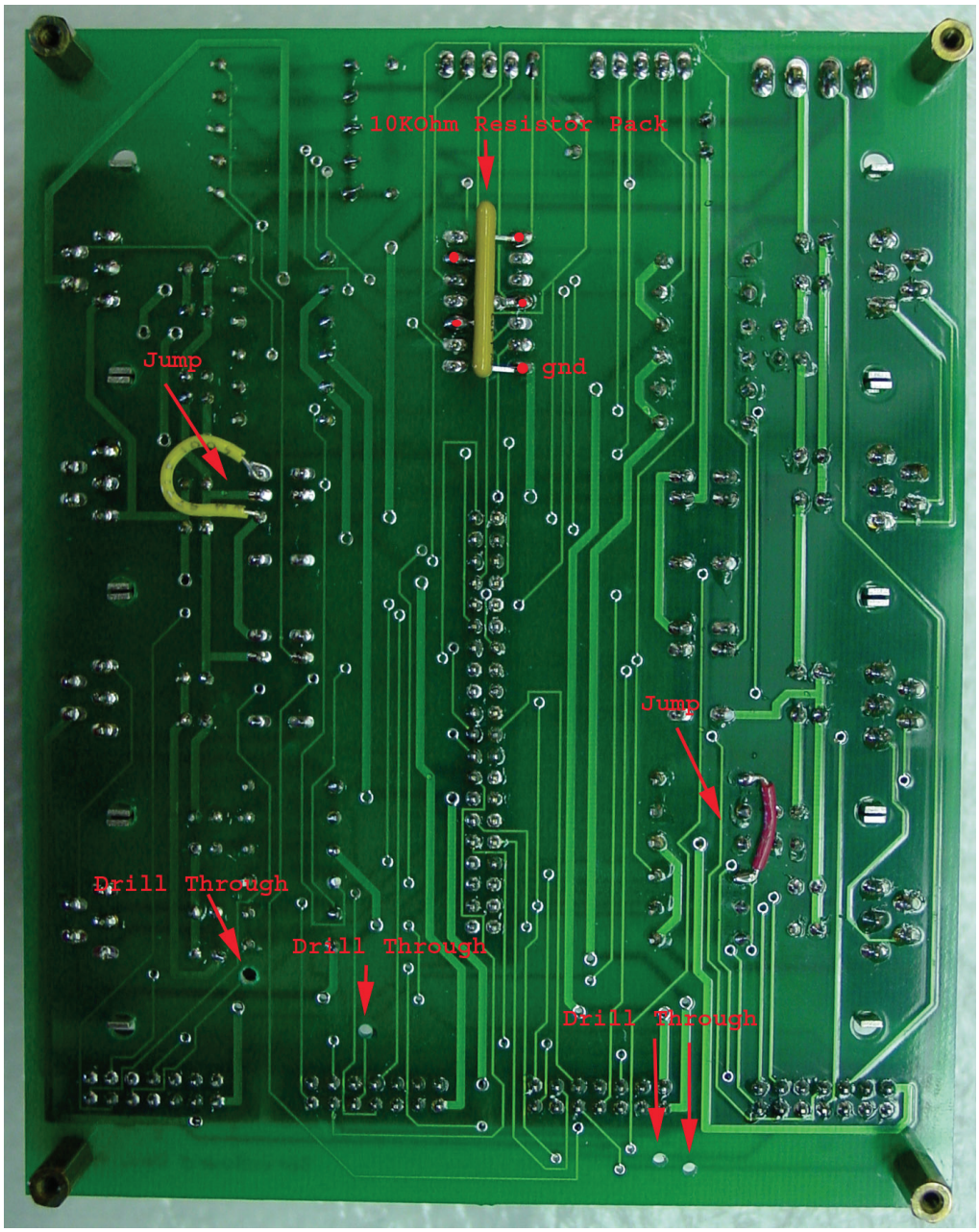

Servo Board Modifications From Rev. A to Rev. B

Parts List for Servo Board Assembly Rev. A

Part	Value	Device	Package	Library
C1	.22uf	C-US025-025X050	C025-025X050	rcl
C2	.22uf	C-US025-025X050	C025-025X050	rcl
C3	.1uf	C-US025-025X050	C025-025X050	rcl
C4	.22uf	C-US025-025X050	C025-025X050	rcl
C5	.22uf	C-US025-025X050	C025-025X050	rcl
C6	.22uf	C-US025-025X050	C025-025X050	rcl
C7	.22uf	C-US025-025X050	C025-025X050	rcl
C8	.22uf	C-US025-025X050	C025-025X050	rcl
C9	.1uf	C-US025-025X050	C025-025X050	rcl
C12	.1uf	C-US025-025X050	C025-025X050	rcl
C13	10uf	CPOL-USE2.5-5	E2,5-5	rcl
C14	10uf	CPOL-USE2.5-5	E2,5-5	rcl
C15	.22uf	C-US025-025X050	C025-025X050	rcl
C16	10uf	CPOL-USE2.5-5	E2,5-5	rcl
C17	.1uf	C-US025-025X050	C025-025X050	rcl
C18	10uf	CPOL-USE2.5-5	E2,5-5	rcl
C19	.1uf	C-US025-025X050	C025-025X050	rcl
C20	10uf	CPOL-USE2.5-5	E2,5-5	rcl
C21	.1uf	C-US025-025X050	C025-025X050	rcl
C22	10uf	CPOL-USE2.5-5	E2,5-5	rcl
C23	.1uf	C-US025-025X050	C025-025X050	rcl
C24	.1uf	C-US025-025X050	C025-025X050	rcl
C25	10uf	CPOL-USE2.5-5	E2,5-5	rcl
C26	10uf	CPOL-USE2.5-5	E2,5-5	rcl
IC1	74AC08N	74AC08N	DIL14	74xx-eu
IC2	LM675T	LM675T	CB367	linear
IC3	LM675T	LM675T	CB367	linear
IC4	LM675T	LM675T	CB367	linear
IC5	LM675T	LM675T	CB367	linear
IC6	LM675T	LM675T	CB367	linear
IC7	LM675T	LM675T	CB367	linear
IC8	LM675T	LM675T	CB367	linear
IC9	LM675T	LM675T	CB367	linear
J1	POWER	MTA04-156	1X4MTA	con-amp
J2	PANEL EN	MTA05-100	10X05MTA	con-amp
J3	LED MOVE	MTA05-100	10X05MTA	con-amp
K1	G5V1	G5V1	G5V1	relay
K2	G5V1	G5V1	G5V1	relay
K3	G5V1	G5V1	G5V1	relay
K4	G5V1	G5V1	G5V1	relay
R1	500k	R-US_0207/10	0207/10	rcl
R2	600k	R-US_0207/10	0207/10	rcl
R3	1	R-US_0207/10	0207/10	rcl

R4	500k	R-US_0207/10	0207/10	rcl
R5	600k	R-US_0207/10	0207/10	rcl
R6	1	R-US_0207/10	0207/10	rcl
R7	500k	R-US_0207/10	0207/10	rcl
R8	600k	R-US_0207/10	0207/10	rcl
R9	1	R-US_0207/10	0207/10	rcl
R10	500k	R-US_0207/10	0207/10	rcl
R11	600k	R-US_0207/10	0207/10	rcl
R12	1	R-US_0207/10	0207/10	rcl
R13	500k	R-US_0207/10	0207/10	rcl
R14	600k	R-US_0207/10	0207/10	rcl
R15	1	R-US_0207/10	0207/10	rcl
R16	500k	R-US_0207/10	0207/10	rcl
R17	600k	R-US_0207/10	0207/10	rcl
R18	1	R-US_0207/10	0207/10	rcl
R19	500k	R-US_0207/10	0207/10	rcl
R20	600k	R-US_0207/10	0207/10	rcl
R21	1	R-US_0207/10	0207/10	rcl
R22	500k	R-US_0207/10	0207/10	rcl
R23	600k	R-US_0207/10	0207/10	rcl
R24	1	R-US_0207/10	0207/10	rcl
R28	10k	R-US_0207/15	0207/15	rcl
R30	10k	R-US_0207/15	0207/15	rcl
R31	10k	R-US_0207/15	0207/15	rcl
R32	10k	R-US_0207/15	0207/15	rcl
R33	10k	R-US_0207/15	0207/15	rcl
R34	10k	R-US_0207/15	0207/15	rcl
R35	10k	R-US_0207/15	0207/15	rcl
R36	10k	R-US_0207/15	0207/15	rcl
X1	057-014-1	057-014-1	057-014-1	con-panduit
X2	057-014-1	057-014-1	057-014-1	con-panduit
X3	057-014-1	057-014-1	057-014-1	con-panduit
X4	057-014-1	057-014-1	057-014-1	con-panduit
X5	057-040-1	057-040-1	057-040-1	con-panduit

Appendix C
Software

C.1. BAM File Structure

```
// Block Count
m_iBlockCount
FOR i = 1 to m_iBlockCount
        // Block ID
        m_iID
        // Path ID
        m_iPathID
        // Block Settings
        m_ulStartTic
        m_bAutoFocus
        m_bBlockEnable
        m_iHeight
        m_iWidth
        m_fCameraLens
        m_iObjective
        m_iOrigin
        m_iArray
        m_lStepX
        m_lStepY
        m_lStepZ
        m_iRows
        m_iCols
        m_iSlices
        m_lULX
        m_lULY
        m_lULZ
        m_lURX
        m_lURY
        m_lURZ
        m_lLRX
        m_lLRY
        m_lLRZ
        m_lZOffset
        // DIC Settings
        m_ulNextDICTic
        m_ulLayerCount
        m_sFileName
        m_sFilePath
        m_sLogFileName
        m_iShutter
        m_lInterval
        // LED Settings
        FOR j = 0 to 4
                m_ulNextLEDTic[j]
                m_ulLEDLayerCount[j]
                m_bLED[j]
                m_sLEDFileName[j]
                m_sLEDFilePath[j]
                m_sLogLEDFileName[j]
                m_iAccumulates[j]
                m_iLEDGain[j]
```

```
                m_iLEDShutter[j]
                m_lLEDInterval[j]
        ENDFOR
        // WayPoint Count
        m_iNumWayPoints
        FOR k = 1 to m_iNumWayPoints
                // WayPoint info
                coord[0]
                coord[1]
                coord[2]
                m_bEnable
                m_iID
        ENDFOR
ENDFOR
```

C.2. Mosaic Block Structure

Type	Name	Description
int	m_iID	A unique ID given to each block
int	m_iPathID	The path the camera will take to collect all images in the mosaic - default is ZigZag. (ZigZag or Linear).
int	m_iOrigin	Logical state of the control waypoints 0x000. Defined UL is 0x100, UR is 0x010, and LR 0x001.
int	m_iArray	State of waypoint calculation. 0 = uncalculated waypoints 1 = calculated waypoints
bool	m_bAutoFocus	0 = Autofocus Off. 1 = Autofocus On
bool	m_bLED[5]	If true, the LED channel for this block has been defined and enabled.
int	m_iGain	Camera gain setting for DIC
int	m_iLEDGain[5]	Camera gain setting for LEDs
int	m_iShutter	Camera shutter setting for DIC
int	m_iLEDShutter[5]	Camera shutter setting for LEDs
int	m_iObjective	Microscope objective lens power value (Usually 5, 10, 20, 40, or 60)
int	m_iAccumulates[5]	The number of images to be collected and summed for the LEDs
float	m_fCameraLens	Camera adapter lens power value (Usually 1.0, 0.5, or 0.4)
int	m_iHeight	Height in pixels of the camera image
int	m_iWidth	Width in pixels of the camera image
long	m_lStepX	Horizontal grid spacing in motor units
long	m_lStepY	Vertical grid spacing in motor units
long	m_lStepZ	Rising grid spacing in motor units
int	m_iRows	The number of rows in the mosaic
int	m_iCols	The number of columns in the mosaic
int	m_iSlices	The number of slices in Z direction for the mosaic block
long	m_lULX	Mosaic Block defined by upper left corner x coordinate
long	m_lULY	Mosaic Block defined by upper left corner y coordinate
long	m_lULZ	Mosaic Block defined by upper left corner z coordinate
long	m_lURX	Mosaic Block defined by upper right corner x coordinate
long	m_lURY	Mosaic Block defined by upper right corner y coordinate
long	m_lURZ	Mosaic Block defined by upper right corner z coordinate
long	m_lLRX	Mosaic Block defined by lower right corner x coordinate
long	m_lLRY	Mosaic Block defined by lower right corner y coordinate
long	m_lLRZ	Mosaic Block defined by lower right corner z coordinate
long	m_lZOffset	A z-offset value in motor units to be applied to each waypoint. It is used to correct for focal drift and persist focal drift corrections. Currently not used as it is easier to reset the origin base point.
long	m_lInterval	Minimum time to cycle between time slices (in seconds)
long	m_lLEDInterval[5]	Minimum time to cycle between fluorescent time slices (in seconds)
int	m_iNumWayPoints	The number of waypoint objects (usually rows * cols)

CObList	m_oWayPoints	This is the object list containing the pointers to all the waypoints
CString	m_sFileName	This is the file name of the DIC raw file
CString	m_sFilePath	This is the path of the DIC raw and log file
CFile*	m_pFile	Pointer to the DIC raw file
CString	m_sLEDFileName[5]	This is the file name of the LED raw files
CString	m_sLEDFilePath[5]	This is the file path of the LED raw and log files
CFile*	m_pLEDFile[5]	Pointer to the LED raw files
CString	m_sLogFileName	This is the file name of the DIC log file
CFile*	m_pLogFile	Pointer to the DIC log raw file
CString	m_sLogLEDFileName[5]	This is the file name of the LED log files
CFile*	m_pLogLEDFile[5]	Pointer to the LED log files
unsigned long	m_ulStartTic	This will be the tick count at the beginning of the experiment
unsigned long	m_ulNextDICTic	The time for the next DIC cycle to start
unsigned long	m_ulNextLEDTic[5]	The time for the next LED cycle to start
unsigned long	m_ulLayerCount	The current number of DIC layers accumulated
unsigned long	m_ulLEDLayerCount[5]	The current number of LED layers collected
bool	m_bBlockEnable	Enabled = 1, Disabled = 0.

References

Anderson, J., Chiu, D., Jackman, R., Cherniavskaya, O., McDonald, J., Whitesides, S., Whitesides, G. (2000). Fabrication of Topologically Complex Three-Dimensional Microfluidic Systems in PDMS by Rapid Prototyping. *Analytical Chemistry, 7,* 3158-3164.

Andrews, P., Harper, I., Swedlow, J. (2002). To 5D and Beyond: Quantitative Fluorescence Microscopy in the Postgenomic Era. *Traffic, 3,* 29-36.

Applegate, R. Jr., Squier, J., Vestad, T., Oakey, J., Marr, D. (2004). Optical trapping, manipulation, and sorting of cells and colloids in microfluidic systems with diode laser bars. *Optics Express, 12(19),* 4390-4398.

Ashkin, A., Dziedzic, J. (1987). Optical Trapping and Manipulation of Viruses and Bacteria. *Science, 235,* 1517-1520.

Astrom, K., Hagglund, T. (1995). *PID controllers: Theory, design and tuning.* North Carolina: Instrument Society of America Research Triangle Park.

Casey, D. (1999). HGP Leaders Confirm Accelerated Timetable for Draft Sequence. *Human Genome News, 10*, 1.

Baker, C., Ulrich, I. (2004). *CMU 1394 Digital Camera Driver.* Retrieved July, 14. 2007, from http://www.cs.cmu.edu/~iwan/1394/

Barron, J., Wu, P., Ladouceur, H., Ringeisen, B. (2004). Biological Laser Printing: A Novel Technique for Creating Heterogeneous 3-Dimensional Cell Patterns. *Biomedical Microdevices, 6(2),* 139-147.

Boland T., Wilson C. (2003). Cell and Organ Printing 1: Protein and Cell Printers. *The Anatomical Record, 272A,* 491-496.

Boland T, Wilson C. (2003). Cell and Organ Printing 2: Fusion of Cell Aggregates in Three-Dimensional Gels. *The Anatomical Record, 272A,* 497-502.

Burglin, T. R. (2000). A two-channel four-dimensional image recording and viewing system with automatic drift correction. *Journal of Microscopy*, *200*(1), 75-80.

Carpenter, A., Ashouri, A., Belmont, A. (2004). Automated Microscopy Identifies Estrogen Receptor Subdomains With Large-Scale Chromatin Structure Unfolding Activity. *Cytometry, 58A*, 157-166.

Chalfie, M., Tu, Y., Euskirchen, G., Ward, W. W., & Prasher, D. C. (1994). Green fluorescent protein as a marker for gene expression. *Science, 263,* 802-805.

Chin, V., Taupin, P., Sanga, S., Scheel, J., Gage, F., Bhatia, S. (2004). Microfabricated Platform for Studying Stem Cell Fates. *Biotechnology and Bioengineering, 88,* 399-414.

Chiu, D., Jeon, N., Huang, S., Kane, R., Wargo, C., Choi, I., Ingber, D., Whitesides, G. (2000). Patterned deposition of cells and proteins onto surfaces by using three-dimensional microfluidic systems. *Proceedings of the National Academy of Sciences, 97,* 2408-2413.

Cox, G. (2006) *Optical Imaging Techniques in Cell Biology*. FL: CRC Press.

Curtis, J., Koss, B., Grier, D. (2002). Dynamic holographic optical tweezers. *Optics Communications, 207*, 169-175.

Dvorak, J., Stotler, W. (1971). A Controlled-Environment Culture System for High Resolution Light Microscopy. *Experimental Cell Research. 68,* 144-148.

Ellson, R., Mutz, M., Browning, B., Lee, L. Jr., Miller. M., Papen, R. (2003). Transfer of Low Nanoliter Volumes between Microplates Using Focused Acoustics—Automation Considerations. *JALA, 8,* 29–34.

Firestone, L., Cook, K., Culp, K., Talsania, N., Preston, K. Jr. (1991). Comparison of Autofocus Methods for Automated Microscopy. *Cytometry, 12,* 196-206.

Forsyth, D., Ponce, J. (2003). *Computer Vision: A Modern Approach*. NJ: Pearson Education Inc.

Geusebroek, J., Cornelissen, F., Smeulders, A., Geerts, H. (2000). Robust Autofocusing in Microscopy. *Cytometry, 39,* 1-9.

Gonzales, R., Woods, R. (2002). *Digital Image Processing*. NJ: Prentice-hall Inc.

Groen, F., Young, I., Ligthart, G. (1985). A Comparison of Different Focus Functions for Use in Autofocus Algorithms. *Cytometry, 6*, 81-91.

Gruber, L., Bradley, K., Lopes, W., Lancelot, R., Plewa, J., Grier, D. (2004). System and method of sorting materials using holographic laser steering. *United States Patent Application: 20040089798.*

Ince, C., Ypey, D., Diesselhoff-Den Dulk, M., Visser, J., De Vos, D., Van Furth, R. (1983). Micro-CO_2-Incubator for Use on a Microscope. *Journal of Immunological Methods, 60,* 269-275.

Inoué, S. (1986). *Video Microscopy*. New York: Plenum Press.

Johnson, E. T., Goforth, L. J. (1974). Metaphase spread detection and focus using closed circuit television. *Journal of Histochemistry and Cytochemistry, 22*, 536–545.

Lalan S, Pomerantseva I, Vacanti J. (2001). Tissue Engineering and Its Potential Impact on Surgery. *World Journal of Surgery. Vol. 25,* 1458-1466.

LaMothe, A. (2003). *Tricks of the 3D Game Programming Gurus. Advanced 3D Graphics and rasterization.* USA: Sams Publishing.

Lamprecht, M., Saatini, D., Carpenter, A. (2007). CellProfiler™: free, versatile software for automated biological image analysis. *BioTechniques, 42(1),* 71-75.

Lewis, P., Yang, C. (1997). *Basic Control Systems Engineering*. New Jersey: Prentice-Hall Inc.

Galil Motion Control Inc. (2006). *DMCWin32 Galil Windows API Tool Kit Manual Rev 2.2*. Retrieved July 23, 2007, from http://www.galilmc.com/support/manuals/dmcwin.pdf

Liu, V., Bhatia, S. (2002). Three-Dimensional Photopatterning of Hydrogels Containing Living Cells. *Biomedical Microdevices, 4(4),* 257-266.

Moogk, D., Hanley, S., Ramunas, J., Blaylock, A., Skorepova, J., Rosenberg, L., Jervis, E. (2007). Design and Analysis of a Long-Term Live-Cell Imaging Chamber for Tracking Cellular Dynamics Within Cultured Human Islets of Langerhans. *Journal of Biotechnology and Bioengineering, Not yet in print.*

Murphy, D. (2001). *Fundamentals of Light Microscopy and Electronic Imaging*. DE: Wiley-Liss Inc.

Mutz, M., *et al*. (2002). Focused acoustic energy for ejecting cells from a fluid. *United States Patent Application: 20020064808*.

Pawley, J. (1995). *Handbook of Biological Confocal Microscopy.* New York: Plenum Press.

Pepperkok, R., Ellenberg, J. (2006). High-throughput fluorescence microscopy for systems biology. *Nature Reviews: Molecular Cell Biology, 7,* 690-696.

Price, J., Gough, D. (1994). Comparison of Phase-Contrast and Fluorescent Digital Autofocus for Scanning Microscopy. *Cytometry, 16*, 283-297.

Ringeinsen, B., Kim, H., Barron, J., Krizman, D., Chrisey, D., Jackman, S., Auyeung, R., Spargo, B. (2004). Laser Printing of Pluripotent Embryonal Carcinoma Cells. *Tissue Engineering, 10,* 483-491.

Schnelle, T., Muller, T., Hagedorn, R., Voigt, A., Fuhr, G. (1999). Single micro electrode dielectrophoretic tweezers for manipulation of suspended cells and particles. *Biochimica et Biophysica Acta, 1429,* 99-105.

Sciperio Inc. (2002). *The Preventative BAT Construct-the Artificial Lymph Node (ALN).* Retrieved Dec. 2002, from http://www.sciperio.com/bio/aln.html

Tan, W., Desai, T. (2004). Layer-by-layer microfluidics for biomimetic three-dimensional structures. *Biomaterials, 25(7-8)*, 1355-64.

Taylor, D. L., Haskins, J. R., Giuliano, K. A. (2007). *High content screening: a powerful approach to systems cell biology and drug discovery.* Totowa, NJ: Humana Press.

Teschler, L. (2005). Precision moves with pint-sized motors. *Machine Design*, *77*(*7*), 96-105.

Uchida, M., Sato-Maeda, M., Tashiro, H. (1995). Whole-Cell manipulation by optical trapping. *Current Biology, 5(4),* 380-382.

White, D., Scribner, K., Olafsen, E. (1999). *MFC programming with Visual C++ 6 Unleashed*. USA: Sams Publishing.

White, J., Amos, W., Fordham, M. (1987). An Evaluation of Confocal Versus Conventional Imaging of Biological Structures by Fluorescence Light Microscopy. *Journal of Cell Biology*, *105*, 41-48.

Wolf, F., Geley, S. (2005). A simple and stable autofocusing protocol for long multidimensional live cell microscopy. *Journal of Microscopy, 221(1)*, 72-77.

Ziegler, J., Nichols, N. (1942). Optimum settings for automatic controllers. *Transactions of the ASME, 64*, 759-768.

Zimmermann W, Melnychenko I, Eschenhagen T. (2004). Engineered heart tissue for regeneration of diseased hearts. *Biomaterials Vol. 25*, 1639-1647.